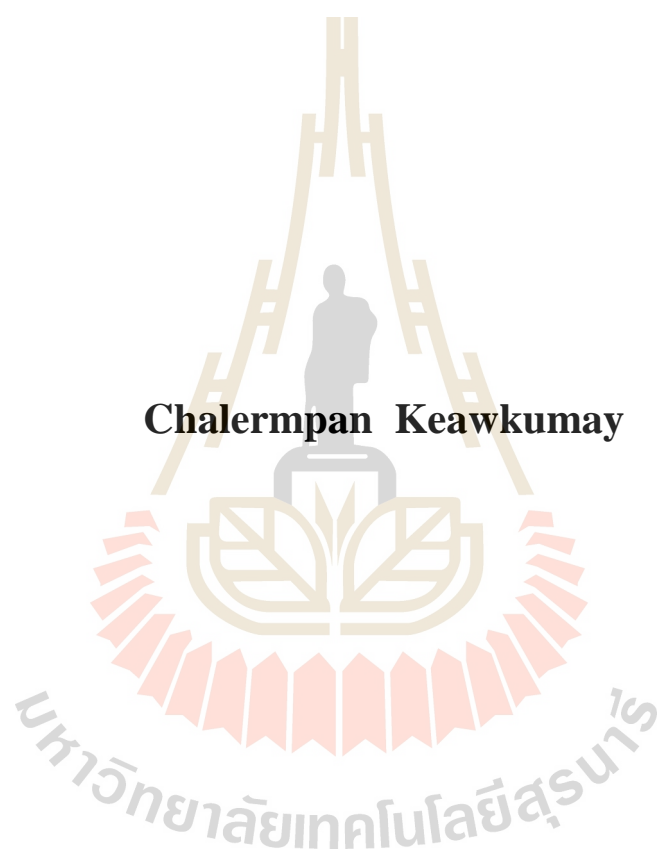


**PREPARATION OF POROUS MATERIALS WITH  
IMPROVED ADSORPTION CAPACITY IN  
AQUEOUS MEDIA**



**A Thesis Submitted in Partial Fulfillment of Requirements for the  
Degree of Doctor of Philosophy in Chemistry  
Suranaree University of Technology  
Academic Year 2017**

# การเตรียมวัสดุพจนที่ปรับเพิ่มความจุการดูดซับในสารละลาย



วิทยานิพนธ์นี้เป็นส่วนหนึ่งของการศึกษาตามหลักสูตรปริญญาวิทยาศาสตรดุษฎีบัณฑิต

สาขาวิชาเคมี

มหาวิทยาลัยเทคโนโลยีสุรนารี

ปีการศึกษา 2560

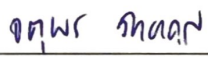
**PREPARATION OF POROUS MATERIALS WITH IMPROVED  
ADSORPTION CAPACITY IN AQUEOUS MEDIA**

Suranaree University of Technology has approved this thesis submitted in partial fulfillments of the requirement for the Degree of Doctor of Philosophy.

Thesis Examining Committee

  
\_\_\_\_\_  
(Asst. Prof. Dr. Sanchai Prayoonpokarach)

Chairperson

  
\_\_\_\_\_  
(Prof. Dr. Jatuporn Wittayakun)

Member (Thesis Advisor)

  
\_\_\_\_\_  
(Dr. Svetlana Mintova)

Member

  
\_\_\_\_\_  
(Asst. Prof. Dr. Nitinat Suppakarn)


Member

  
\_\_\_\_\_  
(Dr. Suwit Suthirakun)

Member

  
\_\_\_\_\_  
(Prof. Dr. Santi Maensiri)

Vice Rector for Academic Affairs  
and Internationalisation

  
\_\_\_\_\_  
(Asst. Prof. Dr. Worawat Meevasana)

Dean of Institute of Science

เฉลิมพันธ์ เขียวคำอ้าย : การเตรียมวัสดุพอร์นที่ปรับเพิ่มความจุการดูดซับในสารละลาย  
(PREPARATION OF POROUS MATERIALS WITH IMPROVED ADSORPTION  
CAPACITY IN AQUEOUS MEDIA). อาจารย์ที่ปรึกษา: ศาสตราจารย์ ดร.จตุพร วิทยาคุณ,  
132 หน้า.

วิทยานิพนธ์นี้ทำการดูดซับพาราควอดในน้ำโดยใช้เคลย์เป็นตัวดูดซับ ได้แก่ มอนท์โมริล  
โลไนท์เคลย์ (Mt) ออร์กาโนเคลย์ที่ปรับเปลี่ยนผิวหน้าเคลย์โดยใช้เตตระเอซิลเอมโมเนียมคลอไรด์  
(TDA-Mt) มีโซพอร์ัสเคลย์ (mesoporous Mt) ที่ปรับเปลี่ยนให้มีรูพอร์น โดยวิธีทำให้เกิดเป็น  
โครงสร้างไมเซลล์บริเวณระหว่างชั้นของเคลย์ แล้วทำการกำจัดสารสร้างไมเซลล์ออก ยิ่งไปกว่า  
นั้น ยังเติมไทเทเนียมเพื่อเพิ่มปริมาณตำแหน่งของการดูดซับ (mesoporous Ti-Mt) ไอโซโทมของ  
การดูดซับพาราควอดบนตัวดูดซับเคลย์ ออร์กาโนเคลย์ และมีโซพอร์ัสเคลย์ เป็นไปตามรูปแบบ  
การดูดซับของแลงเมียร์ โดยมีปริมาณการดูดซับพาราควอด ตามลำดับ ต่อไปนี้ TDA-Mt (52  
มิลลิกรัมต่อกรัม) Mt (38 มิลลิกรัมต่อกรัม) mesoporous Ti-Mt (25 มิลลิกรัมต่อกรัม) และ  
mesoporous Mt (25 มิลลิกรัมต่อกรัม) นอกจากนี้ การเติมไทเทเนียมยังเพิ่มปริมาณการดูดซับ  
พาราควอดได้

เพื่อที่จะปรับปรุงปริมาณการดูดซับให้สูงขึ้น ได้มีการสังเคราะห์ซีโอไลต์ฟูจาไซต์ชนิดควาย  
ในรูปโซเดียมไอออน ที่มีขนาดรูพอร์นในระดับไมโครเมตร (FAU) ให้มีอัตราส่วนระหว่างซิลิกอน  
ต่ออะลูมิเนียม (Si/Al) ที่แตกต่างกันเพื่อใช้เป็นตัวดูดซับ FAU ที่สังเคราะห์โดยวิธีไฮโดรเทอร์มอล  
มี Si/Al อยู่ระหว่าง 2.1 ถึง 2.4 และมีขนาดของอนุภาคอยู่ระหว่าง 100 ถึง 300 นาโนเมตร ผลของ  
การดูดซับพบว่า เป็นไปตามรูปแบบการดูดซับของแลงเมียร์ ซึ่งมีปริมาณการดูดซับในช่วง 210  
ถึง 240 มิลลิกรัมต่อกรัมของตัวดูดซับ ซึ่ง FAU ที่มีอัตราส่วนของซิลิกอนต่ออะลูมิเนียม 2.4 มีค่า  
การดูดซับสูงที่สุด

อาจเป็นไปได้ว่า ปริมาณการดูดซับพาราควอดจะเพิ่มสูงขึ้นได้ ถ้าใช้ตัวดูดซับ FAU การที่มี  
ขนาดอนุภาคในระดับนาโนเมตร ดังนั้น จึงทำการสังเคราะห์ FAU ที่มีขนาดนาโนเมตร (FAU  
nanozeolite) โดยวิธีไฮโดรเทอร์มอล โดยใช้แหล่งของอะลูมิเนียมที่แตกต่างกัน ได้แก่ ผงอะลูมิเนียม  
และ โซเดียมอะลูมิเนต ( $\text{NaAlO}_2$ ) นอกจากนี้มีการใช้น้ำที่มีปริมาตรที่แตกต่างกันด้วย จากการ  
สังเคราะห์ FAU nanozeolite พบว่า FAU ที่ใช้  $\text{NaAlO}_2$  มีผลึกขนาดเล็กกว่า FAU ที่ใช้ผงอะลูมิเนียม  
ยิ่งไปกว่านั้น การสังเคราะห์ FAU nanozeolite ที่ใช้น้ำในปริมาตรที่น้อยทำให้ได้ผลึกที่มีขนาดเล็ก  
กว่าการสังเคราะห์ที่ใช้น้ำในปริมาตรที่มาก ปริมาตรของน้ำในการสังเคราะห์ FAU nanozeolite  
เพิ่มขึ้นเป็นลำดับ ดังต่อไปนี้  $Y1-180 > Y1-140 > Y1-140 > Y1-92$  รูปภาพที่ได้จากกล้อง

จุลทรรศน์แบบส่องกราด แสดงให้เห็นว่า Y1-140 และ Y1-92 มีขนาดของผลึกในระดับนาโนเมตร อย่างไรก็ตาม ผลจากสเปกตรัมจากการเลี้ยวเบนของรังสีเอกซ์ ยืนยันว่า มีเพียง Y1-140 เท่านั้นที่เป็นเฟส FAU บริสุทธิ์

การเติมวานาเดียม (V) ลงใน FAU ที่มีผลึกขนาดนาโนเมตร (V-FAU) อาจจะทำให้เป็นตัวเร่งปฏิกิริยาที่น่าสนใจ ดังนั้น ในส่วนนี้จึงได้ทำการสังเคราะห์ V-FAU ด้วยวิธีไฮโดรเทอร์มอลแบบผสมในขั้นตอนเดียว ที่มีปริมาณของน้ำที่แตกต่างกัน V-FAU จากการสังเคราะห์ที่ใช้ปริมาณน้ำมาก ได้ผลึกที่มีรูปร่างเป็นทรงสี่เหลี่ยม และผลึกมีขนาดเล็กประมาณ 100 ถึง 300 นาโนเมตร ในทางกลับกัน V-FAU จากการสังเคราะห์ที่ใช้ปริมาณน้ำน้อย ได้ผลึกที่มีรูปร่างเป็นทรงกลม และผลึกมีขนาดใหญ่ประมาณ 500 นาโนเมตร วานาเดียมยังถูกตรวจพบในทุกตัวอย่างของ V-FAU จากการทดสอบด้วยเครื่องยูวี-วิสิเบิลแบบการสะท้อนของแสง ยืนยันว่า มีวานาเดียมในโครงสร้างของ V-FAU การวัดหาปริมาณกรดบรอนสเตดและลิวอิส โดยใช้ FAU ที่อยู่ในรูปของโปรตอน (HFAU) พบว่า V-HFAU มีปริมาณกรดสูงกว่า HFAU ซึ่งการที่มีปริมาณกรดสูงจะเป็นประโยชน์สำหรับนำไปใช้เป็นตัวเร่งปฏิกิริยาได้



สาขาวิชาเคมี  
ปีการศึกษา 2560

ลายมือชื่อนักศึกษา เฉลิมพงษ์ เก่งทำชัย  
ลายมือชื่ออาจารย์ที่ปรึกษา อทพร ดนแดน

CHALERMPAN KEAWKUMAY : PREPARATION OF POROUS  
MATERIALS WITH IMPROVED ADSORPTION CAPACITY IN  
AQUEOUS MEDIA. THESIS ADVISOR : PROF. JATUPORN  
WITTAYAKUN, Ph.D. 132 PP.

PARAQUAT ADSORPTION/ CLAY/ FAUJASITE ZEOLITE/ NANOZEOLITE/  
VANADIUM

In this thesis, adsorption of paraquat in water is performed by using clay based adsorbents including montmorillonite (Mt), organoclay (TDA-Mt) from intercalation of Mt with tetradecylammonium chloride, mesoporous Mt from intragallery templating method (with and without Ti addition). Paraquat adsorption isotherms of clay based adsorbent follow Langmuir model and the adsorption capacity is as follows: TDA-Mt (52 mg/g) > Mt (38 mg/g) > mesoporous Ti-Mt (25 mg/g) > mesoporous Mt (18 mg/g). The presence of Ti enhances the adsorption capacity.

In order to improve adsorption capacity, microporous zeolite faujasite Y in sodium form (FAU) with various Si/Al ratios are used as adsorbents. The synthesis of FAU with different Si/Al ratios (2.1 to 2.4) and particle sizes (100-300 nm) is performed using hydrothermal method. The adsorption process obeys the Langmuir model. The capacity of the adsorbents is in the range 210-240 mg/g-adsorbent. The FAU samples with the highest Si/Al ratio (2.4) have the highest adsorption capacity.

It is possible that nanosized FAU has higher adsorption capacity of paraquat than microsized FAU. Thus, FAU is synthesized by using hydrothermal method with different aluminium sources (aluminium powder and sodium aluminate) and water

contents. The crystal size of FAU obtained from sodium aluminate is smaller than that from aluminium powder. Moreover, the smaller size is produced from the synthesis with less water content. The amount of water in the synthesis gel is increased in the following order: Y1-180 > Y1-140 > Y1-92. The SEM images of the FAU samples show that samples Y1-140 and Y1-92 have nanosized crystals. However, the X-ray diffraction (XRD) patterns indicate that only Y1-140 sample has a pure FAU phase.

Incorporation of vanadium (V) in nanosized FAU could make it an interesting catalyst. In this part nanosized FAU incorporated with vanadium (V-FAU) is synthesized by one-pot hydrothermal method with various water contents. V-FAU from the synthesis gel with the high water content has a rectangular crystal shape around 100-300 nm. In contrast, V-FAU from the synthesis gel with the lower water content has a spherical shape with size of 500 nm. Vanadium is detected in all V-FAU samples and its incorporation in FAU structure is confirmed by diffuse reflectance ultraviolet-visible (DR UV-Vis) spectroscopy. Amount of Brønsted and Lewis acid site of V-HFAU is more than that of HFAU. The higher acidity of V-HFAU is beneficial for catalytic reactions.

School of Chemistry

Academic Year 2017

Student's Signature บณลิตพพนธ์ ภิงวาศำอำว

Advisor's Signature อศพว อศกร

## ACKNOWLEDGEMENTS

I am deeply indebted to my thesis advisor, Professor Dr. Jatuporn Wittayakun, for giving me a chance to study in School of Chemistry, Suranaree University of Technology (SUT) and kind suggestions and supports throughout the study period. Furthermore, I gratefully thank Dr. Svetlana Mintova for accepting me to work in her research group at Laboratoire Catalyse et Spectrochimie (LCS), ENSICAEN, Université Caen-Normandie, France, and teaching me several techniques in nanozeolite synthesis.

I also thank Asst. Prof. Dr. Sanchai Prayoonpokarach, Asst. Prof. Dr. Nitinat Suppakarn and Dr. Suwit Suthirakun for their valuable suggestions and guidance given as thesis examination committee.

I wish to acknowledge Suranaree University of Technology for financial supports from a SUT-PhD scholarship (SUT-PhD/11/2554). I would like to express my appreciation to the faculty and staff of School of Chemistry and Center for Scientific and Technological Equipment, SUT. Special thanks are extended to Mr. Suriyan Rakmae and all member of catalysis group at SUT for their help, support and encouragement.

Last but not least, I would like to thank my parents, Mr. Jaras and Mrs. Boonmee Keawkumay, and my younger brother, Mr. Rachane Keawkumay, who give me a valuable life and protect my mind from an evil with their unconditional love.

Chalermpan Keawkumay



# CONTENTS

	<b>Page</b>
ABSTRACT IN THAI.....	I
ABSTRACT IN ENGLISH.....	III
ACKNOWLEDGEMENTS.....	V
CONTENTS.....	VI
LIST OF TABLES.....	XII
LIST OF FIGURES.....	XIV
SYMBOLS AND ABBREVIATIONS.....	XVII
<b>CHAPTER</b>	
<b>I INTRODUCTION.....</b>	<b>1</b>
1.1 Introduction.....	1
1.2 Research objectives.....	3
1.3 Scope and limitation of the study.....	3
1.4 References.....	4
<b>II LITERATURE REVIEW.....</b>	<b>11</b>
2.1 Adsorption of paraquat.....	11
2.2 Background of adsorbents.....	17
2.2.1 Zeolite.....	17
2.2.2 Clay (Montmorillonite; Mt).....	18

## TABLE OF CONTENTS (Continued)

	<b>Page</b>
2.2.3 Organoclay .....	19
2.2.4 Mesoporous clay (Pillar clay) .....	22
2.3 Background of nanozeolites .....	23
2.4 Background of vanadium incorporated zeolites.....	24
2.5 References .....	25
<b>III ADSORPTION OF PARAQUAT BY</b>	
<b>MONTMORILLONITE MODIFIED WITH</b>	
<b>TETRADECYLAMMONIUM CHLORIDE AND</b>	
<b>INTRAGALLERY TEMPLATING METHOD .....</b>	<b>35</b>
3.1 Introduction.....	36
3.2 Experiment.....	38
3.2.1 Materials .....	38
3.2.2 Preparation of organoclays.....	38
3.2.3 Preparation of mesoporous-Mt and mesoporous Ti-Mt.....	39
3.3 Material characterization.....	40
3.3.1 Phase composition .....	40
3.3.2 N <sub>2</sub> adsorption-desorption isotherms.....	40
3.3.3 Morphology.....	41
3.3.4 Functional groups.....	41

## TABLE OF CONTENTS (Continued)

	<b>Page</b>
3.4 Adsorption study .....	41
3.4.1 Adsorption isotherms .....	42
3.4.2 Effect of pH for paraquat adsorption on Mt samples .....	43
3.5 Results and discussion .....	44
3.5.1 Structures of clay and organoclays .....	44
3.5.2 N <sub>2</sub> adsorption-desorption isotherms .....	46
3.5.3 Morphologies .....	49
3.5.4 Functional groups .....	50
3.5.5 Adsorption of paraquat on Mt and modified samples .....	52
3.6 Conclusions .....	58
3.7 References .....	59
<b>IV PARAQUAT ADSORPTION ON ZEOLITE FAU Y WITH VARIOUS SILICON/ALUMINIUM RATIO .....</b>	<b>64</b>
4.1 Introduction .....	65
4.2 Experiment .....	67
4.2.1 Synthesis of zeolite NaY .....	67
4.2.2 Characterization of zeolite NaY .....	68
4.2.3 Paraquat adsorption .....	69
4.3 Results and discussion .....	70
4.3.1 Structure and Si/Al ratio of NaY .....	70
4.3.2 N <sub>2</sub> adsorption-desorption isotherms .....	71

## TABLE OF CONTENTS (Continued)

	<b>Page</b>
4.3.3 Morphology.....	75
4.3.4 Functional groups.....	76
4.3.5 Basicity of NaY.....	78
4.4 Paraquat adsorption.....	79
4.5 Conclusions.....	82
4.6 References.....	82
<b>V EFFECT OF ALUMINIUM SOURCE AND WATER CONTENT ON TEXTURAL PROPERTY AND MORPHOLOGY OF FAUJASITE NANOZEOLITE.....</b>	<b>87</b>
5.1 Introduction.....	88
5.2 Experiment.....	90
5.2.1 Synthesis of Y1-140 and Y1-180.....	90
5.2.2 Synthesis of Y1-180 and Y1-140 using aluminium powder.....	92
5.2.3 Synthesis of Y1-180 and Y1-140 using aluminium powder.....	92
5.2.4 Aging and crystallization.....	92
5.3 Characterization.....	93
5.3.1 X-ray diffraction (XRD) analysis.....	93
5.3.2 N <sub>2</sub> adsorption-desorption analysis.....	93

## TABLE OF CONTENTS (Continued)

	<b>Page</b>
5.3.3 Scanning electron microscopy (SEM) .....	93
5.3.4 Dynamic light scattering (DLS) analysis .....	93
5.3.5 Chemical analysis .....	94
5.4 Results and discussion .....	94
5.4.1 Phase and crystallinity of FAU Y with different aluminium sources .....	94
5.4.2 Morphology of FAU Y nanozeolites .....	97
5.4.3 N <sub>2</sub> adsorption-desorption isotherms of FAU Y zeolite.....	100
5.4.4 Chemical composition of FAU Y zeolite.....	102
5.4.5 Optimization of water content for FAU Y synthesis .....	102
5.5 Conclusions.....	105
5.6 References.....	105
<b>VI INCORPORATION OF VANADIUM IN FAUJASITE NANOZEOLITE.....</b>	<b>109</b>
6.1 Introduction.....	110
6.2 Experimental .....	113
6.2.1 Synthesis of V-Y83, V-Y90 and V-Y100.....	113
6.3 Characterization .....	114
6.3.1 X-ray diffraction (XRD) analysis.....	114
6.3.2 N <sub>2</sub> adsorption-desorption analysis.....	114

## TABLE OF CONTENTS (Continued)

	<b>Page</b>
6.3.3 Scanning electron microscopy (SEM) .....	115
6.3.4 Transmission electron microscopy (TEM).....	115
6.3.5 Chemical analysis .....	115
6.3.6 Pyridine adsorption .....	115
6.3.7 Diffuse reflectance (DR) UV-Vis spectroscopy.....	116
6.4 Results and discussion .....	117
6.4.1 Phase and crystallinity of V-FAU .....	117
6.4.2 Morphology of V-FAU Y with different water contents .....	120
6.4.3 N <sub>2</sub> adsorption-desorption isotherms of V-FAU .....	122
6.4.4 Chemical composition of V-FAU zeolites.....	124
6.4.5 Pyridine adsorption .....	125
6.4.6 Characterization of V-FAU by DRUV-Vis.....	126
6.5 Conclusions.....	128
6.6 References.....	128
CURRICULUM VITAE .....	132

## LIST OF TABLES

Table	Page
3.1	2 Theta ( $2\theta$ ) and interlayer spacing of Mt and modified Mt..... 44
3.2	Surface area, total pore volume and average pore diameter of Mt samples ..... 47
3.3	FTIR assignments of Mt and modified Mt ..... 52
3.4	Langmuir parameters for paraquat adsorption on Mt and modified Mt ..... 54
3.5	Maximum adsorption capacities of Mt, organoclay (based Mt) and mesoporous Mt..... 57
4.1	Si/Al ratio, surface area and total pore volume of NaY and NaY adsorbed paraquat samples ..... 72
4.2	Basicity amount of NaY samples ..... 78
4.3	Langmuir parameters of paraquat adsorption on NaY with various Si/Al ratio ..... 81
5.1	Amounts of materials for the synthesis of FAU Y (Y1-180 and Y1-140) with aluminium powder ..... 91
5.2	Amounts of materials for the synthesis of FAU Y (Y1-180 and Y1-140) with sodium aluminate ( $\text{NaAlO}_2$ )..... 91
5.3	Textural properties of Y1-180 and Y1-140 with different aluminium sources ..... 101
5.4	Chemical composition of Y1-180 and Y1-140 with different aluminium sources ..... 102

## LIST OF TABLES (Continued)

<b>Table</b>		<b>Page</b>
6.1	Amount of materials in gram for the synthesis of V incorporated FAU Y zeolite with various water contents .....	114
6.2	Textural properties of V-Y83, V-Y92 and V-Y100 .....	124
6.3	Chemical composition of V-Y83, V-Y92 and V-Y100.....	124
6.4	Peak area and number of acid site .....	126
6.5	Vanadium species in V-FAU zeolite based on DR UV-Vis analysis (Chao et al., 1997).....	127



## LIST OF FIGURES

Figure	Page
2.1	Chemical structures of paraquat..... 11
2.2	Structure of zeolite NaY (Baerlocher and McCusker, Database of Zeolite Structures: <a href="http://www.iza-structure.org/databases/">http://www.iza-structure.org/databases/</a> )..... 18
2.3	Structure of clay minerals represented by montmorillonite. They are built up from combinations of tetrahedral and octahedral sheets whose basic units are usually Si–O tetrahedron and Al–O octahedron, respectively (Alexandre and Dubois, 2000) Zeolite Structures: <a href="http://www.iza-structure.org/databases/">http://www.iza-structure.org/databases/</a> )..... 20
3.1	Chemical structures of (a) Tetradecylamine (TDA), (b) Cetyltrimethyl- ammonium bromide (CTAB), (c) Tetraethoxy silane (TEOS) and (d) Tetrabutyl titanate ..... 39
3.2	XRD pattern of (a) Mt and TDA-Mt, and (b) mesoporous Mt and Mesoporous Ti-Mt ..... 45
3.3	N <sub>2</sub> adsorption-desorption isotherms of (a) Mt and TDA-Mt, and (b) mesoporous Mt and Mesoporous Ti-Mt..... 48
3.4	Morphology of Mt, TDA-Mt, mesoporous Mt and Mesoporous Ti-Mt ..... 49
3.5	FTIR spectra of Mt, TDA-Mt, mesoporous Mt and Mesoporous Ti-Mt ..... 51
3.6	Adsorption isotherm of paraquat on Mt and modified Mt samples ..... 53
3.7	XRD of a) Mt and TDA-Mt, b) Mt and TDA-Mt with paraquat ..... 55

## LIST OF FIGURES (Continued)

Figure	Page
3.8	Effect of pH on the adsorption of paraquat using Mt samples as adsorbents .....56
4.1	XRD pattern of (a) NaY with various Si/Al ratio and (b) paraquat adsorbed NaY .....73
4.2	N <sub>2</sub> adsorption-desorption isotherm of (a) NaY with various Si/Al ratio and (b) paraquat adsorbed NaY .....74
4.3	SEM images of NaY with various Si/Al ratio .....75
4.4	FTIR spectra of (a) NaY with various Si/Al ratio and (b) paraquat adsorbed NaY .....77
4.5	TCD signal of NaY with various Si/Al .....79
4.6	Adsorption isotherm of paraquat on Mt and modified Mt samples .....80
5.1	Intensity corresponded crystallinity of FAU Y samples .....95
5.2	XRD pattern of Y1-180 and Y1-140 with different aluminium sources .....96
5.3	SEM images of Y1-180 and Y1-140 with different aluminium sources (A) Y1-180-Alpowder, (B) Y1-180-NaAlO <sub>2</sub> , (C) Y1-140-Alpowder and (D) Y1-140-NaAlO <sub>2</sub> . .....98
5.4	DLS curves of Y1-180 and Y1-140 with different aluminium sources .....99
5.5	N <sub>2</sub> adsorption-desorption isotherm of Y1-180 and Y1-140 with different aluminium sources ..... 101
5.6	XRD pattern of Y1-180, Y1-140 and Y92 using sodium aluminate ..... 103

## LIST OF FIGURES (Continued)

Figure	Page
5.7	SEM images of Y1-180, Y1-140 and Y1-92 using sodium aluminate ..... 104
6.1	XRD patterns of V-Y83, V-Y92, V-Y100 comparing to NaY ..... 117
6.2	XRD patterns of V-FAU synthesized from the gels with different water content.. ..... 118
6.3	Pattern fitting (Le Bail method) of V-Y92. Vertical ticks correspond to line indexing of the FAU phase. Difference plots between calculated and experimental points are shown at the bottom of the pattern..... 119
6.4	SEM images of V-FAU with different water content ..... 121
6.5	TEM images of V-Y92 with nanosized particles with high magnification ..... 122
6.6	N <sub>2</sub> adsorption-desorption isotherm of V-FAU nanozeolites..... 123
6.7	FTIR spectra of HY and V-HY samples after pyridine adsorption..... 125
6.8	DR UV-Vis spectra of V-Y83, V-Y92 and V-Y100..... 128

## SYMBOLS AND ABBREVIATIONS

%	=	Percent
°	=	Degree
°C	=	Degree Celsius
CEC	=	Cation exchange capacity
XRD	=	X-Ray diffractometer
FTIR	=	Fourier transform infrared spectrometer
BET	=	Brunauer-Emmett-Teller
BJH	=	Barrett-Joyner-Halenda
SEM	=	Scanning electron microscope
TEM	=	Transmission electron microscope
DLS	=	Dynamic light scattering
ICP	=	Inductively coupled plasma
UV-Vis	=	Ultraviolet-visible spectroscopy
DR-UV-Vis	=	Diffuse reflectance ultraviolet-visible spectroscopy
Mt	=	Montmorillonite
FAU	=	Faujasite zeolite
TDA	=	Tetradecylamine
CTAB	=	Cetyltrimethyl ammonium bromide
TEOS	=	Tetraethoxy silane
mg	=	Milligram

**SYMBOLS AND ABBREVIATIONS (Continued)**

g	=	Gram
Å	=	Angstrom
min	=	Minute
mm	=	Millimeter
µm	=	Micrometer
nm	=	Nanometer
m <sup>2</sup>	=	Square meter
cm <sup>3</sup>	=	Cubic centimeter
m <sup>3</sup>	=	Cubic meter
cm <sup>-1</sup>	=	Reciprocal centimeter
ml	=	Milliliter
meq	=	Milliequivalent
mol	=	Mole
wt%	=	Percent by weight
conc	=	Concentrated
ca	=	Circa

# CHAPTER I

## INTRODUCTION

### 1.1 Introduction

This thesis is divided into 4 main parts. The first two parts are about adsorption of paraquat on clay, adsorbents derived from clay and zeolite FAU Y. Paraquat is used widely in large areas in Nakhon Ratchasima, Thailand, to control weeds. However, it can accumulate in the environment and contaminate water reservoirs. Adsorption is a method to remove paraquat in aqueous solution. The first part (Chapter III), Montmorillonite clay (Mt) is modified to an organoclay and mesoporous materials to increase the paraquat adsorption capacity. The second part (Chapter IV) is the synthesis of microporous FAU Y with various Si/Al ratios to improve the adsorption capacity.

Faujasite (FAU) zeolite is one of the most promising materials because of its well-defined channels making a large supercage ( $11.0 \times 13.0 \text{ \AA}$ ) with a large pore size ( $7.4 \times 7.4 \text{ \AA}$ ), large surface area, and excellent thermal stability. FAU zeolite can be used in a several applications such as ion exchange, adsorption, catalysis and membrane separation (Mintova and Valtchev 1999; Nakrani et al., 2016; Dang et al., 2017).

Small crystalline size could improve the textural properties of zeolites including pore volume, external surface area and surface reactivity (Awala et al., 2015; Nakrani et al., 2017). Therefore, the third part (Chapter V) is an optimization of a synthesis of nanocrystalline FAU Y. In the final part (Chapter VI), vanadium

incorporated FAU nanozeolite is synthesized by a one-pot hydrothermal method in order to increase the performance and catalytic ability of FAU nanozeolite.

Recently, the syntheses of nanocrystalline zeolites are achieved. Nanocrystalline zeolites are materials with dimension less than 100 nm with special properties, such as large accessible surface area and activities and shorter diffusion pathways than micrometer-sized zeolite (Valtchev et al., 2004; Azizi et al., 2014; Mintova et al., 2016). Nanosized crystals of FAU type zeolite without organic templates are successfully synthesized by using hydrothermal method at low temperature (50°C) for 45 h (Awala et al., 2015). Small crystallites (10-15 nm) with a narrow particle size distribution, micropore volumes ( $0.30 \text{ cm}^3 \text{ g}^{-1}$ ) and high crystalline yields (above 80%) are obtained. Therefore, nanosized crystallines and high micropore volumes could improve the adsorption capacity of paraquat.

Vanadium incorporated zeolites have been used as selective oxidation catalysts. The activity and selectivity of vanadium containing zeolite are sensitive to the nature of vanadium species in the zeolites including oxidation state, coordination, dispersion (Roozeboom et al., 1980; Went et al., 1990; Das et al., 1993; Whittington and Anderson, 1993; Chao et al., 1997; Teixeira-Neto et al., 2009). There are many methods for the incorporation vanadium into zeolites, i.e. impregnation, encapsulation, ion exchange, one-pot hydrothermal method (Huang et al., 1990; Kim et al., 1997; Dzwigaj et al., 1998; Kozlov et al., 1998; Kozlov et al., 1999; Hagiwara et al., 2003; Maurya et al., 2011; Pal et al., 2014; El-Roz et al., 2017; and Silva et al., 2017). Vanadium incorporated zeolites prepared by one-pot synthesis are still the best fulfill the compromise between vanadium concentration and metal dispersion (Teixeira-Neto et al., 2009). Many techniques, including  $^{51}\text{V}$  nuclear magnetic

resonance (NMR), X ray photoelectron spectroscopy (XPS), electron paramagnetic resonance (EPR) and diffuse reflectance UV-visible spectroscopy (DR-UV-Vis) are used to identify the coordination vanadium sites in the zeolite structure (Centi et al., 1992).

## **1.2 Research objectives**

The aims of this research are as follows:

1.2.1 To prepare and characterize adsorbents for paraquat removal, including NaY, organoclay and mesoporous clay.

1.2.2 To investigate paraquat adsorption on NaY with various Si/Al ratios, montmorillonite, organoclay and pillar clay.

1.2.3 To optimize the synthesis of FAU nanozeolites.

1.2.4 To explore the incorporation of vanadium into FAU nanozeolites.

## **1.3 Scope and limitation of the study**

1.3.1 Montmorillonite clay is modified by two methods: organoclay and mesoporous clay with and without addition of titanium by methods from literature (Keawkumay et al., 2012; Mao et al., 2015).

1.3.2 Microporous NaY with various Si/Al ratios are synthesized from rice husk silica by a method from the literature (Wittayakun et al., 2008).

1.3.3 FAU nanozeolites are synthesized by adapting hydrothermal method from Awala et al., 2015. The synthesis of FAU Y nanozeolites is performed by using different aluminium sources and water contents.



1.3.4 Vanadium incorporated FAU nanozeolites are synthesized by using one-pot hydrothermal method adapting from Awala et al., 2015. The synthesis of FAU Y nanozeolites is done by using different of water contents. The existence of vanadium in FAU nanozeolite is also determined.

## 1.4 References

- Alexandre, M. and Dubois, P. (2000). Polymer-layered silicate nanocomposites: preparation, properties and uses of a new class of material. **Material Science and Engineering**. 28: 1-63.
- Awala, H., Gilson, J.-P., Retoux, R., Boullay, P., Goupil, J.-M., Valtchev, V., and Mintova, S. (2015). Template-free nanosized faujasite-type zeolites. **Nature Materials**. 14: 447-451.
- Azizi, S. N., Ghasemi, S., and Kaviani, S. (2014). Synthesis and characterization of NaX nanozeolite using stem sweep as silica source and application of Ag-modified nanozeolite in electrocatalytic reduction of H<sub>2</sub>O<sub>2</sub>. **Biosensors and Bioelectronics**. 62:1-7.
- Baba, T., Sawada, H., Takahashi, T., and Abe, M. (2002). Chemisorption study of hydrogen and methane by <sup>1</sup>H MAS NMR and conversion of methane in the presence of ethylene on Ag-Y zeolite. **Applied Catalysis A, General**. 231: 55-63.
- Bouras, O., Bollinger, J. C., Baudu, M., and Khalaf, H. (2007). Adsorption of diuron and its degradation products from aqueous solution by surfactant-modified pillar clays. **Applied Clay Science**. 37: 240-250.

- Centi, G., Perathoner, S., Trifiro, F., Aboukais, A., Aissi, C. F., and Guelton, M. (1992). Physicochemical characterization of V-silicalite. **The Journal of Physical Chemistry**. 96: 2617-2629.
- Chao, K. J., Wu, C. N., Chang, H., Lee, L. J., and Hu, S. (1997). Incorporation of vanadium in mesoporous MCM-41 and microporous AFI zeolites. **The Journal of Physical Chemistry B**. 101: 6341-6349.
- Chatterjee, D., Dasgupta, S., and Rao N. N. (2006). Visible light assisted photodegradation of halocarbons on the dye modified TiO<sub>2</sub> surface using visible light. **Solar Energy Materials & Solar Cells**. 90: 1013-1020.
- Chen, Y., Wang, K., and Lou, L. (2004). Photodegradation of dye pollutants on silica gel supported TiO<sub>2</sub> particles under visible light irradiation. **Journal of Photochemistry and Photobiology A: Chemistry**. 163: 281-287.
- Chun, H., Yizhong, W., and Hongxiao, T. (2001). Influence of adsorption on the photodegradation of various dyes using surface bond-conjugated TiO<sub>2</sub>/SiO<sub>2</sub> photocatalyst. **Applied Catalysis B: Environmental**. 35: 95-105.
- Cundy, C. S. and Cox, P. A. (2005). The hydrothermal synthesis of zeolites: Precursors, intermediates and reaction mechanism. **Microporous and Mesoporous Materials**. 82: 71-78.
- Dang, S., Zhao, L., Yang, Q., Zheng, M., Zhang, J., Gao, J., and Xu, C. (2017). Competitive adsorption mechanism of thiophene with benzene in FAU zeolite: The role of displacement. **Chemical Engineering Journal**. 328: 172-185.

- Das, N., Eckert, H., Hu, H., Wachs, I. E., Walzer, J. F., and Feher, F. J. (1993). Bonding states of surface vanadium(V) oxide phases on silica: structural characterization by vanadium-51 NMR and Raman spectroscopy. **The Journal of Physical Chemistry**. 97: 8240-8243.
- El-Roz, M., Lakiss, L., Telegeiev, I., Lebedev, O. I., Bazin, P., Vicente, A., and Valtchev, V. (2017). High-visible-light photoactivity of plasma-promoted vanadium clusters on nanozeolites for partial photooxidation of methanol. **ACS Applied Materials and Interfaces**. 9: 17846-17855.
- Eneji, I. S., Buncel, E., and Vanloon, G. W. (2002). Degradation and sorption of pirimiphos-methyl in two Nigerian soils. **Journal of Agricultural and Food Chemistry**. 50: 5634-5639.
- Ganigar, R., Rytwo, G., Gonen, Y., Radian, A., and Mishael, Y. G. (2010). Polymer-clay nanocomposites for the removal of trichlorophenol and trinitrophenol from water. **Applied Clay Science**. 49: 311-316.
- Guisnet, M. and Gilson, J. P. (2002). **Zeolites for cleaner technologies**. Imperial College Press, London.
- Hagiwara, K., Ebihara, T., Urasato, N., Ozawa, S., and Nakata, S. (2003). Effect of vanadium on USY zeolite destruction in the presence of sodium ions and steam - Studies by solid-state NMR. **Applied Catalysis A: General**. 249: 213-228.
- Hamid, S. B. A., Tan, T. L., Lai, C. W., and Samsudin, E. M. (2014). Multiwalled carbon nanotube/TiO<sub>2</sub> nanocomposite as a highly active photocatalyst for photodegradation of Reactive Black 5 dye. **Chinese Journal of Catalysis**. 35: 2014-2019.

- Huang, M., Shan, S., Yuan, C., Li, Y., and Wang, Q. (1990). Introduction of vanadium into Y zeolite by solid-state ion exchange. **Zeolites**. 10: 772-777.
- Kozlov, A., Asakura, K., and Iwasawa, Y. (1998). Synthesis and characterization of vanadium (IV) complexes in NaY zeolite supercages. **Microporous and Mesoporous Materials**. 21: 571-579.
- Kozlov, A., Kozlova, A., Asakura, K., and Iwasawa, Y. (1999). Zeolite-encapsulated vanadium picolinate peroxo complexes active for catalytic hydrocarbon oxidations. **Journal of Molecular Catalysis A: Chemical**. 137: 223-237.
- Kusic, H., Koprivanac, N., and Bozic, A. L. (2013). Environmental aspects on the photodegradation of reactive triazine dyes in aqueous media. **Journal of Photochemistry and Photobiology A: Chemistry**. 252: 131-144.
- Leite, M. P., dos Reis, L. G. T., Robaina, N. F., Pacheco, W. F., and Cassella, R. J. (2013). Adsorption of paraquat from aqueous medium by Amberlite XAD-2 and XAD-4 resins using dodecylsulfate as counter ion. **Chemical Engineering Journal**. 215-216: 691-698.
- Mao, H., Li, B., Li, X., Yue, L., Xu, J., Ding, B., Gao, X., and Zhou, Z. (2010). Facile synthesis and catalytic properties of titanium containing silica-pillar clay derivatives with ordered mesoporous structure through a novel intra-gallery templating method. **Microporous and Mesoporous Materials**. 130: 314-321.
- Maurya, M. R., Kumar, A., and Costa Pessoa, J. (2011). Vanadium complexes immobilized on solid supports and their use as catalysts for oxidation and functionalization of alkanes and alkenes. **Coordination Chemistry Reviews**. 255: 2315-2344.

- Mintova, S., Grand, J., and Valtchev, V. (2016). Nanosized zeolites: Quo Vadis? **Comptes Rendus Chimie**. 19: 183-191.
- Mintova, S., and Valtchev, V. (1999). Synthesis of nanosized FAU-type zeolite. **Studies in Surface Science and Catalysis**. 125: 141-148.
- Mohamed, R. M., Mkhallid, I. A., and Barakat, M. A. (2015). Rice husk ash as a renewable source for the production of zeolite NaY and its characterization. **Arabian Journal of Chemistry**. 8: 48-53.
- Ngoula, F., Watcho, P., Dongmo, M. C., Kenfack, A., Kamtchoung, P., and Tchoumboue, J. (2001). Effects of pirimiphos-methyl (an organophosphate insecticide) on the fertility of adult male rats. **African Health Sciences**. 7 (1): 3-9.
- Pal, N., Pramanik, M., Bhaumik, A., and Ali, M. (2014). Highly selective and direct oxidation of cyclohexane to cyclohexanone over vanadium exchanged NaY at room temperature under solvent-free conditions. **Journal of Molecular Catalysis A: Chemical**. 392: 299-307.
- Patakioutas, G. and Albanis, T. A. (2002). Adsorption-desorption studies of alachlor, metolachlor, EPTC, chlorothalonil and pirimiphos-methyl in contrasting soils. **Pest Management Science**. 58: 352-362.
- Patakioutas, G. I., Karras, G., Hela, D., and Albanis, T. A. (2002). Pirimiphos-methyl and benalaxyl losses in surface runoff from plots cultivated with potatoes. **Pest Management Science**. 58: 1194-1204.
- Paul, B., Yang, D., Yang, X., Ke, X., Frost, R., and Zhu, H. (2010). Adsorption of the herbicide simazine on moderately acid-activated beidellite. **Applied Clay Science**. 49: 80-83.

- Petkowicz, D. I., Rigo, R. T., Radtke, C., Pergher, S. B., and Santos, J. H. Z. (2008). Zeolite NaA from Brazilian chrysotile and rice husk. **Microporous and Mesoporous Materials**. 116: 548-554.
- Roozeboom, F., Mittelmeijer-Hazeleger, M. C., Moulijn, J. A., Medema, J., De Beer, V. H. J., and Gellings, P. J. (1980). Vanadium oxide monolayer catalysts. 3. A Raman spectroscopic and temperature-programmed reduction study of monolayer and crystal-type vanadia on various supports. **Journal of Physical Chemistry**. 84: 2783-2791.
- Rouquerol, F., Rouquerol, J., and Sing, K. (1999). Adsorption by powders and porous solids: principles, methodology and applications. Academic Press, London, pp. 18-212.
- Sakthivel, S., Shankar, M. V., Palanichamy, M., Arabindoo, B., and Murugesan, V. (2002). Photocatalytic decomposition of leather dye Comparative study of TiO<sub>2</sub> supported on alumina and glass beads. **Journal of Photochemistry and Photobiology A: Chemistry**. 148: 153-159.
- Silva, T. Q., dos Santos, M. B., Santiago, A. A. C., Santana, D. O., Cruz, F. T., Andrade, H. M. C., and Mascarenhas, A. J. S. (2017). Gas phase glycerol oxidative dehydration over bifunctional V/H-zeolite catalysts with different zeolite topologies. **Catalysis Today**. 289: 38-46.
- Su, F., Lu, C., Kuo, S. C., and Zeng, W. (2010). Adsorption of CO<sub>2</sub> on aminefunctionalized Y-type zeolites. **Energy Fuels**. 24: 1441-1448.
- Suntres, Z. E. (2002). Role of antioxidants in paraquat toxicity. **Toxicology**. 180: 65-77.

- Tan, W. C., Yap, S. Y., Matsumoto, A., Othman, R., and Yeoh, F. Y. (2011). Synthesis and characterization of zeolites NaA and NaY from rice husk ash. **Adsorption**. 17: 863-868.
- Teixeira-Neto, Â. A., Marchese, L., and Pastore, H. O. (2009). Vanadium-modified molecular sieves: Preparation, characterization and catalysis. **Quimica Nova**. 32: 463-468.
- Valtchev, V. P., and Bozhilov, K. N. (2004). Transmission Electron Microscopy Study of the Formation of FAU-Type Zeolite at Room Temperature. **The Journal of Physical Chemistry B**. 108: 15587-15598.
- Went, G. T., Oyama, S. T., and Bell, A. T. (1990). Laser Raman spectroscopy of supported vanadium oxide catalysts. **The Journal of Physical Chemistry**. 94: 4240-4246.
- Whittington, B. I., and Anderson, J. R. (1993). Nature and activity of some vanadium catalysts. **The Journal of Physical Chemistry**. 97: 1032-1041.
- WHO. (1984). Paraquat and diquat. **Environment Health Criteria**. 39, Geneva, Switzerland.
- Wittayakun, J., Khemthong, P., and Prayoonpokarach, S. (2008). Synthesis and characterization of zeolite NaY from rice husk silica. **Korean Journal of Chemical Engineering**. 25: 861-864.
- Zainal, Z., Lee, C. Y., Hussein, M. Z., Kassim, A., and Yusof, N. A., (2007). Electrochemical-assisted photodegradation of mixed dye and textile effluents using TiO<sub>2</sub> thin films. **Journal of Hazardous Materials**. 146: 73-80.

## CHAPTER II

### LITERATURE REVIEW

#### 2.1 Adsorption of paraquat

Nakhon Ratchasima, Thailand is one of the largest producers of agricultural products, such as corn, cassava and sugarcane. The major problems are weed and grass. Therefore, herbicides are used in a large amount to solve those problems. The widely used herbicide is 1,1'-dimethyl-4,4'-bipyridinium dichloride, also known as paraquat, due to its low cost and effective performance. The structure of paraquat is shown in Figure 2.1.

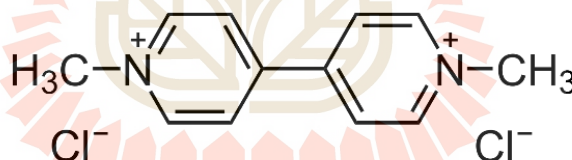


**Figure 2.1** Chemical structure of paraquat.

Paraquat is toxic to human and animals when exposed via ingestion, skin contact, or splash to eyes (Suntres, 2002). Paraquat causes gastrointestinal irritation, abdominal pain, nausea, vomiting and diarrhea when contacted by ingestion. It also causes skin burns and dermatitis from a direct contacts to skin. If splashed to eyes, it causes irritation, burns, corneal damage and scarring of the eyes. High accumulation of paraquat can cause injury to lungs as well as other organs. However, the main



damage occurs in the lungs where paraquat can transform the available oxygen into free radicals, culminating in respiratory failure and death (WHO, 1984; Leite et al., 2013). In the environment, paraquat binds to suspended or precipitated sediment, resulting in persistence in the aquatic environment. The excessive use of paraquat can lead to water pollution. For this reason, removal of paraquat by natural adsorbents is studied in this work.

Paraquat contamination in water can be removed by adsorption with natural adsorbents such as clay minerals (Mithyantha et al., 1975; Rytwo et al., 2002; Seki and Yurdakoç, 2005; Tsai and Lai, 2006; Brigante et al., 2010 and Iglesias et al., 2010), rice husk (Hsu et al., 2009; Rongchapo et al., 2013), and mesoporous silica (Brigante and Schulz, 2011). Rongchapo et al. (2013) compared paraquat adsorption on RHS, MCM-41, NaBEA and NaY. The adsorption capacity depended on the Si/Al ratio and NaY gave the highest capacity. They further studied the adsorption on Al-MCM-41 with various Al ratios and NaX, which had similar structure to NaY but higher Al content (Rongchapo et al., 2015). The adsorption capacity of Al-MCM-41 was higher than that of MCM-41. NaX had lower capacity than NaY. This was because interaction of Na<sup>+</sup> cation in NaX was stronger than that in NaY, making it less exchangeable with paraquat (Rongchapo et al., 2017). However, too much Al was not favorable for the paraquat adsorption. Therefore, NaY with various Si/Al ratios is further investigated for the adsorption of paraquat in this work. Paraquat adsorption capacity was improved by NaY/SBA-15 composite. The interaction of C and N atoms in paraquat molecules with oxygen atom on NaY/SBA-15 was observed (Osakoo et al., 2017).

The adsorption of paraquat varies largely with the nature of the adsorbent. Paraquat adsorbs strongly on clay minerals and somewhat less on activated carbon and humic substances due to its highly polar nature of expanding lattice clay, like montmorillonite (Brigante et al., 2010). Mithyantha et al. (1975) studied the adsorption paraquat using bentonite and montmorillonite. The maximum adsorption capacity of bentonite and montmorillonite were 15.2 and 25.2 mg/g, respectively. The adsorption of paraquat obeys the Freundlich isotherm. Draoui et al. (1999) studied the adsorption of paraquat on kaolinite, illite and montmorillonite. The adsorption isotherm and the thermodynamic parameters were determined. All clays showed H-type isotherm of Giles classification corresponding to a high-affinity adsorption. The adsorption enthalpies varied between -20 and -50 kJ/mol. The adsorption of the paraquat molecule on kaolinite, illite and montmorillonite is governed by electrostatic interactions. Ait Sidhoum et al. (2013) studied the adsorption of paraquat on the Algerian bentonite by using batch experiments in an aqueous solution. The effect of calcination temperature on the adsorption capacity was evaluated. The adsorption isotherm was also investigated. The adsorption data was fitted to the Langmuir isotherm model in order to calculate the maximum adsorption capacities. The adsorption capacity of the calcined samples greatly decreased with heat treatment. The maximum adsorption capacity of bentonite and calcined bentonite were 111 and 100 mg/g, respectively. The analysis of FTIR spectrum of paraquat-adsorbent complex confirmed that the proposed adsorption mechanism might be mainly controlled by cation exchange. Seki and Yurdakoç (2005) used clay minerals including sepiolite, bentonite and illite to prepare organoclays by modification with nonylammonium chloride (9 carbon atoms) and dodecylammonium chloride (12

carbon atoms). The organoclays were used as adsorbents for paraquat and the illite modified with nonylammonium chloride had the highest maximum adsorption capacity (57 mg/g) compared to unmodified illite (54 mg/g) (as shown in Table 2.1). The adsorption capacities of paraquat on dodecylammonium modified illite (24 mg/g) decreased because of low surface area dodecylammonium modified clays. Gu et al. (2015) reported that Na-Mt modified with zwitterionic surfactant (3-(N,N-dimethylhexadecylammonio) propanesulfonate, DHAPS) improve the adsorption capacity because their anionic group on one side interacted strongly with paraquat dication. In contrast, the lower capacity was obtained from CTAB-Mt. This was because there was just partition adsorption between the long carbon chain of CTAB and herbicides due to the similar intermiscibility of the modifier and adsorbate. Guégan et al. (2015) studied the adsorption of paraquat using Mt modified with benzyl decyltrimethyl ammonium (BDTA) cationic surfactant and the triethylene glycol mono n-decyl ether (C<sub>10</sub>E<sub>3</sub>) nonionic surfactant. BDTA-Mt as a cationic organoclay was ineffective for the adsorption of paraquat while C<sub>10</sub>E<sub>3</sub>-Mt nonionic organoclay can adsorb paraquat.

Ibrahim and Jbara (2009) reported that the adsorption of paraquat on a natural zeolitic material such as phillipsite-faujasite stuff was strongly enhanced when the adsorbent was thermally activated and/or modified with monovalent cations such as K<sup>+</sup> and Na<sup>+</sup>. Cation exchange was reported to play a key role on the adsorption process. Shieh et al. (2013) showed that the adsorption of paraquat on amino acid-functionalized SBA-15 strongly depends on the time and pH of the solution, but not on the temperature. The adsorption mechanism was related to  $\pi$ - $\pi$  stacking interactions between the adsorbent and the adsorbate. Brigante and Avena (2014)

studied the adsorption of paraquat on mesoporous silica with a MCM-41 type structure. The adsorption was fast and strongly dependent on pH, increasing as pH decreases. The adsorption mechanism of was related to electrostatic attractions and outer sphere complexes (or ionic pairs) formations between the functional groups of the pesticide and the silica active sites, as deduced from adsorption experiments performed at different ionic strengths and temperatures. The maximum adsorption capacity was 107 mg/g. Rongchapo et al. (2013) compared paraquat adsorption on RHS, MCM-41, NaBEA and NaY. The adsorption capacity depended on the Si/Al ratio and NaY gave the highest capacity. The adsorption mechanism was proposed to be cation exchange. They further studied the adsorption on Al-MCM-41 with various Al ratios and NaX, which had similar structure to NaY but higher Al content. The adsorption capacity of Al-MCM-41 was higher than that of MCM-41. However, NaX had lower capacity than NaY, suggesting that too much Al was not favorable for the paraquat adsorption (Rongchapo et al., 2015).

**Table 2.1** Maximum adsorption capacities of clay, organoclay and zeolites.

Adsorbent	$q_{\max}$ (mg/g)	Reference
Bentonite	42.4	Seki and Yurdakoç, 2005
Organoclays	9.8-57.3	Seki and Yurdakoç, 2005
Phillipsite–faujasite	7.0	Ibrahim and Jbara, 2005
Modified zeolite Y	69.4	Zhang et al., 2006
SBA-15 SiO <sub>2</sub>	55.0	Shieh et al., 2013
Rice husk silica	18.9	Rongchapo et al., 2013
MCM-41	21.3	Rongchapo et al., 2013
NaY	185.2	Rongchapo et al., 2013
NaBEA	122.0	Rongchapo et al., 2013
NaX	120.0	Rongchapo et al., 2015
Al-MCM-41	52.0	Rongchapo et al., 2015
MCM-41 SiO <sub>2</sub>	107.0	Brigante and Avena, 2014
Na-Mt	134	Guégan et al., 2015
BDTA-Mt	-	Guégan et al., 2015
C <sub>10</sub> E <sub>3</sub> -Mt	39	Guégan et al., 2015
Na-Mt	Low	Gu et al., 2015
CTAB-Mt	6.4-6.9	Gu et al., 2015
DHAPS-Mt	70.8-75.5	Gu et al., 2015
SDS-Mt	85.2-90.9	Gu et al., 2015

## 2.2 Background of adsorbents

In this work, the adsorbents for paraquat are zeolite NaY with various Si/Al ratio, montmorillonite clay (MMT), organoclay and pillar clay from MMT modification. Backgrounds of those materials are provided in this part.

### 2.2.1 Zeolite

Zeolites are microporous aluminosilicate materials. Structures of zeolites are crystalline polymers based on arrangement of  $[\text{SiO}_4]$  or  $[\text{AlO}_4^-]$  tetrahedral linked to each other by sharing oxygen atoms to form a framework of cavities and channels. Framework oxygens connecting tetrahedral Si and Al atoms attach with hydroxyl groups and cations. Amount of cationic sites is parallel to the amount of aluminum atoms (Guisnet and Gilson, 2002). Those cations can be ion-exchanged with paraquat.

Zeolite Linde type Y in sodium form (NaY) belongs to the faujasite (FAU) family with a framework containing double 6 rings linked through sodalite cages generating supercages with average pore diameter of 7.4 Å (Figure 1.2). NaY are commonly applied as catalysts and adsorbents for the removal of volatile organic compounds (Baba et al., 2002; Su et al., 2010), adsorption of paraquat (Rongchapo et al., 2013) and fluid cracking catalysts (Cundy and Cox, 2005). Several methods to prepare NaY from rice husk are reported (Wittayakun et al., 2008; Tan et al., 2011; Saceda et al., 2011; Mohamed et al., 2015). In general, NaY can be synthesized in two steps to avoid the formation of other phases, especially zeolite NaP (Petkowicz et al., 2008; Wittayakun et al., 2008).

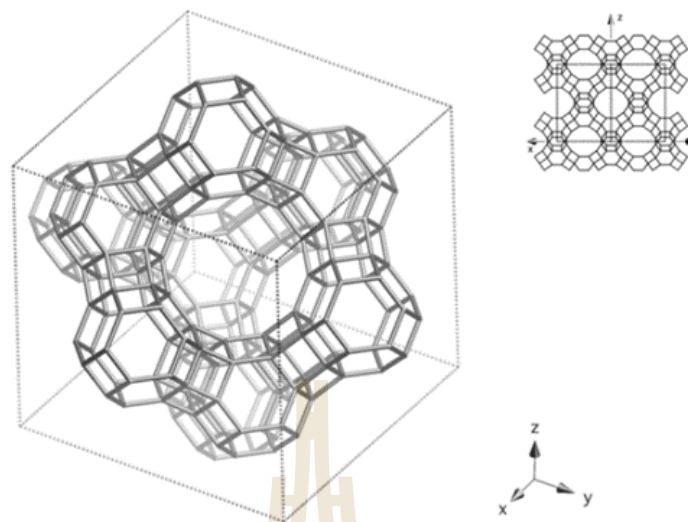


**Figure 2.2** Structure of zeolite NaY (Baerlocher and McCusker, Database of Zeolite

Structures: <http://www.iza-structure.org/databases/>).

### 2.2.2 Clay (Montmorillonite; Mt)

Clay minerals are hydrous aluminum silicates and are generally classified as layered silicates. The layered silicates of clay are generated by a combination of silicon tetrahedral sheet and aluminium octahedral sheets. Such minerals include both natural clays and synthetic clays (Tjong, 2006; Zeng et al., 2005).

The commonly used layered silicates belong to the smectite family with the structure consisting of aluminium octahedral sheet sandwiched in between two silicon tetrahedral sheets as called 2:1 layered silicates (Zeng et al., 2005). The most commonly used 2:1 layered silicates is montmorillonite (Mt). As shown in Figure 2.2, Mt consists of layers made up of two tetrahedrally coordinated silicon atoms fused to an edge-shared octahedral sheet of either aluminum or magnesium

hydroxide. The layer thickness is around 1 nm and the lateral dimensions of these layers may vary from 30 nm to several microns or larger, depending on types of layered silicate (Alexandre and Dubois, 2000). Mt clays are the main components of soils and possess a negative charge that is compensated for by exchangeable cations, on their surfaces, such as  $\text{Na}^+$  and  $\text{Ca}^{2+}$  (Seki and Yurdakoç, 2005). The cation exchange capacity (CEC) and the nature of the compensating cations are important in the interactions of organic compounds with the solid surfaces of clays. Therefore, surface modification of the clay is the main parameter to remove the organic pollutants. Such modified clays are commonly called organoclays.

### 2.2.3 Organoclay

Normally, the modification of clay surface can be done via ion exchange of the inorganic cations, such as  $\text{Na}^+$  or  $\text{Ca}^{2+}$  with those of organic surfactants, for example, organic ammonium cations as shown in Eq. 2.1 (Vansant and Peeter, 1978).



From the Eq. 2.1, NaMMt is montmorillonite with  $\text{Na}^+$  as interlayer cations and R is the alkyl chain of the acidified primary amine surfactant. After modification, the surface of the clay becomes organophilic. Organic surfactants for clay modification include primary, secondary, tertiary and quaternary alkylammonium cations which are water soluble. So, most cation exchange can be carried out in aqueous suspensions.



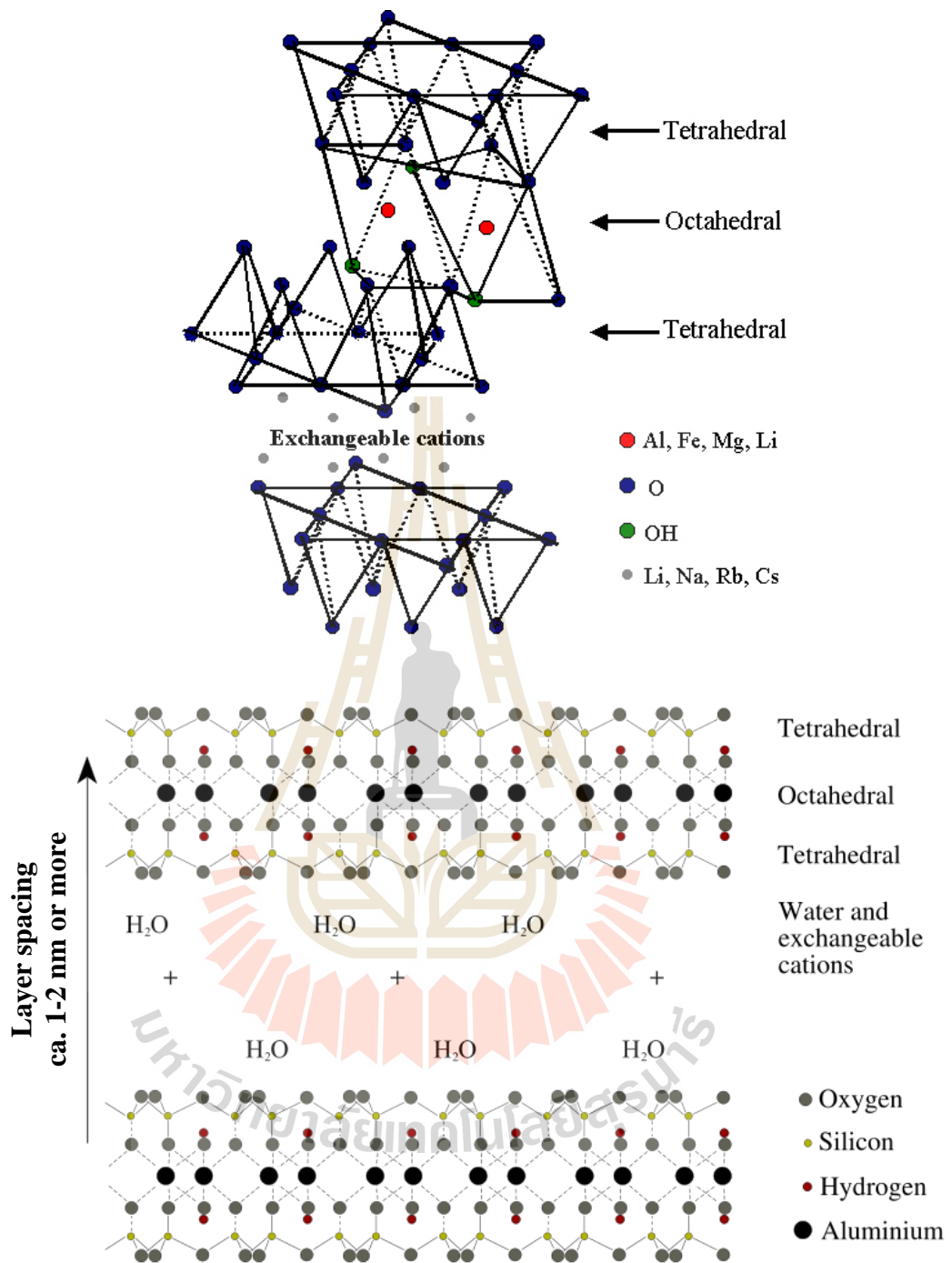


**Figure 2.3** Structure of clay minerals represented by montmorillonite. They are built up from combinations of tetrahedral and octahedral sheets whose basic units are usually Si–O tetrahedron and Al–O octahedron, respectively (Alexandre and Dubois, 2000).

Arroyo et al. (2003) modified MMT clay with octadecylamine (ODA). The result showed that interlayer spacing of modified MMT was higher than that of the unmodified MMT. To confirm the appearance of adsorbed surfactant in clay layer, FTIR was used to investigate the intercalated surfactant. Two peaks at 2918 and 2850  $\text{cm}^{-1}$  attributed to the C-H asymmetric and symmetric stretching vibrations of ODA surfactant, respectively were observed. Magaraphan et al. (2003) modified surface of MMT clay using a primary amine (dodecylamine, tetradecylamine, hexadecylamine, octadecylamine) and quaternary ammonium surfactants (hexadecyltrimethyl ammonium bromide, octadecyltrimethyl ammonium chloride). Octadecylamine-modified clay showed the highest interlayer spacing. The result indicated that the long alkyl chain of amine surfactants played an important role in the expansion of clay layers.

Keawkumay et al. (2012) modified MMT surface using octadecylamine (ODA), a primary amine surfactant with  $\text{C}_{18}$  chain. The ODA-modified MMT had a higher interlayer spacing than the unmodified one because of the intercalation of ODA molecules in the clay layers. The change may make it suitable for adsorption of the paraquat. However, the organic cation with a long carbon chain could affect adsorption capacity of paraquat on organoclay. This was because the organic molecules may hinder the intercalation of the paraquat molecules into the interlayer of clay (Seki and Yurdakoc, 2005). Therefore, TDA which is an aliphatic amine with  $\text{C}_{14}$  chain is selected to modify the MMT in this work.

#### 2.2.4 Mesoporous clay (Pillar clay)

One of the drawbacks of using the clay mineral as adsorbent for organic pollutant is the low surface area. Therefore, the clay mineral can be modified to increase the surface area. Pillar clays (PILC) can provide large surface area and pore volumes, which are beneficial for organic compounds and intermediates to reach and leave the active sites on the surface. The design and synthesis of inorganic porous clay with a controlled pore structure is interesting due to their potential applications as catalysts, supports, selective adsorbents, separating agents, and porous matrixes for encapsulation of specific functional molecules (Li et al., 2009). The PILC can be synthesized using cationic surfactant as gallery templates which formed micelle within the interlayer of clay. After that, silica source (tetraethoxysilicate; TEOS) was incorporated with clay layers by hydrolysis and condensation, followed by calcinations at high temperature. The obtained product formed ordered mesoporous structure (Li et al., 2009). Moreover, titanium-containing mesoporous materials have potential applications as catalysts and adsorbents in various industrial processes (Trong On et al., 2001; Poladi et al., 2002; Jin et al., 2008). The titanium was incorporated in the frame of the interlayer silica pillar structure to obtain products with ordered mesoporous structure and high surface area (Mao et al., 2010; Yang et al., 2013; Sahel et al., 2014). Therefore, the surface area of clay mineral can be increased by generating mesopores by pillaring method.

### 2.3 Background of nanozeolites

The nanosized particles of zeolites have been used in various applications including catalysts, adsorbent, medical materials, and membrane materials, etc (Mintova and Valtchev, 1999; Tosheva and Valtchev, 2005; Ghasemi et al., 2011; Mintova and Ng, 2013). Recently, nanosized zeolites have gained attention due to their special properties, for example, high external surface area and activities, more accessible active sites and shorter diffusion pathways, compared with microsized zeolite crystals (Tosheva and Valtchev, 2005 and Ansari et al., 2014).

Tosheva and Valtchev (2005) reviewed the large number of researchers on synthesis of nanosized zeolites. Various nanosized zeolites were successfully synthesized via a hydrothermal method using clear aluminosilicate solutions with organic templates, such as NaA, FAU Y, FAU X and ZSM-5. Mintova and Valtchev (1999) synthesized the nanocrystalline FAU-type zeolites using the hydrothermal method with tetramethylammonium (TMA) as an organic template. The organic templates were used to reduce the crystal sizes (Schoeman, 1994; Davis, 2002; and Ansari et al., 2014).

Zhan et al. (2002) synthesized various nanocrystallines of FAU X zeolite by developing an organic-template-free approach using silicate source and controlling hydrothermal crystallization conditions. Wang et al. (2003) prepared nanosized crystals of zeolite FAU X and A using thermoreversible polymer hydrogel to control the zeolite growth rate but this polymer was expensive. Aly et al. (2012) synthesized mordenite zeolite without organic template using hydrothermal method. Ansari et al. (2014) synthesized nanosized FAU X using microwave-assisted hydrothermal method. The pure phase of nanosized FAU X zeolite was obtained at the

crystallization temperature of 90°C for 3 h. Awala et al. (2015) successfully synthesized nanosized FAU zeolites using hydrothermal approach with the crystallization at 50°C for 45 h. The nanosized crystallines of FAU zeolites with a mean crystal size 10-15 nm were obtained.

## 2.4 Background of vanadium incorporated zeolites

Vanadium incorporated zeolites have been used as catalysts for the various oxidations of hydrocarbons, for example, oxidation of cyclohexane, benzene, phenol, etc., and also dehydration of glycerol (Maurya et al., 2011; and Siva et al., 2017). Dzwigaj et al. (2000) reported that the V(V); ( $\text{NH}_4\text{VO}_3$ ) and V(IV); ( $\text{VOSO}_4$ ) precursors were incorporated with silanol groups of vacant T-sites of SiBEA zeolite by ion-exchange process. Hagiwara et al. (2003) introduced vanadium into USY zeolite by impregnation method. Cristiano-Torres et al. (2008) prepared the vanadium containing USY zeolite by impregnation method using vanadium naphthenate as a precursor. Pal et al. (2014) studied the vanadium exchanged zeolite by simple ion-exchange on NaY as a heterogeneous catalyst for highly selective and direct one-pot liquid phase oxidation of cyclohexane to cyclohexanone. Silva et al. (2017) reported that the ammonium metavanadate ( $\text{NH}_4\text{VO}_3$ ) precursor was impregnated on zeolite ZSM-5, Beta (BEA), ferrierite (FER), FAU Y, offretite (OFF) and mordenite (MOR) by used as vanadium catalysts for the oxidative dehydration of glycerol to acrylic acid.

A large number of preparation method was one-pot synthesis, preparing by the introduction of the vanadium source i.e.  $\text{V}_2\text{O}_5$ ,  $\text{VOSO}_4$  in the synthesis gel to form vanadosilicate. Vanadium incorporated zeolites prepared by one-pot synthesis are still

the best fulfill the compromise between vanadium concentration and metal dispersion (Teixeira-Neto et al., 2009). Kim et al. (1997) reported the incorporation of vanadium into ZSM-5, MOR and FAU Y zeolites by using one-pot hydrothermal method. The substitution of vanadium into the zeolite framework structure could be applied to the large pore zeolites and the vanadium containing zeolites had selective catalytic properties in various oxidation reactions. Moreover, there are many techniques to determined vanadium species in zeolites such as  $^{51}\text{V}$  nuclear magnetic resonance (NMR), X-ray photoelectron spectroscopy (XPS), diffuse reflectance UV-visible spectroscopy (DR-UV-Vis) and Raman spectroscopy (Centi et al., 1992; Dzwigaj et al., 1998; Teixeira-Neto et al., 2009).

## 2.5 References

- Ait Sidhoum, D., Socias-Viciana, M. M., Urena-Amate, M. D., Derdour, A., Gonzalez-Pradas, E., and Debbagh-Boutarbouch, N. (2013). Removal of paraquat from water by an Algerian bentonite. **Applied Clay Science**. 83-84: 441-448.
- Aly, H. M., Moustafa, M. E., and Abdelrahman, E. A. (2013). Influence of Aluminum Source on the Synthesis of Nanosized ZSM-5 Zeolite. **Der Chemica Sinica**. 4: 68-72.
- Akpan, U. G. and Hameed, B. H. (2009). Parameters affecting the photocatalytic degradation of dyes using  $\text{TiO}_2$ -based photocatalysts: A review. **Journal of Hazardous Materials**. 170: 520-529.

- Alexandre, M. and Dubois, P. (2000). Polymer-layered silicate nanocomposites: preparation, properties and uses of a new class of material. **Material Science and Engineering**. 28: 1-63.
- Ansari, M., Aroujalian, A., Raisi, A., Dabir, B., and Fathizadeh, M. (2014). Preparation and characterization of nano-NaX zeolite by microwave assisted hydrothermal method. **Advanced Powder Technology**. 25: 722-727.
- Arroyo, M., Lopez-Manchado, M. A., and Herrero, B. (2003). Organo-montmorillonite as substitute of carbon black in natural rubber compounds. **Polymer**. 44: 2447-2453.
- Baba, T., Sawada, H., Takahashi, T., and Abe, M. (2002). Chemisorption study of hydrogen and methane by  $^1\text{H}$  MAS NMR and conversion of methane in the presence of ethylene on Ag-Y zeolite. **Applied Catalysis A: General**. 231: 55-63.
- Brigante, M. and Avena, M. (2014). Synthesis, characterization and application of a hexagonal mesoporous silica for pesticide removal from aqueous solution, **Microporous and Mesoporous Materials**. 191: 1-9.
- Brigante, M. and Schulz, P. C. (2011). Adsorption of paraquat on mesoporous silica modified with titania: Effects of pH, ionic strength and temperature. **Journal of Colloid and Interface Science**. 363: 355-361.
- Brigante, M., Zanini, G., and Avena, M. (2010). Effect of humic acids on the adsorption of paraquat by goethite. **Journal of Hazardous Materials**. 184: 241-247.

- Centi, G., Perathoner, S., Trifiro, F., Aboukais, A., Aissi, C. F., and Guelton, M. (1992). Physicochemical characterization of V-silicalite. **Journal of Physical Chemistry**. 96: 2617–2629.
- Cristiano-Torres, D. V., Osorio-Pérez, Y., Palomeque-Forero, L. A., Sandoval-Díaz, L. E., and Trujillo, C. A. (2008). The action of vanadium over Y zeolite in oxidant and dry atmosphere. **Applied Catalysis A: General**. 346: 104–111.
- Davis, M. E. (2002). Ordered porous materials for emerging applications. **Nature**. 417: 813-821.
- Cundy, C. S. and Cox, P. A. (2005). The hydrothermal synthesis of zeolites: Precursors, intermediates and reaction mechanism. **Microporous and Mesoporous Materials**. 82: 71-78.
- Diebold, U. (2003). The surface science of titanium dioxide. **Surface Science Report**. 48: 53-229.
- Draoui, K., Denoye, R., Chgoura, M., and Rouquerol, J. (1999). Adsorption of paraquat on minerals A thermodynamic study. **Journal of Thermal Analysis and Calorimetry**. 58: 597-606.
- Dzwigaj, S., Peltre, M. J., Massiani, P., Davidson, A., Che, M., Sen, T., and Sivasanker, S. (1998). Incorporation of vanadium species in a dealuminated  $\beta$  zeolite. **Chemical Communications**. 1: 87–88.
- Eneji, I. S., Buncel, E., and Vanloon, G. W. (2002). Degradation and sorption of pirimiphos-methyl in two Nigerian soils. **Journal of Agricultural and Food Chemistry**. 50: 5634-5639.



- Ghasemi, Z., Younesi, H., and Kazemian, H. (2011). Synthesis of nanozeolite sodalite from rice husk ash without organic additives. **Canadian Journal of Chemical Engineering**. 89: 601-608.
- Gu, Z., Gao, M., Lu, L., Liu, Y., and Yang, S. (2015). Montmorillonite Functionalized with Zwitterionic Surfactant as a Highly Efficient Adsorbent for Herbicides. **Industrial and Engineering Chemistry Research**. 54: 4947-4955.
- Guégan, R., Giovanela, M., Warmont, F., and Motelica-Heino, M. (2015). Nonionic organoclay: A 'Swiss Army knife' for the adsorption of organic micro-pollutants? **Journal of Colloid and Interface Science**. 437: 71-79.
- Guisnet, M. and Gilson, J. P. (2002). **Zeolites for Cleaner Technologies**. Imperial College Press, London.
- Hagiwara, K., Ebihara, T., Urasato, N., Ozawa, S., and Nakata, S. (2003). Effect of vanadium on USY zeolite destruction in the presence of sodium ions and steam - Studies by solid-state NMR. **Applied Catalysis A: General**. 249: 213-228.
- Hsu, S.-T., Chen, L.-C., Lee, C.-C., Pan, T.-C., You, B.-X., and Yan, Q.-F. (2009). Preparation of methacrylic acid-modified rice husk improved by an experimental design and application for paraquat adsorption. **Journal of Colloid and Interface Science**. 171: 465-470.
- Ibrahim, K. M. and Jbara, H. A. (2009). Removal of paraquat from synthetic wastewater using phillipsite-faujasite tuff from Jordan. **Journal of Hazardous Materials**. 163: 82-86.

- Iglesias, A., López, R., Gondar, D., Antelo, J., Fiol, S., and Arce, F. (2010). Adsorption of paraquat on goethite and humic acid-coated goethite. **Journal of Colloid and Interface Science**. 183: 664-668.
- Jin, C., Li, G., Wang, X., Wang, Y., Zhao, L., and Sun, D. (2008). A titanium containing micro/mesoporous composite and its catalytic performance in oxidative desulfurization. **Microporous and Mesoporous Materials**. 111: 236-242.
- Kaneko, M. and Okura, I. (2002). **Photocatalysis: Science and Technology**. Springer, New York.
- Keawkumay, C., Jarukumjorn, K., Wittayakun, J., and Suppakarn, N. (2012). Influences of surfactant content and type on physical properties of natural rubber/organoclay nanocomposites. **Journal of Polymer Research**. 19: 9917.
- Kim, G.-J., Kim, J.-H., and Shoji, H. (1997). Incorporation of Vanadium into ZSM-5, Mordenite and Y Type Zeolite and Their Catalytic Properties. **Progress in Zeolite and Microporous Materials Studies in Surface Science and Catalysis**. 105: 1101-1108.
- Li, B., Mao, H, Li, X., Ma, W., and Liu, Z. (2009). Synthesis of mesoporous silica-pillar clay by intragallery ammonia-catalyzed hydrolysis of tetraethoxysilane using quaternary ammonium surfactants as gallery templates. **Journal of Colloid and Interface Science**. 336: 244-249.
- Magaraphan, R., Thaijaroen, W., and Lim-ochakun, R. (2003). Structure and properties of natural rubber and modified montmorillonite nanocomposites. **Rubber Chemistry and Technology**. 76: 406-418.

- Mao, H., Li, B., Li, X., Yue, L., Xu, J., Ding, B., Gao, X., and Zhou, Z. (2010). Facile synthesis and catalytic properties of titanium containing silica-pillar clay derivatives with ordered mesoporous structure through a novel intra-gallery templating method. **Microporous and Mesoporous Materials**. 130: 314-321.
- Maurya, M. R., Kumar, A., and Costa Pessoa, J. (2011). Vanadium complexes immobilized on solid supports and their use as catalysts for oxidation and functionalization of alkanes and alkenes. **Coordination Chemistry Reviews**. 255: 2315-2344.
- Mintova, S. and Ng, E. P. (2013). Zeolite Nanoparticles. **Comprehensive Inorganic Chemistry II (Second Edition): From Elements to Applications**. 5: 285-302.
- Mintova, S. and Valtchev, V. (1999). Synthesis of nanosized FAU-type zeolite. **Studies in Surface Science and Catalysis**. 125: 141-148.
- Mithyantha, M. S., Rao, K. B., Biddappa, C. C., Lillaram, N. T., and Perur, N. G. (1975). Paraquat adsorption on clay minerals. **Bulletin of the Indian National Science Academy**. 50: 293-298.
- Mohamed, R. M., Mkhallid, I. A., and Barakat, M. A. (2015). Rice husk ash as a renewable source for the production of zeolite NaY and its characterization. **Arabian Journal of Chemistry**. 8: 48-53.
- Osakoo, N., Pansakdanon, C., Sosa, N., Deekamwong, K., Keawkumay, C., Rongchapo, W., Prayoonpokarach, S., and Wittayakun, J. (2017). Characterization and comprehension of zeolite NaY/mesoporous SBA-15 composite as adsorbent for paraquat. **Materials Chemistry and Physics**. 193: 470-476.

- Patakioutas, G. and Albanis, T. A. (2002). Adsorption–desorption studies of alachlor, metolachlor, EPTC, chlorothalonil and pirimiphos-methyl in contrasting soils. **Pest Management Science**. 58: 352-362.
- Pal, N., Pramanik, M., Bhaumik, A., and Ali, M. (2014). Highly selective and direct oxidation of cyclohexane to cyclohexanone over vanadium exchanged NaY at room temperature under solvent-free conditions. **Journal of Molecular Catalysis A: Chemical**. 392: 299-307.
- Petkowicz, D. I., Rigo, R. T., Radtke, C., Pergher, S. B., and Santos, J. H. Z. (2008). Zeolite NaA from Brazilian chrysotile and rice husk. **Microporous and Mesoporous Materials**. 116: 548-554.
- Poladi, R. H. P. R. and Landry, C. C. (2002). Oxidation of octane and cyclohexane using a new porous substrate, Ti-MMM-1. **Microporous and Mesoporous Materials**. 52: 11-18.
- Rongchapo, W., Deekamwong, K., Loiha S., Prayoonpokarach, S., and Wittayakun, J. (2015). Paraquat adsorption on NaX and Al-MCM-41. **Water Science and Technology**. 71: 1347-1353.
- Rongchapo, W., Sophiphun, O., Rintramee, K., Prayoonpokarach, S., and Wittayakun, J. (2013). Paraquat adsorption on porous materials synthesized from rice husk silica. **Water Science and Technology**. 68.4: 863-869.
- Rongchapo, W., Keawkumay, C., Osakoo, N., Deekamwong, K., Chanlek, N., Prayoonpokarach, S., and Wittayakun, J. (2017). Comprehension of paraquat adsorption on faujasite zeolite X and Y in sodium form. **Adsorption Science & Technology**. 1-10.

- Rouquerol, F., Rouquerol, J., and Sing, K. (1999). Adsorption by powders and porous solids: principles, methodology and applications. Academic Press, London, pp. 18-212.
- Rytwo, G., Tropp, D., and Serban, C. (2002). Adsorption of diquat, paraquat and methyl green on sepiolite: experimental results and model calculations. **Applied Clay Science**. 20: 273-282.
- Saceda, J. J. F., de Leon, R. L., Rintramee, K., Prayoonpokarach, S., and Wittayakun, J. (2011). Properties of silica from rice husk and rice husk ash and their utilization for zeolite Y synthesis. **Química Nova**. 34: 1394-1397.
- Sahel, K. Bouhent, M., Belkhadem, F., Ferchichi, M., Dappozze, F., Guillard, C., and Figueras, F. (2013). Photocatalytic degradation of anionic and cationic dyes over TiO<sub>2</sub> P25, and Ti-pillar clays and Ag-doped Ti-pillar clays. **Applied Clay Science**. 95: 205-210.
- Sahoo, C., Gupta, A. K., and Pal, A. (2005). Photocatalytic degradation of Methyl Red dye in aqueous solutions under UV irradiation using Ag<sup>+</sup> doped TiO<sub>2</sub>. **Desalination**. 181: 91-100.
- Schoeman, B. J., Sterte, J., and Otterstedt, J. E. (1994). Colloidal zeolite suspensions. **Zeolites**. 14: 110-116.
- Seki, Y. and Yurdakoç, K. (2005). Paraquat adsorption onto clays and organoclays from aqueous solution. **Journal of Colloid and Interface Science**. 287: 1-5.
- Silva, T. Q., dos Santos, M. B., Santiago, A. A. C., Santana, D. O., Cruz, F. T., Andrade, H. M. C., and Mascarenhas, A. J. S. (2017). Gas phase glycerol oxidative dehydration over bifunctional V/H-zeolite catalysts with different zeolite topologies. **Catalysis Today**, 289: 38-46.

- Singh, N. (2009). Adsorption of herbicides on coal fly ash from aqueous solutions. **Journal of Hazardous Materials**. 168: 233-237.
- Sobczyński, A., and Dobosz, A. (2001). Water purification by photocatalysis on semiconductors. **Polish Journal of Environmental Studies**. 10: 195-205.
- Su, F., Lu, C., Kuo, S. C., and Zeng, W. (2010). Adsorption of CO<sub>2</sub> on aminefunctionalized Y-type zeolites. **Energy Fuels**. 24: 1441-1448.
- Tan, W. C., Yap, S. Y., Matsumoto, A., Othman, R., and Yeoh, F. Y. (2011). Synthesis and characterization of zeolites NaA and NaY from rice husk ash. **Adsorption**. 17: 863-868.
- Teixeira-Neto, Â. A., Marchese, L., and Pastore, H. O. (2009). Vanadium-modified molecular sieves: Preparation, characterization and catalysis. **Química Nova**. 32: 463-468.
- Tjong, S. C. (2006). Structural and mechanical properties of polymer nanocomposites. **Materials Science and Engineering**. 53: 73-197.
- Tosheva, L. and Valtchev, V. P. (2005). Nanozeolites: Synthesis, crystallization mechanism, and applications. **Chemistry of Materials**. 17: 2494-2513.
- Trong On, D., Lutic, D., and Kaliaguine, S. (2001). An example of mesostructured zeolitic material: UL-TS-1. **Microporous and Mesoporous Materials**. 44-45: 435-444.
- Tsai, W.-T. and Lai, C.-W. (2006). Adsorption of herbicide paraquat by clay mineral regenerated from spent bleaching earth. **Journal of Hazardous Materials**. B134: 144-148.
- Vansant, E. F. and Peeters, G. (1978). The exchange of alkylammonium ions on Na-laponite. **Clays and Clay Minerals**. 26: 279-284.

- Wang, H., Holmberg, B. A., and Yan, Y. (2003). Synthesis of template-free zeolite nanocrystals by using in situ thermoreversible polymer hydrogels. **Journal of the American Chemical Society**. 125: 9928-9929.
- Wittayakun, J., Khemthong, P., and Prayoonpokarach, S. (2008). Synthesis and characterization of zeolite NaY from rice husk silica. **Korean Journal of Chemical Engineering**. 25: 861-864.
- Zeng, Q. H., Yu, A. B., Lu, G. Q., and Paul, D. R. (2005). Clay-based polymer nanocomposites: research and commercial development. **Journal of Nanoscience and Nanotechnology**. 5: 1574-1592.
- Zhan, B.-Z., White, M. A., Lumsden, M., Mueller-Neuhaus, J., Robertson, K. N., Cameron, T. S., and Gharghour, M. (2002). Control of Particle Size and Surface Properties of Crystals of NaX Zeolite. **Chemistry of Materials**. 14: 3636-3642.
- Zhang, H., Kim, Y., and Dutta, P.K. (2006) Controlled release of paraquat from surface-modified zeolite Y. **Microporous and Mesoporous Materials**. 88: 312-318.

# CHAPTER III

## ADSORPTION OF PARAQUAT BY

### MONTMORILLONITE MODIFIED WITH

### TETRADECYLAMMONIUM CHLORIDE AND

### INTRAGALLERY TEMPLATING METHOD

#### Abstract

Adsorption of paraquat in water is performed on four adsorbents including montmorillonite (Mt), organoclay (TDA-Mt) from intercalation of Mt with tetradecylammonium chloride, and mesoporous Mt from intragallery templating method (with and without Ti addition). The adsorbents are characterized by X-ray diffraction, N<sub>2</sub> adsorption-desorption and transmission electron microscopy. Paraquat adsorption isotherms follow Langmuir model and the adsorption capacity is as follows: TDA-Mt > Mt > mesoporous Ti-Mt > mesoporous Mt. The adsorption mechanism on TDA-Mt and Mt might be via ion exchange. The adsorption on mesoporous samples is on the external surface with negative charge. The presence of Ti enhances the adsorption capacity.



### 3.1 Introduction

Herbicides and insecticides are used widely in agricultural activities. Despite the main advantage to increase the product yield, they are considered to be water pollutants when they leach from soil. A herbicide which is widely used in Thailand is paraquat. It is toxic and persistent in the environment (WHO, 1984). Paraquat in water can be removed by adsorption with natural adsorbents such as clay minerals (Mithyantha et al., 1975; Rytwo et al., 2002; Seki and Yurdakoç, 2005).

Clay minerals are hydrous aluminum phyllosilicates which consist of layers made up of silicon in tetrahedral coordination and aluminum, magnesium or iron in octahedral coordination. Montmorillonite (Mt) is a member of the smectite family, a 2:1 layer (two tetrahedral and one octahedral sheet) with cationic substitution. Negative charges are generated by substitution of Si by Al in the tetrahedral sheet and the replacement of Al by Mg, Fe, Li or other small atoms in the octahedral sheet (Rouquerol et al., 1999). The charge distribution and internal surface area may make Mt a suitable adsorbent for cationic herbicides. There are several factors affecting the adsorption ability, for example, surface area, porosity, types of exchangeable cation, interlayer spacing and the presence of water molecules between the layers (Ganigar et al., 2010; Paul et al., 2010).

The adsorption ability of the clay mineral can be improved by intercalation with cationic surfactant via ion exchange. The produced materials are known as organoclays (Seki and Yurdakoç, 2005). For example, Churchman (2002) modified bentonite by using a quaternary ammonium cation to improve toluene removal. Seki and Yurdakoç (2005) modified bentonite (B), also in a smectite family by nonylammonium chloride (NA, with C9 chain) and dodecylammonium chloride

(DCA, with C12 chain). The modification by both ammonium salts increased the clay interlayer spacing and changed the paraquat adsorption capacity. The adsorption increased on Na-bentonite but decreased in DCA-bentonite. The adsorption ability is related to the exchange ability of ammonium cation with the clay interlayer cation. In addition, the paraquat interaction to the organoclays depended on the thickness of the organic layer and size of paraquat molecules (Seki and Yurdakoç, 2005).

Keawkumay et al. (2012) reported an intercalation of Mt by octadecylammonium chloride. The modification increased the interlayer spacing (1.38 nm of Mt to 1.62 nm of ODA-Mt) and the obtained material is suitable as a filler of rubber nanocomposite. Such sample may work as an adsorbent for paraquat but the long carbon chain could lower the adsorption capacity (Seki and Yurdakoç, 2005). Therefore, tetradecylammonium chloride (TDA) which has a shorter carbon chain is selected instead for the Mt modification in this work.

Another way to modify the clay is intra-gallery templating method that surfactant molecules can form micelles in the clay interlayer and pillars are created around the micelle by an addition of silicates. The surfactant molecules can be removed by calcination and mesopores are generated. An example of the intra-gallery templating method is the modification of Mt using CTAB with and without an addition of Ti (Mao et al., 2010). Their method is employed in this work and the obtained mesoporous materials are used as adsorbents.

The objectives of this work are to prepare and characterize adsorbents from Mt including organoclay (TDA-Mt) and mesoporous materials from Mt and use as adsorbents for paraquat. In this study, the new organoclay TDA-Mt is prepared from

modification of Mt with tetradecylammonium chloride. Thus, it is the first time that TDA-Mt and mesoporous Mt and Ti-Mt are used as adsorbents for paraquat.

## 3.2 Experiment

### 3.2.1 Materials

Calcium montmorillonite clay ( $\text{Ca}^{2+}$ -MMT) with cation exchange capacity (CEC) value of 80 meq/100g is supplied by Thai Nippon Co., Ltd. Tetradecylamine (TDA:  $\text{CH}_3(\text{CH}_2)_{13}\text{NH}_2$ ) is purchased from Acros. Cetyltrimethylammonium bromide (CTAB:  $(\text{CH}_3)_3(\text{CH}_2)_{16}\text{NH}_2$ ) is purchased from Unilab. Tetraethoxy silane (TEOS:  $\text{Si}(\text{OC}_2\text{H}_5)_4$ ) and tetrabutyl titanate ( $\text{Ti}(\text{OBU})_4$ ) are purchased from Fluka and Aldrich, respectively. Chemical structures of these surfactants are shown in Figure 3.1.

### 3.2.2 Preparation of organoclays

Mt with cation exchange capacity (CEC) of 80 meq/100g had the contents by weight percent in oxide form on the product label are as follows:  $\text{Al}_2\text{O}_3$ , 6.59;  $\text{SiO}_2$ , 68.24;  $\text{CaO}$ , 3.39;  $\text{K}_2\text{O}$ , 3.36;  $\text{Fe}_2\text{O}_3$ , 11.52; and  $\text{TiO}_2$ , 2.40. Mt is modified by tetradecylammonium chloride with a method adapted from Keawkumay et al. (2012). The content of TDA is equivalent to the CEC. 10 g of Mt is dispersed in 200 mL hot deionized water (70 °C) with a continuous stirring. Tetradecylamine 1.71 g in 100 mL hot deionized water is protonated by concentrate hydrochloric acid 1 mL and added to the clay-water dispersion. Then, the mixture is stirred vigorously for 2 h, filtered, washed repeatedly with hot deionized water, vacuum-filtered, dried at 90 °C. The obtained organoclay is notated TDA-Mt.

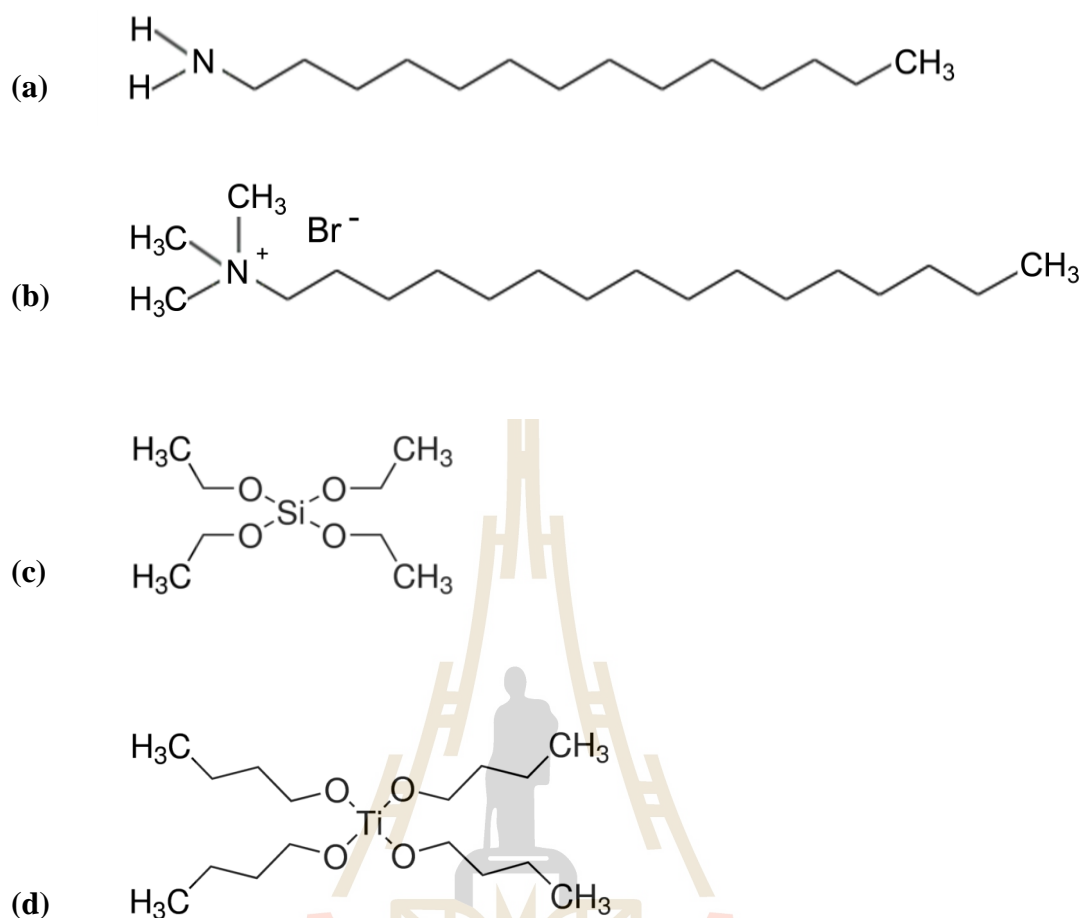


**Figure 3.1** Chemical structures of (a) Tetradecylamine (TDA), (b) Cetyltrimethylammonium bromide (CTAB), (c) Tetraethoxy silane (TEOS) and (d) Tetrabutyl titanate.

### 3.2.3 Preparation of mesoporous-Mt and mesoporous-Ti-Mt

Mesoporous-Ti-Mt is synthesized by intra-gallery templating method (Mao et al., 2010). 10 g of Mt is dispersed in 30 mL of DI water and stirred for 10 min. 10.23 g of CTAB is dissolved in 65 mL of ethanol, added with a mixture from 63 mL of tetraethoxy silane and 4.8 mL of tetrabutyl titanate and stirred for 30 min to produce a clear solution. The solution is dropped slowly to the clay dispersion and

stirred at room temperature for 1 h. The pH of the obtained gel is adjusted to 10 by an ammonia solution. The mixture is stirred for 2 h, filtered, dried at 90 °C and calcined at 600 °C for 6 h with heating rate of 2 °C/min. This sample is referred to as mesoporous-Ti-Mt. In addition, mesoporous-Mt without the addition of Ti(OBu)<sub>4</sub> is synthesized with the same procedure.

### **3.3 Material characterization**

#### **3.3.1 Phase composition**

The phase composition of all samples is characterized by X-ray diffractometer (XRD, Bruker D8 ADVANCE) with a Cu K<sub>α</sub> radiation ( $\lambda = 1.5418 \text{ \AA}$ ) operated at a voltage of 40 kV. The XRD patterns are recorded with a step size of 0.02 and a scan speed of 0.2 °/min. The interlayer spacing of Mt is calculated from the XRD peak position using Bragg's law.

#### **3.3.2 N<sub>2</sub> adsorption-desorption isotherms**

N<sub>2</sub> adsorption-desorption isotherms of the adsorbents are obtained from a Micromeritics ASAP 2010 instrument. The samples are degassed at 300 °C for 8 h before the measurement. An exception is on TDA-Mt which is degassed at 150 °C to preserve the organic composition. The specific surface areas (SBET) are calculated using the Brunauer–Emmett–Teller (BET) equation. The pore size distribution of mesoporous-Mt and mesoporous-Ti-Mt is calculated using the Barrett-Joyner-Halenda (BJH) method.

### 3.3.3 Morphology

The pore structure of clay, organoclay and pillar clay samples is determined by transmission electron microscopy (TEM) on a Tecnai G<sup>2</sup> with an accelerating voltage of 200 kV. The samples are prepared by ultrasonic dispersion, using absolute alcohol as a solvent and micro grit as a support membrane.

### 3.3.4 Functional groups

Functional groups of all adsorbents before and after adsorption of 500 ppm paraquat are identified by a Fourier transform infrared spectrometer (FTIR) (Perkin Elmer Spectrum GX) using KBr pellet technique. The spectrum is recorded in the 4000-400 cm<sup>-1</sup> region with 2 cm<sup>-1</sup> resolution.

## 3.4 Adsorption study

A commercial paraquat solution (27.6% w/v) is purchased from a local store and used for a preparation of a stock solution. Its concentration is spectrometrically determined using an external standard method. The adsorption kinetics is performed by adding 0.100 g of the adsorbent to a polypropylene (PP) bottle containing 20 mL of paraquat solution with the concentration of 500 ppm. The mixture is agitated by using a magnetic stirrer at the speed of 400 rpm for various times. Then 10 mL of the samples in each bottle is collected and immediately filtered using a 0.45 µm syringe filter. The amount of remaining paraquat in the solution is determined using a UV-Vis spectrophotometer (Varian CARY 300) at a wavelength corresponding to the maximum absorbance,  $\lambda_{\text{max}}$  at 257 nm. The kinetic models (pseudo-first-order, pseudo-second-order) are used to determine the adsorption kinetic mechanisms.

The pseudo-first-order model explains adsorption in solid-liquid systems based on the adsorption capacity of solid (Hameed, 2007; Boparai et al., 2011; Fatimah and Huda, 2013). The pseudo-first-order model is described by Eq. 1:

$$\log (q_e - q_t) = \log q_e - \frac{k}{2.303} t \quad (1)$$

where  $k$  is the pseudo-first-order rate constant (1/min),  $q_t$  is the amount of paraquat adsorbed at time  $t$  (mg/g). From the plot of  $\log (q_e - q_t)$  versus  $t$ ,  $k$  and  $q_e$  can be directly obtained from the slope and intercept, respectively.

The pseudo-second-order rate expression, Eq. 2, is applied in the analysis of chemisorption from aqueous solutions (Tsai et al., 2005; Boparai et al., 2011):

$$\frac{t}{q_t} = \frac{1}{k q_e^2} + \frac{t}{q_e} \quad (2)$$

where  $k$  is the pseudo-second-order rate constant (g/mg min),  $q_t$  is the amount of paraquat adsorbed at time  $t$  (mg/g). From the plot of  $(t/q_t)$  versus  $t$ ,  $k$  and  $q_e$  are obtained from the intercept and slope, respectively.

### 3.4.1 Adsorption isotherms

Adsorption isotherms are obtained by using 0.100 g of adsorbent and paraquat concentration ranging from 100 to 1000 ppm. The paraquat solution (20 mL) is added into a 100 mL polypropylene bottle containing the adsorbent at room temperature, stirred for 1 h and filtered through a 0.45  $\mu\text{m}$  syringe filter. The amount of remaining paraquat in the solution is determined using a UV-Vis spectrophotometer at a wavelength corresponding to the maximum absorbance,  $\lambda_{\text{max}}$  at

257 nm. The adsorption data is analyzed according to linear form of Langmuir and Freundlich isotherms.

Langmuir and Freundlich models are commonly applied to explain the adsorption behavior. The Langmuir isotherm assumes that the adsorbate forms monolayer on the adsorbent and the maximum adsorption could be determined by the equation (Thomas and Crittenden, 1998; Singh, 2009; Tan and Xiao, 2009; Boparai et al., 2011) given as:

$$\frac{C_e}{q_e} = \frac{1}{K_L q_m} + \frac{C_e}{q_m} \quad (3)$$

where  $K_L$  is the Langmuir constant related to the affinity of binding site (L/mg) and  $q_m$  is the maximum adsorption capacity (mg/g). Both  $K_L$  and  $q_m$  can be determined from the linear plot of  $C_e/q_e$  versus  $C_e$ .

### 3.4.2 Effect of pH for paraquat adsorption on Mt samples

The effect of pH is performed by adding 0.10 g of the adsorbents to a PP bottle containing 20 mL of 500 mg/g of paraquat solution with various pH (1.5, 3.5, 5.5 (as-prepared), 7.5, 9.5). The mixture is agitated by using a magnetic stirrer at the speed of 400 rpm for 60 min before sampling and analysis by UV-Vis spectrophotometer.



## 3.5 Results and discussion

### 3.5.1 Structures of clay and organoclays

XRD spectroscopy is a common technique used in investigating surfactant intercalation and expansion of Mt. As Mt interlayer spacing can expand or contract, the peak position in the XRD spectrum of Mt shifts proportionally. Then, the interlayer spacing of Mt can be calculated from the XRD peak position using Bragg's law:

$$d = \lambda / (2 \sin\theta) \quad (3.1)$$

where  $d$  is the interlayer spacing of clay,  $\lambda$  is the X-ray wavelength of  $\text{CuK}_\alpha$  equal to 1.5418 Å, and  $\theta$  is the incident angle of X-ray.

**Table 3.1** 2 Theta ( $2\theta$ ) and interlayer spacing of Mt and modified Mt.

Clay sample	2 Theta (degree)	Interlayer spacing (nm)
Mt	5.74	1.54
TDA-Mt	2.74, 5.18	3.22, 1.70
Mesoporous-Mt	1.30	6.79
Mesoporous-Ti-Mt	2.28	3.87

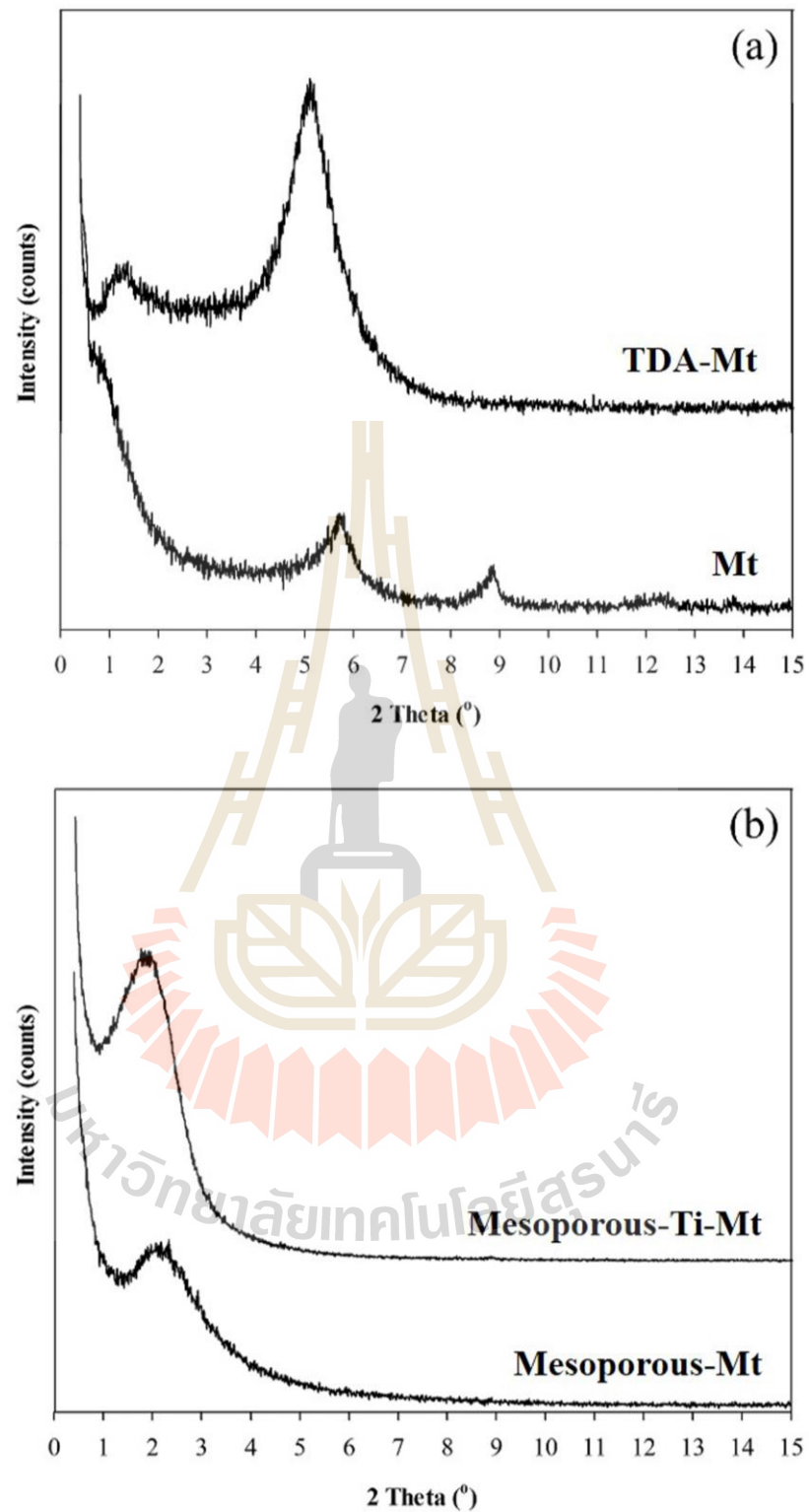


**Figure 3.2** XRD pattern of (a) Mt and TDA-Mt, and (b) mesoporous Mt and Mesoporous Ti-Mt.

XRD patterns of Mt and TDA-Mt are shown in Figure 3.2a and those of mesoporous Mt and Ti-Mt shown in Figure 3.2b. The XRD peaks of Mt occurred at  $5.7^\circ$  and  $8.9^\circ$ . The first peak corresponded to the plane 001 and the interlayer spacing of 1.54 nm as shown in Table 3.1. The major XRD peak of TDA-Mt at  $5.2^\circ$  corresponds to an interlayer spacing of 1.73 nm. The increase spacing from that of Mt corresponds to intercalation of TDA into the interlayers (de Paiva et al., 2008). The change depended on the chain length of surfactant. For example, the larger increase from 1.22 nm of Na-Mt to 3.92 and 2.14 nm of Mt functionalized with a zwitterionic surfactant (3-(N,N-dimethylhexadecylammonio)propanesulfonate, DHAPS) (Gu et al., 2015). The expansion from 0.97 nm of untreated Na-Mt to 1.40 nm in an organoclay from Na-Mt and benzyl decyltrimethyl ammonium is also reported (Guégan et al., 2015). An increase of interlayer spacing is also reported on bentonite modified with nonylammonium chloride and dodecyl-ammonium chloride (Seki and Yurdakoç, 2005).

The XRD patterns of mesoporous Mt and mesoporous Ti-Mt show a broad peak corresponding to a plane (001) in an ordered lamellar clay material (Mao et al., 2010; Yang et al., 2013). The peak from mesoporous Ti-Mt has a higher intensity than that from mesoporous Mt suggesting a more uniform structure. Both samples do not show peaks corresponding to hexagonal mesoporous silica (Brigante and Avena, 2014).

### 3.5.2 N<sub>2</sub> adsorption-desorption isotherms

N<sub>2</sub> adsorption-desorption isotherms of Mt and TDA-Mt are shown in Figure 3.3a. The adsorption isotherm (filled symbols) of Mt and TDA-Mt are type II according to the IUPAC classification (Sing, 1982). The samples are non-porous or

macroporous. The adsorbed volume to form monolayer is low and the multilayer adsorption began afterward. TDA-Mt has a lower adsorbed volume than Mt (Table 3.2) due to the presence of the surfactant within the interlayer. The decrease of surface area is also reported when Na-Mt contained a zwitterionic surfactant (Gu et al., 2015). The desorption isotherm (empty symbols) of Mt does not overlap with the adsorption forming a H3 hysteresis loop in the  $P/P_0$  range 0.45-1.0. The H3 loop is a characteristic of aggregates of plate-like particles possessing non-rigid slit-shaped pores (Sing, 1982; Rouquerol et al., 1999). The term “pseudo type II” or “type IIb” are also used to classify the isotherm of natural montmorillonite (Rouquerol et al., 1999). Similar hysteresis loops are reported by Gu et al., 2015.

The isotherm of mesoporous Mt and mesoporous Ti-Mt are shown in Figure 3.3b. Both samples had type IV adsorption isotherm according to the IUPAC classification with a hysteresis loop type H3 (Sing, 1982; Rouquerol et al., 1999). The adsorbed volume from mesoporous Ti-Mt is higher than that without Ti indicating a larger surface area (Table 3.2).

**Table 3.2** Surface area, total pore volume and average pore diameter of Mt samples.

Adsorbent	Surface area ( $S_{BET}$ ) ( $m^2 g^{-1}$ )	Total pore volume ( $cm^3 g^{-1}$ )	Average pore diameter (nm)
Mt	49	0.1078	8.72
TDA-Mt	26	0.1355	20.77
mesoporous Mt	379	0.2846	3.00
mesoporous Ti-Mt	716	0.5871	3.28

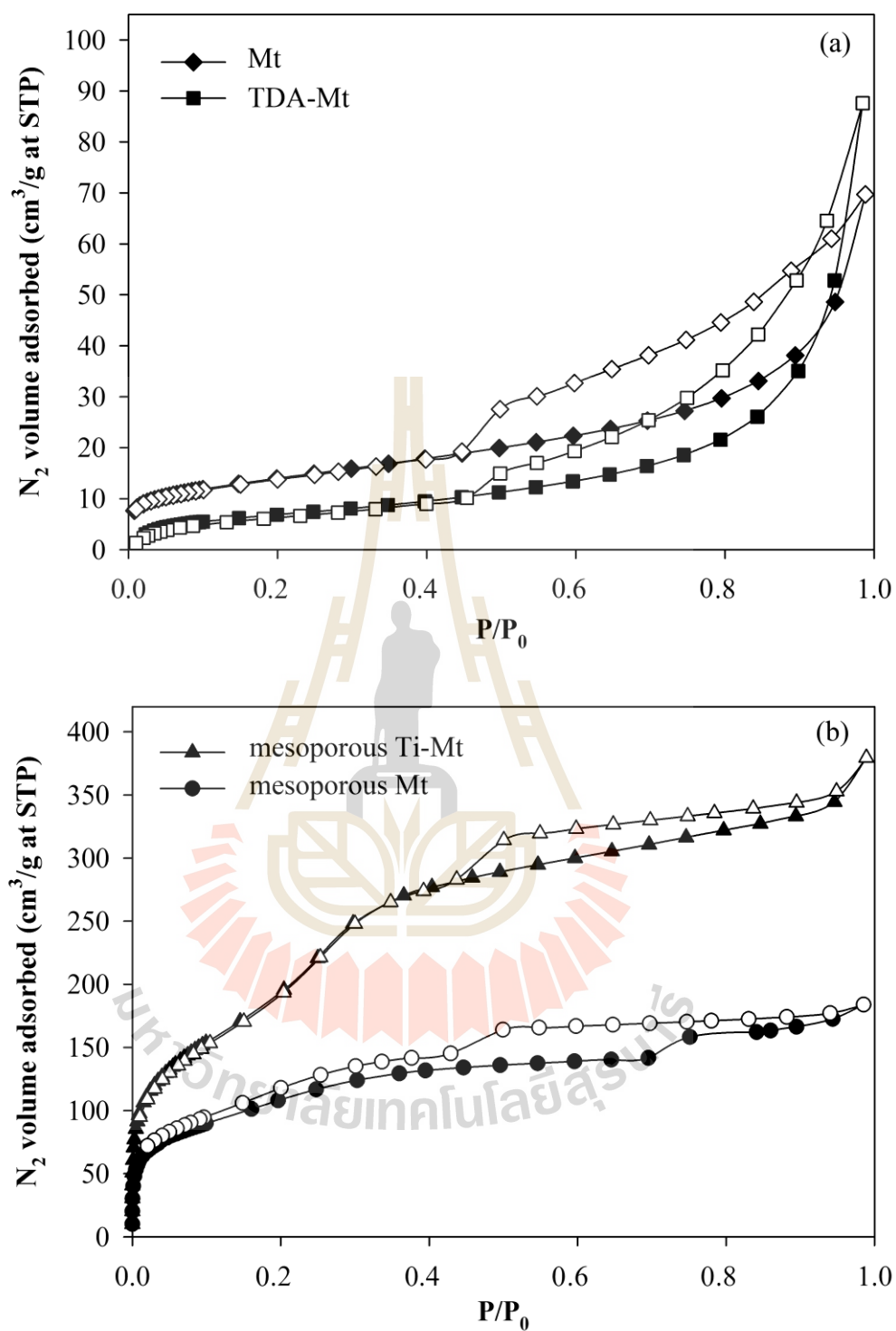


**Figure 3.3**  $N_2$  adsorption-desorption isotherms of (a) Mt and TDA-Mt, and (b) mesoporous Mt and Mesoporous Ti-Mt.

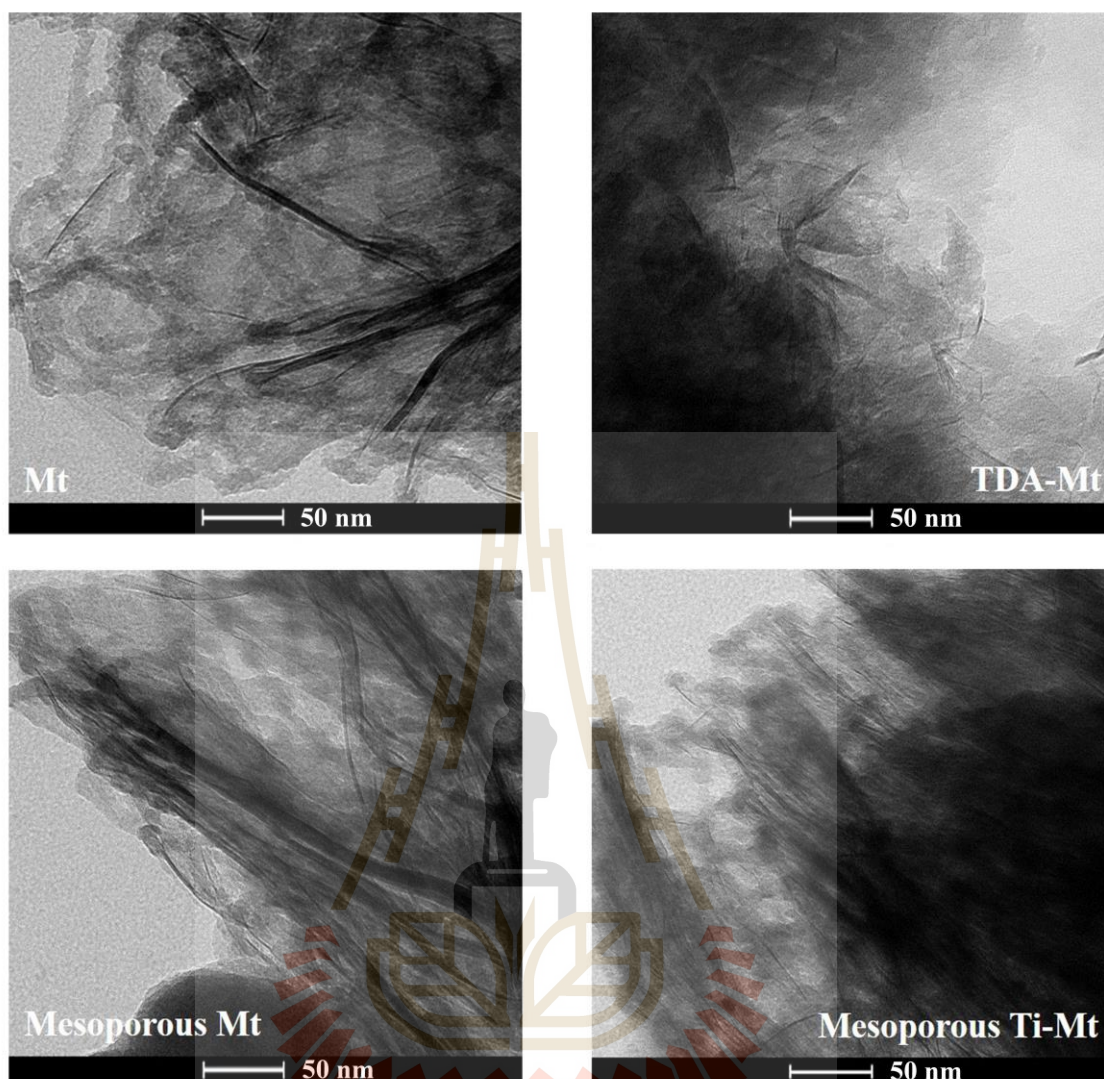


**Figure 3.4** Morphology of Mt, TDA-Mt, mesoporous Mt and mesoporous Ti-Mt.

### 3.5.3 Morphologies

The morphologies of the Mt and modified Mt samples from TEM are shown in Figure 3.4. Mt showed aggregation of several layers with varied sizes and orientations. TDA-Mt exhibits the intercalation of TDA into the clay layers and the particles may be exfoliated. In the images of mesoporous Mt and mesoporous Ti-Mt, the clay layers are discernible as solid dark lines. The pores appear in lighter contrast

between the layers which consists of uniform layered structure. Furthermore, the uniform gallery pores are observed between the dark layers (Mao et al., 2009; Gao et al., 2012; Yang et al., 2013; Mao et al., 2014; Mao et al., 2015).

#### 3.5.4 Functional groups

FTIR is used to identify functional groups of Mt and modified Mt. Figure 3.5 showed FTIR spectra of Mt, TDA-Mt, mesoporous Mt and Mesoporous Ti-Mt and the assignments are showed in Table 3.3. The spectrum of Mt, mesoporous Mt and Mesoporous Ti-Mt show a broad band between 3644-3324  $\text{cm}^{-1}$  corresponding to the OH stretching vibration of water, and a band at 1638  $\text{cm}^{-1}$  corresponding to the OH bending vibration of the interlayer water of the Mt. In addition, a sharp band corresponding to the Si-O stretching vibration of the layered silicate is observed at 1038  $\text{cm}^{-1}$ . Furthermore, the Si-O and Al-O bending vibration bands are observed at 600-400  $\text{cm}^{-1}$ .

FTIR spectrum of TDA-Mt showed four additional peaks compared with that of Mt. Bands around 2920  $\text{cm}^{-1}$  and 2850  $\text{cm}^{-1}$  attributed to the C-H asymmetric and C-H symmetric, stretching vibration of alkyl chains, respectively. Bands around 1470  $\text{cm}^{-1}$  and 1380  $\text{cm}^{-1}$  corresponded to the C-H asymmetric and symmetric bending vibration of alkyl chains, respectively. These results indicate that the surfactants may intercalate into Mt galleries or adsorb on the surface of Mt.

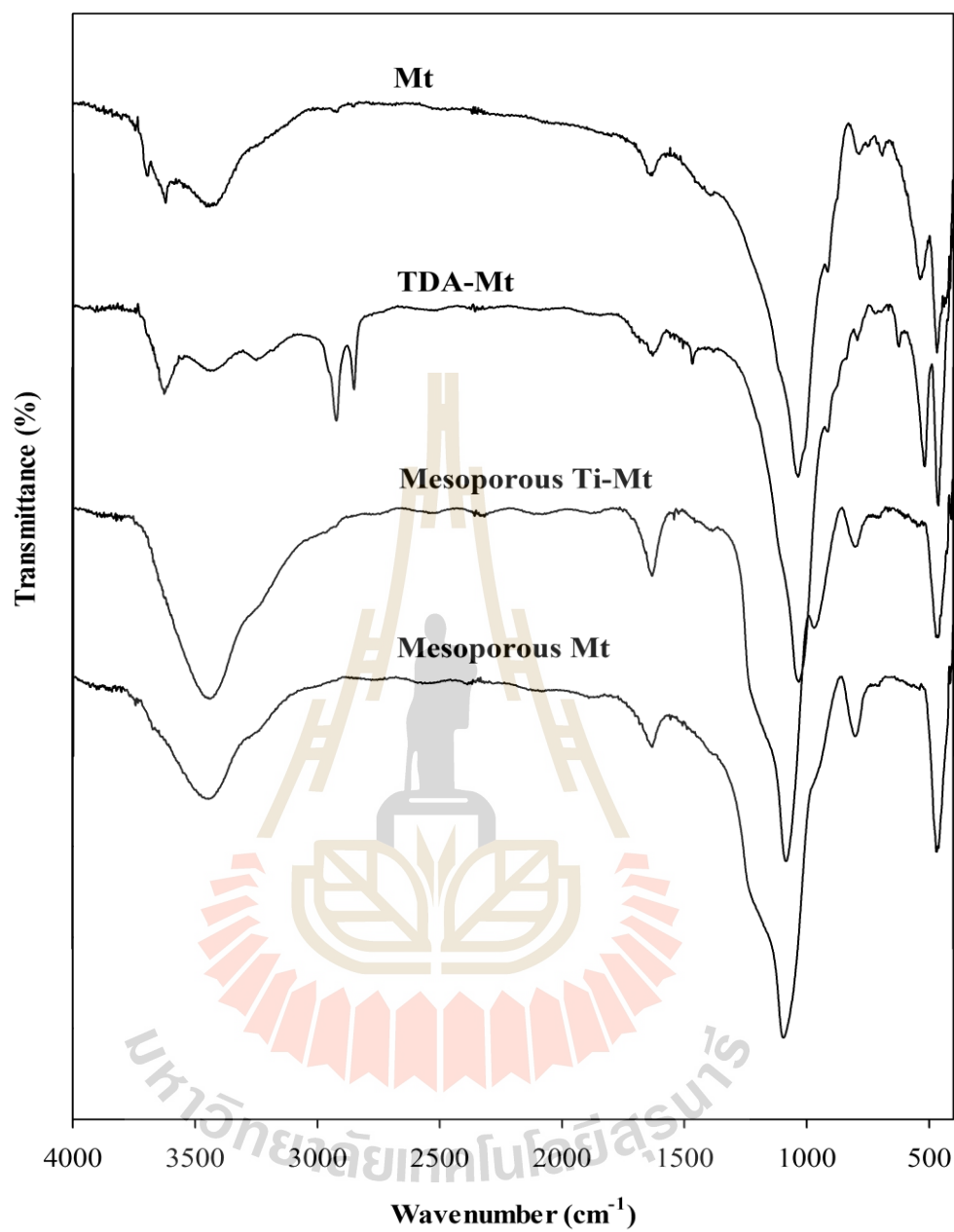


**Figure 3.5** FTIR spectra of Mt, TDA-Mt, mesoporous Mt and Mesoporous Ti-Mt.



**Table 3.3** FTIR assignments of Mt and modified Mt.

Wavenumber (cm <sup>-1</sup> )				Assignment
Mt	TDA-Mt	Mesoporous Mt	Mesoporous Ti-Mt	
3644-3324	3644-3324	3644-3324	3644-3324	O-H stretching of water
-	2920-2850	-	-	CH <sub>2</sub> asymmetric stretching of TDA
1638	1637	1638	1635	H-O-H bending vibration of water
1043	1042	1043	1042	Si-O-Si stretching
916	914	912	912	Al-OH-Al
850	850	850	850	Si-O-Al, Al-OH-Mg
795	795	795	795	OH bending vibration of hydrated water
625	627	627	629	Si-O-Mg, Mg-OH
527	522	523	522	Si-O-Al deformation
467	463	460	463	Si-O-Mg

### 3.5.5 Adsorption of paraquat on Mt and modified samples

Amount of paraquat adsorbed on all adsorbents at various equilibrium concentrations are shown in Figure 3.6. The amount of paraquat adsorbed on all adsorbents increases sharply at very low equilibrium concentrations implying that paraquat adsorption on these adsorbents are chemisorption. The isotherms of paraquat adsorbed on Mt samples based on Giles classification (Giles et al., 1960) are class H (high affinity) sub-group 2 which is a strong adsorption. The adsorption curve tends to

be a plateau indicating a formation of paraquat monolayer on the adsorbent surface. The similar adsorption behavior is reported on montmorillonite-zirconium(IV) cross-linked compound (González-Pradas et al., 2000), Algerian bentonite (Ait Sidhoum et al., 2013) and DHAPS-Mt (Gu et al., 2015).

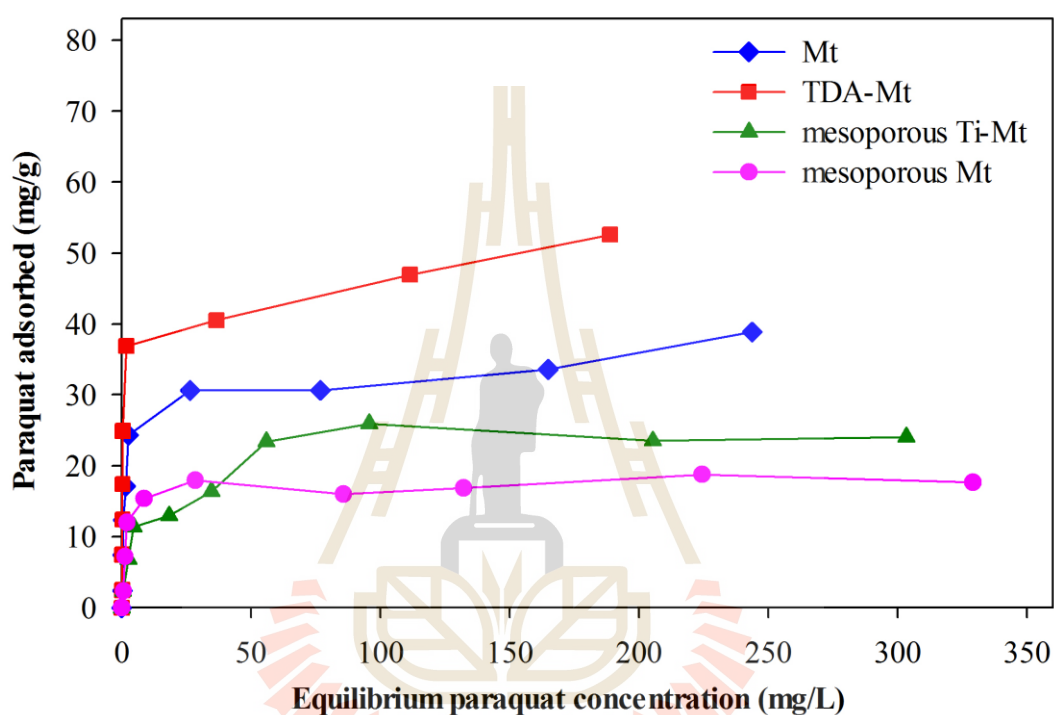


**Figure 3.6** Adsorption isotherm of paraquat on Mt and modified Mt samples.

The adsorption of paraquat on Mt samples follows Langmuir isotherm indicating a monolayer adsorption. The Langmuir parameters are summarized in Table 3.4. The adsorption of paraquat on TDA-Mt has the highest  $K_L$  values indicating that the highest affinity of paraquat molecules to the binding sites (Giles et al., 1960). The maximum adsorption capacity ( $q_m$ ) of the adsorbents on TDA-Mt is the highest (52 mg/g-adsorbent) followed by Mt, mesoporous Ti-Mt and mesoporous Mt. Although TDA-Mt has the lowest surface area, it has the highest adsorption

capacity. Paraquat dication could exchange with TDA and cations in the clay layers of TDA-Mt and Mt, respectively.

**Table 3.4** Langmuir parameters for paraquat adsorption on Mt and modified Mt.

Adsorbent	Langmuir parameter for paraquat		
	$q_m$ ( $\text{mg g}^{-1}$ )	$K_L$ ( $\text{L mg}^{-1}$ )	$R^2$
Mt	38	0.211	0.9908
TDA-Mt	52	0.374	0.9950
mesoporous Mt	18	0.132	0.9959
mesoporous Ti-Mt	25	0.348	0.9975

To confirm the exchange hypothesis, the Mt and TDA-Mt samples containing paraquat are characterized by XRD and the results are shown in Figure 3.7. The XRD pattern of Mt containing paraquat (Mt-PQ) shows the main peak at  $7.0^\circ$  corresponding to the interspacing layer 1.26 nm. The decrease of the interlayer spacing indicates ion exchange between hydrated cations and paraquat dication. Similar behavior is also reported on ion exchange of hydrated  $\text{Na}^+$  from Na-Mt by alkyl ammonium, glycine ethylester and ethylenediammonium (Laura and Cloos, 1975; Bala et al., 2000; Khan et al., 2009; Khan et al., 2012). The XRD pattern of TDA-Mt containing paraquat (TDA-Mt-PQ) shows the main peak at  $7.0^\circ$  corresponding to the interlayer spacing 1.27 nm. The spacing is similar to that of paraquat adsorbed on untreated Mt indicating that paraquat exchanged with the TDA.

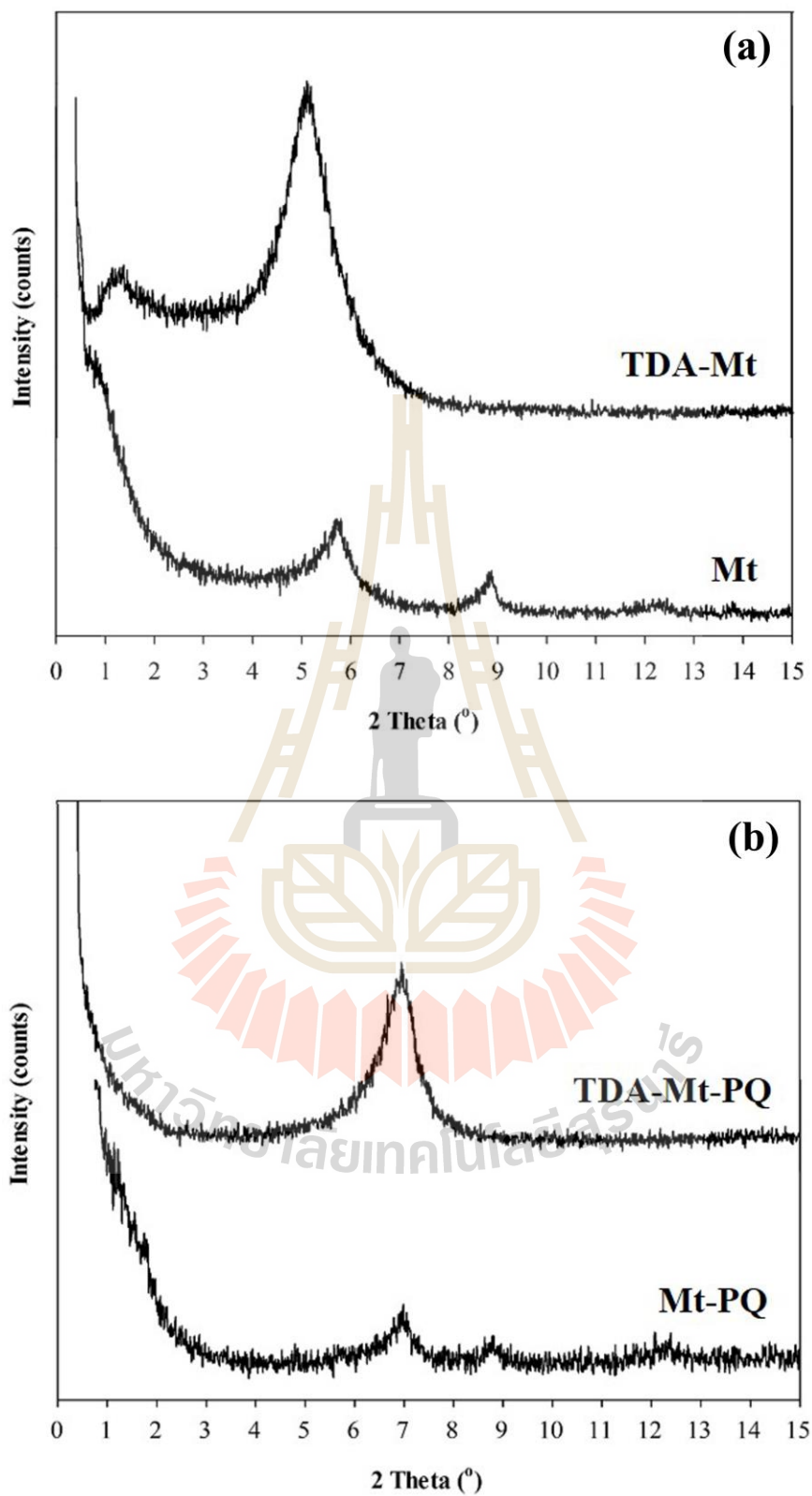


**Figure 3.7** XRD of a) Mt and TDA-Mt, b) Mt and TDA-Mt with paraquat.

The influence of pH on the adsorption of paraquat is shown in Figure 3.8. The lower amount adsorbed at the lower pH indicates a competition between proton and paraquat to the adsorption sites. A similar effect is reported on adsorption of paraquat on silica (Brigante and Avena, 2014).

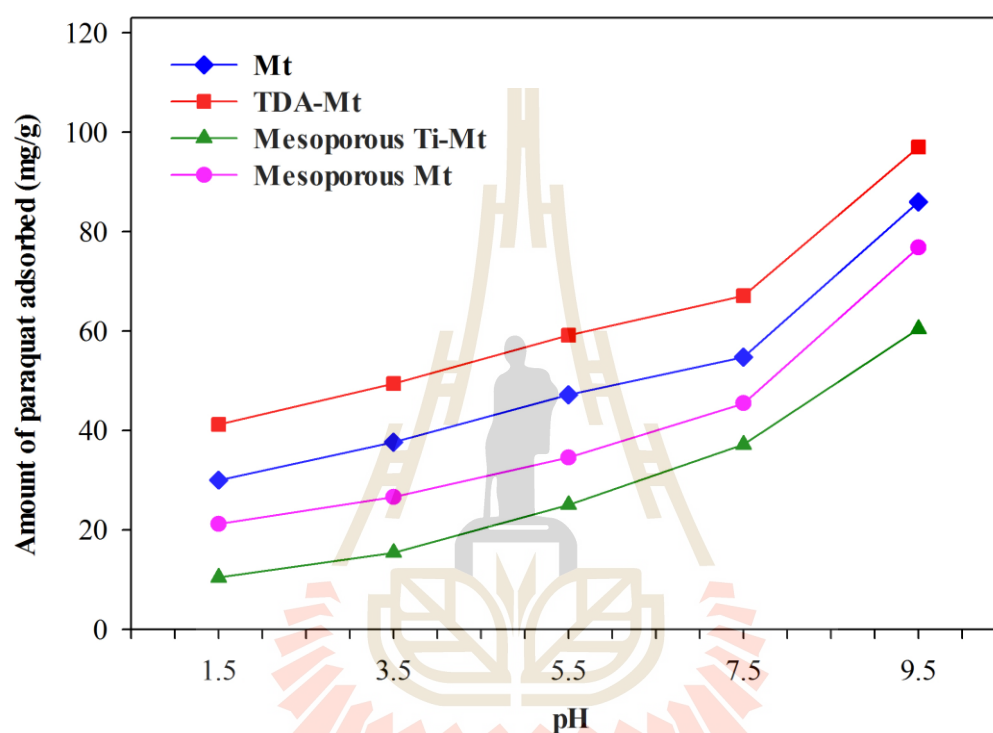


**Figure 3.8** Effect of pH on the adsorption of paraquat using Mt samples as adsorbents.

Table 3.5 compares paraquat adsorption capacities from this work and literature. The adsorption capacities of Mt from different studies seem to depend on composition and treatment method. From other works, samples from Mt modified with cationic or non-ionic surfactant have lower capacities than the un-modified one due to the difficulty to exchange (Guégan et al., 2015; Gu et al., 2015). Zwitterion surfactants could improve the adsorption capacity because their anionic group on one side interacts strongly with paraquat dication (Gu et al., 2015).

**Table 3.5** Maximum adsorption capacities of Mt, organoclay (based Mt) and mesoporous Mt.

Adsorbent	Type of surfactant in orgnoclay	$q_{\max}$ (mg g <sup>-1</sup> )	Reference
Mt		38	This work
TDA-Mt	cationic	52	This work
Na-Mt		134	Guégan et al., 2015
BDTA-Mt	cationic	-	Guégan et al., 2015
C <sub>10</sub> E <sub>3</sub> -Mt	non-ionic	39	Guégan et al., 2015
Na-Mt		Low	Gu et al., 2015
CTAB-Mt	cationic	6.4 & 6.9	Gu et al., 2015
DHAPS-Mt	zwitterionic	70.8 & 75.5	Gu et al., 2015
SDS-Mt	zwitterionic	85.2 & 90.9	Gu et al., 2015
Mesoporous Mt		18	This work
Mesoporous Ti-Mt		25	This work
MCM-41		21.3	Rongchapo et al., 2013
Al-MCM-41		66.4	Rongchapo et al., 2015
Mesoporous silica		107	Brigante and Avena, 2014

TDA = tetradecylammonium

BDTA = benzyl decyltrimethyl ammonium

C<sub>10</sub>E<sub>3</sub> = triethylene glycol mono n-decyl ether

CTAB = cetyltrimethylammonium bromide

DHAPS = (3-(N,N-dimethylhexadecylammonio)propanesulfonate

SDS = sodium dodecyl sulfonate

In the case of mesoporous Ti-Mt and mesoporous Mt, the adsorption capacity is low despite the large surface area. The results indicated that adsorption occurs on the external surface. The presence of Ti generates negative charge surface and enhanced the adsorption. With the similar reason, the presence of Al in mesoporous MCM-41 leads to higher adsorption capacities (Rongchapo et al., 2013; Rongchapo et al., 2015). Moreover, the higher adsorption capacity is reported on mesoporous silica with uniform particle size prepared with a mixed surfactant (Brigante and Avena, 2014).

### 3.6 Conclusions

Montmorillonite (Mt) is modified by tetradecylammnium chloride (TDA) to produce TDA-Mt. The intercalation of TDA resulted in the increase of interlayer spacing and decrease in the surface area. Moreover, Mt is modified by intragallery templating to produce mesoporous Mt and mesoporous Ti-Mt. Both samples have lamellar structure with significantly higher surface area than the parent Mt due to the presence of mesopores. The paraquat adsorption capacity is as follows: TDA-Mt > Mt > mesoporous Ti-Mt > mesoporous Mt. The adsorption isotherm fits with Langmuir model. The adsorption on TDA-Mt and Mt is ion exchange. For mesoporous materials, the adsorption occurred on external surface and the presence of Ti increases the adsorption capacity. The adsorption decreases in acidic conditions.

### 3.7 References

- Ait Sidhoum, D., Socias-Viciano, M. M., Urena-Amate, M. D., Derdour, A., Gonzalez-Pradas, E., and Debbagh-Boutarbouch, N. (2013). Removal of paraquat from water by an Algerian bentonite. **Applied Clay Science**. 83-84: 441-448.
- Bala, P. B., Samantaray, K., and Srivastava, S. K. (2000). Synthesis and characterization of Na-montmorillonitealkylammonium intercalation compounds. **Materials Research Bulletin**. 35: 1717-1724.
- Boparai, H. K., Joseph, M., and O'Carroll, D. M. (2011). Kinetics and thermodynamics of cadmium ion removal by adsorption onto nanozerovalent iron particles. **Journal of Hazardous Materials**. 186: 458-465.
- Brigante, M. and Avena, M. (2014). Synthesis, characterization and application of a hexagonal mesoporous silica for pesticide removal from aqueous solution. **Microporous and Mesoporous Materials**. 191: 1-9.
- Churchman, G. J. (2002). Formation of complexes between bentonite and different cationic polyelectrolytes and their use as sorbents for non-ionic and anionic pollutants. **Applied Clay Science**. 21: 177-189.
- de Paiva, L. B., Morales, A. R., and Diaz, F. R. V. (2008) Organoclays: Properties, preparation and applications. **Applied Clay Science**. 42: 8-24.
- Ganigar, R., Rytwo, G., Gonen, Y., Radian, A., and Mishael, Y. G. (2010). Polymer-clay nanocomposites for the removal of trichlorophenol and trinitrophenol from water. **Applied Clay Science**. 49: 311-316.



- Gao, X., Mao, H., Lu, M., Yang, J., and Li, B. (2012). Facile synthesis route to NiO-SiO<sub>2</sub> intercalated clay with ordered porous structure: Intragallery interfacially controlled functionalization using nickel-ammonia complex for deep desulfurization. **Microporous and Mesoporous Materials**. 148: 25-33.
- Giles, C. H., Macewan, T. H., Nakhwa, S. N., and Smith, D. (1960). Study in adsorption Part XI. A system of classification of solution adsorption isotherm, and its use in diagnosis of adsorption mechanism and in measurement of specific surface areas of solids. **Journal of the Chemical Society**. 4: 3973-3993.
- González-Pradas, E., Villafranca-Sanchez, M., Rey-Bueno, F. D., Urena-Amate, M. D., and Fernandez-Perez, M. (2000). Removal of paraquat and atrazine from water by montmorillonite-(Ce or Zr) phosphate cross-linked compounds. **Pest Management Science**. 56: 565-570.
- Gu, Z., Gao, M., Lu, L., Liu, Y., and Yang, S. (2015). Montmorillonite Functionalized with Zwitterionic Surfactant as a Highly Efficient Adsorbent for Herbicides. **Industrial and Engineering Chemistry Research**. 54: 4947-4955.
- Guégan, R., Giovanela, M., Warmont, F., and Motelica-Heino, M. (2015). Nonionic organoclay: A 'Swiss Army knife' for the adsorption of organic micro-pollutants? **Journal of Colloid and Interface Science**. 437: 71-79.
- Keawkumay, C., Jarukumjorn, K., Wittayakun, J., and Suppakarn, N. (2012). Influences of surfactant content and type on physical properties of natural rubber/organoclay nanocomposites. **Journal of Polymer Research**. 19: 9917.

- Khan, A. H., Bala, P., Nurnabi, M., and Mustafizur Rahman, A. F. M. (2012). Investigations on microstructural and layer disorder parameters of Na-montmorillonite glycine intercalation compounds. **Dhaka University Journal of Science**. 60(1): 25-29.
- Khan, A. H., Nurnabi, M., and Bala, P. (2009). Studies on thermal transformation of Na-montmorillonite-glycine intercalation compounds. **Journal of Thermal Analysis and Calorimetry**. 96: 929-935.
- Laura, R. D., and Cloos, P. (1975). Adsorption of ethylenediamine (EDA) on montmorillonite saturated with different cations; III, Na-, K- and Li-montmorillonite; ion-exchange, protonation, co-ordination and hydrogen-bonding. **Clays Clay Minerals**. 23: 61-69.
- Mao, H., Li, B., Li, X., Liu, Z., and Ma, W. (2009). Mesoporous nickel (or cobalt)-doped silica-pillared clay: Synthesis and characterization studies. **Materials Research Bulletin**. 47: 1569-1575.
- Mao, H., Li, B., Li, X., Yue, L., Xu, J., Ding, B., Gao, X., and Zhou, Z. (2010). Facile synthesis and catalytic properties of titanium containing silica-pillared clay derivatives with ordered mesoporous structure through a novel intra-gallery templating method. **Microporous and Mesoporous Materials**. 130: 314-321.
- Mao, H., Zhu, K., Li, B., Yao, C., and Kong, Y. (2014). Document Synthesis of titania modified silica-pillared clay (SPC) with highly ordered interlayered mesoporous structure for removing toxic metal ion Cr(VI) from aqueous state. **Applied Surface Science**. 292: 1009-1019.

- Mao, H., Zhu, K., Lu, X., Zhang, G., Yao, C., Kong, Y., and Liu, J. (2015). Restructuring of silica-pillared clay (SPC) through posthydrothermal treatment and application as phosphotungstic acid supports for cyclohexene oxidation. **Journal of Colloid and Interface Science**. 446: 141-149.
- Mithyantha, M. S., Rao, K. B., Biddappa, C. C., Lillaram, N. T., and Perur, N.G. (1975). Paraquat adsorption on clay minerals. **Bulletin of the Indian National Science Academy**. 50: 293-298.
- Paul, B., Yang, D., Yang, X., Ke, X., Frost, R., and Zhu, H. (2010). Adsorption of the herbicide simazine on moderately acid-activated beidellite. **Applied Clay Science**. 49: 80-83.
- Rongchapo, W., Deekamwong, K., Loiha, S., Prayoonpokarach, S., and Wittayakun, J. (2015). Paraquat adsorption on NaX and Al-MCM-41. **Water Science and Technology**. 71: 1347-1353.
- Rongchapo, W., Sophiphun, O., Rintramee, K., Prayoonpokarach, S., and Wittayakun, J. (2013). Paraquat adsorption on porous materials synthesized from rice husk silica. **Water Science and Technology**. 68: 863-869.
- Rouquerol, F., Rouquerol, J., and Sing, K. (1999). **Adsorption by powders and porous solids: principles, methodology and applications**. London: Academic Press. 18-212.
- Rytwo, G., Tropp, D., and Serban, C. (2002). Adsorption of diquat, paraquat and methyl green on sepiolite: experimental results and model calculations. **Applied Clay Science**. 20: 273-282.
- Seki, Y. and Yurdakoç, K. (2005). Paraquat adsorption onto clays and organoclays from aqueous solution. **Journal of Colloid and Interface Science**. 287: 1-5.

- Sing, K. S. W. (1982). Reporting physisorption data for gas/solid systems with special reference to the determination of surface area and porosity. **Pure & Applied Chemistry**. 54: 2201-2218.
- Singh, N. (2009). Adsorption of herbicides on coal fly ash from aqueous solutions. **Journal of Hazardous Materials**. 168: 233-237.
- Tan, G. and Xiao, D. (2009). Adsorption of cadmium ion from aqueous solution by ground wheat stems. **Journal of Hazardous Materials**. 164: 1359-1363.
- Thomas, W. J. and Crittenden, B. (1998). **Adsorption technology and design**. Boston: Butterworth-Heinemann. 38-50.
- WHO. (1984). Paraquat and diquat. **Environment Health Criteria**. 39, Geneva, Switzerland.
- Yang, S., Liang, G., Gu, A., and Mao, H. (2013). Synthesis of TiO<sub>2</sub> pillared montmorillonite with ordered interlayer mesoporous structure and high photocatalytic activity by an intra-gallery templating method. **Materials Research Bulletin**. 48: 3948-3954.

# CHAPTER IV

## PARAQUAT ADSORPTION ON FAU Y ZEOLITE WITH VARIOUS SILICON/ALUMINIUM RATIO

### Abstract

Paraquat is widely used for agricultural purposes. It is a water pollutant leaching from soil. Moreover, paraquat is highly toxic to human. The objective of this study is to synthesize FAU type zeolite with various Si/Al ratios for the adsorption of herbicide paraquat. The synthesis of zeolite FAU with different Si/Al ratios (2.1 to 2.4) and particle sizes (100-300 nm) is performed using hydrothermal method. The samples exhibit the X-ray diffraction patterns corresponding to pure FAU phase. The crystal size, morphology and chemical composition are controlled by changing the conditions of hydrothermal treatment. Paraquat adsorption is performed in a batch system. The results show that the adsorption process could be described with the Langmuir model. The capacity of the adsorbents is in the range of 210-240 mg/g-adsorbent. After paraquat adsorption, the surface areas of the samples decrease from 800 to 30 m<sup>2</sup>/g indicating that paraquat adsorbs in the zeolite. The FAU samples with the higher Si/Al ratio (2.4) has the higher adsorption capacity.

## 4.1 Introduction

Zeolite Linde type Y in sodium form (NaY) belongs to faujasite (FAU) family with a framework containing double 6 rings linked through sodalite cages generating supercages with average pore diameter of 7.4 Å. NaY is commonly applied as catalysts and adsorbents for the removal of volatile organic compounds (Baba et al., 2002, Su et al., 2010), adsorption of paraquat (Rongchapo et al., 2013) and fluid cracking catalysts (Cundy and Cox, 2005). Several methods to prepare NaY from rice husk are reported (Wittayakun et al., 2008; Tan et al., 2011; Saceda et al., 2011; Mohamed et al., 2015). In general, NaY can be synthesized in two steps to avoid the formation of other phases, especially zeolite NaP (Wittayakun et al., 2008; Petkowicz et al., 2008). NaY can be synthesized using various starting silica and alumina sources. Normally, a conventional method of NaY synthesis uses commercial silica ( $\text{SiO}_2$ ) and alumina ( $\text{Al}_2\text{O}_3$ ). To reduce costs of synthesis, agricultural wastes can be used as the silica source in the synthesis of zeolite instead of chemical sources. Some countries in south-east Asia, especially, Thailand, produce large quantities of rice husk (RH) as a byproduct from the rice milling industry. This husk has low commercial value and is usually burnt as a fuel. About 20 wt% of ash is produced and the ash contains 85-98 wt% silica with low amounts of traced metallic elements impurities. Silica from RH has a uniform dispersion by molecular units, very fine amorphous particle size, high purity and surface area (Liou et al., 2004).

Changing aluminium content in the zeolite Y framework provides an additional way of controlling the number, strength, and distribution of the acid sites, and thus the catalytic activity (Kaduk and Faber, 1995). Zeolite Y can be synthesized with lower and higher critical point of Si/Al value in zeolite Y composition (Lutz,

2015). Furthermore, Si/Al ratio relates to hydrophobicity and hydrophilicity of zeolite Y. The decrease amount of aluminium could increase the hydrophobicity of the  $\equiv\text{Si}-\text{O}-\text{Si}\equiv$  bonds. In addition, zeolite with a higher amount of aluminium is more hydrophilic due to the  $\equiv\text{Si}-\text{O}-(\text{Al}^{(-)})\equiv$  bonds (Chen, 1976; Lutz, 2015).

Paraquat is a herbicide which is widely used in Thailand, including in Nakhon Ratchasima province to control weeds and grasses. However, paraquat is highly toxic to humans and animals when contacted via ingestion, skin contact and splash to eyes (Suntres, 2002). Paraquat can contaminate water due to high solubility. Therefore, it is important to study a removal of paraquat from aqueous solution by using natural adsorbents i.e. clay, activated carbon, zeolite.

Ibrahim and Jbara (2009) study the adsorption of paraquat on natural phillipsite-faujasite tuff from Jordan. This adsorbent consists of 65% zeolites (45% faujasite and 20% phillipsite), 30% palagonite and 5% of calcite. Paraquat readily ion exchanges into faujasite. When the faujasite tuff (F) is activated by  $\text{Na}^+$ ,  $\text{K}^+$ ,  $\text{Ca}^{2+}$  and  $\text{Mg}^{2+}$ , the adsorption capacities are high. Nur et al. (2005) study the adsorption of commercial paraquat using a commercial NaY zeolite with surface area of  $900 \text{ m}^2/\text{g}$ . Paraquat at a concentration of 300 ppm is removed completely in less than 10 min by 0.4 g of NaY. When NaY particles are covered with alkylsilane, the zeolite hydrophilicity decreased. The paraquat adsorption slightly decreases (but still more than 95%) and blue dye (Cibacron Blue 35A) is also removed. Rongchapo et al. (2013) study the adsorption of commercial paraquat on porous material derived from rice husk silica, including MCM-41, NaBEA, NaY and NaX. Those materials are different in pore structure, surface area and Si/Al ratio. NaY, which is in the faujasite family with a Si/Al ratio of 2.3, has the highest maximum adsorption capacity (185

mg/g) and the mechanism is cation exchange. Since the adsorption depends on Si/Al ratio, they further use the adsorbent with higher Al content including Al-MCM-41 and NaX. The adsorption capacity on Al-MCM-41 is higher than MCM-41. However, the capacity on NaX is lower than that on NaY (Rongchapo et al., 2015). Thus, an influence of Si/Al ratio in a narrow range on the paraquat adsorption is investigated in this work.

## 4.2 Experiment

### 4.2.1 Synthesis of zeolite NaY

The zeolite NaY is synthesized with a procedure modified from that by Robson (2001). The Si/Al ratio is varied to be slightly more or less than 2.2.  $\text{Na}_2\text{SiO}_3$  solution is prepared by dissolving of 57.4 g RHS in NaOH solution prepared from dissolving of 23.00 g NaOH in 119.60 g DI water. A seed gel with a molar ratio of  $10.67\text{Na}_2\text{O}:\text{Al}_2\text{O}_3:10\text{SiO}_2:180\text{H}_2\text{O}$  is prepared. NaOH (4.09 g) is dissolved in 20.00 g of DI water in a PE bottle, then, anhydrous  $\text{NaAlO}_2$  (varied from lower 20% to higher 20% of normal sodium aluminate content, Riedel-de Haën<sup>®</sup>, 41.383%  $\text{Na}_2\text{O}$ , 58.604%  $\text{Al}_2\text{O}_3$ ) is added to NaOH solution. The mixture is stirred for 10 min until the solution is clear before an addition of 22.72 g  $\text{Na}_2\text{SiO}_3$  solution to the solution of  $\text{NaAlO}_2$ . The mixture is stirred for 10 min, capped, and aged at room temperature for 24 h.

A feedstock gel with molar ratio  $4.30\text{Na}_2\text{O}:\text{Al}_2\text{O}_3:10\text{SiO}_2:180\text{H}_2\text{O}$  is prepared with a similar procedure to that of the seed gel except that it is used immediately without aging. NaOH (0.14 g) is dissolved in DI water (131.97 g) in a PE bottle, then,  $\text{NaAlO}_2$  (varied from lower 20% to higher 20% of normal sodium aluminate content) is added, stirred for 10 min and, then,  $\text{Na}_2\text{SiO}_3$  solution (143.43 g)



is added to the NaAlO<sub>2</sub> solution. The synthesized NaY samples are called NaY1 (+20% Al), NaY2 (+10% Al), NaY3 (normal), NaY4 (-10% Al) and NaY5 (-20% Al).

#### 4.2.2 Characterization of zeolite NaY

NaY samples are characterized by X-ray diffractometer (XRD, Bruker D8 ADVANCE) with a Cu K $\alpha$  radiation ( $\lambda = 1.5418 \text{ \AA}$ ) operated at a voltage of 40 kV. The XRD patterns are recorded with a step size of 0.02 and a scan speed of 0.2 °/min. In addition, the adsorbents containing paraquat are characterized with the similar procedure. Those samples are treated with paraquat (500 ppm) with a procedure similar to the adsorption study, washed by DI water and dried at 90 °C overnight. The Si/Al ratios are determined by X-ray fluorescence spectrometry (ED-XRF, Horiba 5200). Morphology of the NaY is studied by an SEM (CARL ZEISS-AURIGA).

N<sub>2</sub> adsorption-desorption isotherms are obtained from N<sub>2</sub> adsorption-desorption analyzer (Bel Sorp mini II) at a liquid nitrogen temperature and surface area is calculated using a Brunauer–Emmett–Teller (BET) method. The samples are degassed at 300 °C to remove physisorbed gas. The spent adsorbents are degassed at 150 °C to preserve the organic content.

Functional groups of all adsorbents before and after adsorption of paraquat (500 ppm) are identified by a Fourier transform infrared spectrometer (FTIR) on a Perkin Elmer Spectrum GX using KBr pellet technique. The spectrum is recorded in the 4000-400 cm<sup>-1</sup> region with 2 cm<sup>-1</sup> resolution.

The basicity of the NaY is analyzed by temperature-programmed desorption of carbon dioxide (CO<sub>2</sub>-TPD) in a Belcat-B equipped with a thermal conductivity detector. A sample weight of 100 mg is packed in a tubular U-shaped

quartz cell. Each sample is preheated at 300 °C with a heating rate of 10 °C/min in a He flow (50 mL/min) for 360 min to eliminate physisorbed species before cooling to 70 °C. Then a constant flow of 50 mL/min of CO<sub>2</sub>/Ar gas mixture is introduced over the samples for 30 min to achieve saturation. After that, the sample is flushed with He for 30 min, heated up to 100 °C with a heating rate of 10 °C/min and held for 3 h to remove physisorbed species. The CO<sub>2</sub>-TPD measurement is performed from 130 to 800 °C with a heating rate of 10 °C/min with He as a carrier gas. The number of basic sites is calculated from the peak area compared to a reference material that is analyzed with the same conditions.

#### 4.2.3 Paraquat adsorption

The adsorption of paraquat is performed using a commercial paraquat solution (27.6% w/v in water) purchased from a local agro store. The exact concentration is determined from a calibration curve constructed from the chemical grade reagents. The adsorption is performed by adding 0.10 g of the adsorbent to a conical flask containing 20 mL of paraquat solutions with various concentrations. The mixture is agitated by using a magnetic stirrer at the speed of 400 rpm for 60 min. Then 10 mL of the samples in each flask is collected and immediately filtered using a 0.45 µm syringe filter. The amount of remaining paraquat in the solution is determined using a UV-Vis spectrophotometer (Varian CARY 300) at a wavelength corresponding to the maximum absorbance,  $\lambda_{\max}$  at 257 nm. The amount of paraquat or pirimiphos-methyl adsorbed at equilibrium ( $q_e$ ) is calculated by Eq. 1 (Tan and Xiao 2009; Boparai et al., 2011).

$$q_e = \frac{(C_0 - C_e) \times V}{w} \quad (1)$$

$C_0$  and  $C_e$  are the initial and equilibrium concentration of paraquat (mg/L), respectively.  $V$  is the volume of paraquat solution (L) and  $w$  is the amount of adsorbent (g).

In order to determine the maximum adsorption capacity of paraquat on NaY samples, the Langmuir isotherm is used. This isotherm assumes that the adsorbate forms monolayer on the adsorbent with uniform sites. (Thomas and Crittenden, 1998; Singh, 2009; Tan and Xiao, 2009; Boparai et al., 2011).

$$\frac{C_e}{q_e} = \frac{1}{K_L q_m} + \frac{C_e}{q_m} \quad (4)$$

where  $K_L$  is the Langmuir constant related to the affinity of binding site (L/mg) and  $q_m$  is the maximum adsorption capacity (mg/g). Both  $K_L$  and  $q_m$  can be determined from the linear plot of  $C_e/q_e$  versus  $C_e$ .

## 4.3 Results and discussion

### 4.3.1 Structure and Si/Al ratio of NaY

Figure 4.1(a) and 4.1(b) show the XRD pattern of the zeolite NaY paraquat adsorption with different Si/Al ratio and without paraquat adsorption. All diffraction peaks of NaY are similar to those of the standard NaY (Treacy and Higgins, 2007). The XRD patterns exhibit sharp characteristic peaks of NaY from  $2\theta = 5^\circ$ - $80^\circ$  indicating that the obtained NaY are in the crystalline form of all ratio.

Moreover, the diffraction peaks also revealed that no other significant peaks correspond to other zeolites appeared. It is confirmed that NaY of high purity is successfully synthesized from rice husk silica. After paraquat adsorption (Figure 4.1(b)), the XRD peaks of all NaY adsorbents are similar to fresh NaY indicating that the structure of NaY samples is not collapsed after the adsorption. This evidences confirmed that paraquat adsorption on NaY with various Si/Al ratio does not change the zeolite structure. However, intensities of the plane (220) and (311) from the pattern of paraquat adsorbed NaY are different from those of NaY samples. The intensity ratio  $I_{(220)}/I_{(311)}$  explains a change in distribution of sodium ions ( $\text{Na}^+$ ) from their random positions in supercages to specific sites by an incorporation of a large ion (Kozlov et al., 1998; Nakayama et al., 2003). The  $I_{(220)}/I_{(311)}$  changes after paraquat adsorption indicating that the amount of  $\text{Na}^+$  in NaY are changed. The result confirms that paraquat adsorption occurs through cation exchange. A similar result is reported on zeolite NaY and NaX (Rongchapo et al., 2017).

The Si/Al ratio of the synthesized NaY is shown in Table 4.1, the Si/Al ratio of NaY3 is 2.25. Decreasing the Al in seed gel and feed stock gel processes, the Si/Al ratios of NaY1 and NaY2 increase to 2.40 and 2.31, respectively. Increasing the Al in seed gel and feed stock gel processes, the Si/Al ratio of NaY4 and NaY5 decreased to 2.19 and 2.15, respectively. The results confirm that the Si/Al of synthesized NaY with various Al contents is in the range of FAU zeolite NaY (Lutz, 2014).

#### 4.3.2 $\text{N}_2$ adsorption-desorption isotherms

The nitrogen adsorption-desorption isotherm of all NaY samples with and without paraquat adsorption are shown in Figure 4.2, respectively. All samples

possessed a type I isotherm, the volume of nitrogen uptake increased quickly at low relative pressure ( $P/P_0 = 0-0.1$ ) by adsorption in micropores and external surface which is characteristic of microporous materials. The volume adsorbed to give monolayer is reached at low relative pressure. After the monolayer adsorption, the nitrogen uptake is nearly constant and the steep adsorption step at high relative pressure ( $P/P_0 = 0.9-1.0$ ) related to the narrow pore size distributions (Khemthong et al., 2010).

The surface areas of zeolite NaY samples are shown in Table 4.1. The surface area of zeolite NaY samples is in the range of 789-856  $m^2/g$ . Surface area increased with decreasing Al content. After paraquat adsorption, the surface areas of paraquat adsorbed NaY samples decrease significantly to 23-40  $m^2/g$ . This is due to the occupation of paraquat molecules in micropore of NaY.

**Table 4.1** Si/Al ratio, surface area and total pore volume of NaY and NaY adsorbed paraquat samples.

Adsorbent	Si/Al ratio	NaY		NaY adsorbed paraquat	
		Surface area ( $m^2/g$ )	Total pore volume ( $cm^3/g$ )	Surface area ( $m^2/g$ )	Total pore volume ( $cm^3/g$ )
NaY1 (-20% Al)	2.40	789	0.4267	21.4	0.1102
NaY2 (-10% Al)	2.31	804	0.4485	23.8	0.1460
NaY3 Normal	2.25	844	0.4639	26.5	0.1673
NaY4 (+10% Al)	2.19	849	0.4991	28.8	0.1889
NaY5 (+20% Al)	2.15	856	0.5345	38.6	0.2297

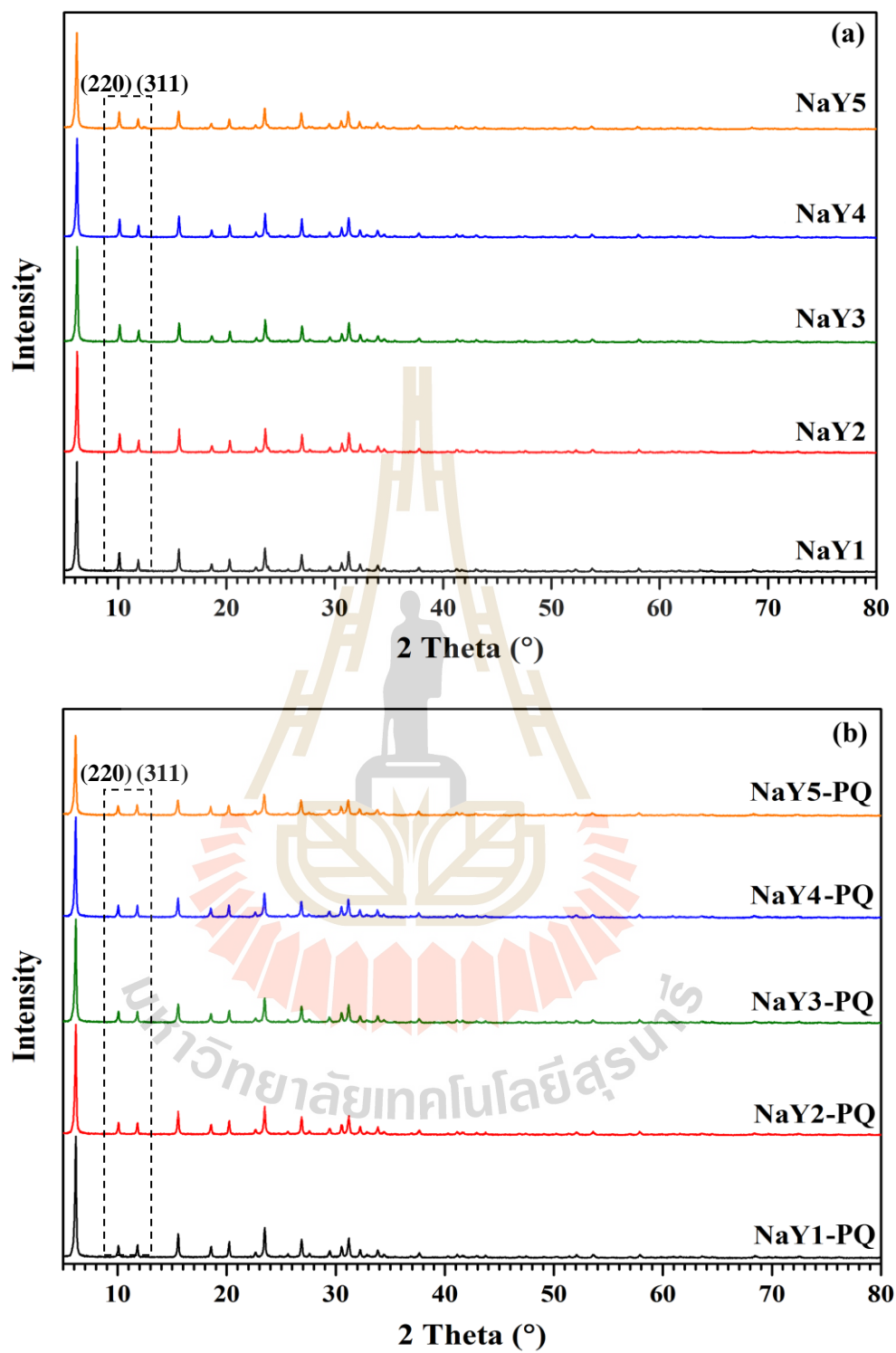


**Figure 4.1** XRD pattern of (a) NaY with various Si/Al ratio and (b) paraquat adsorbed NaY.

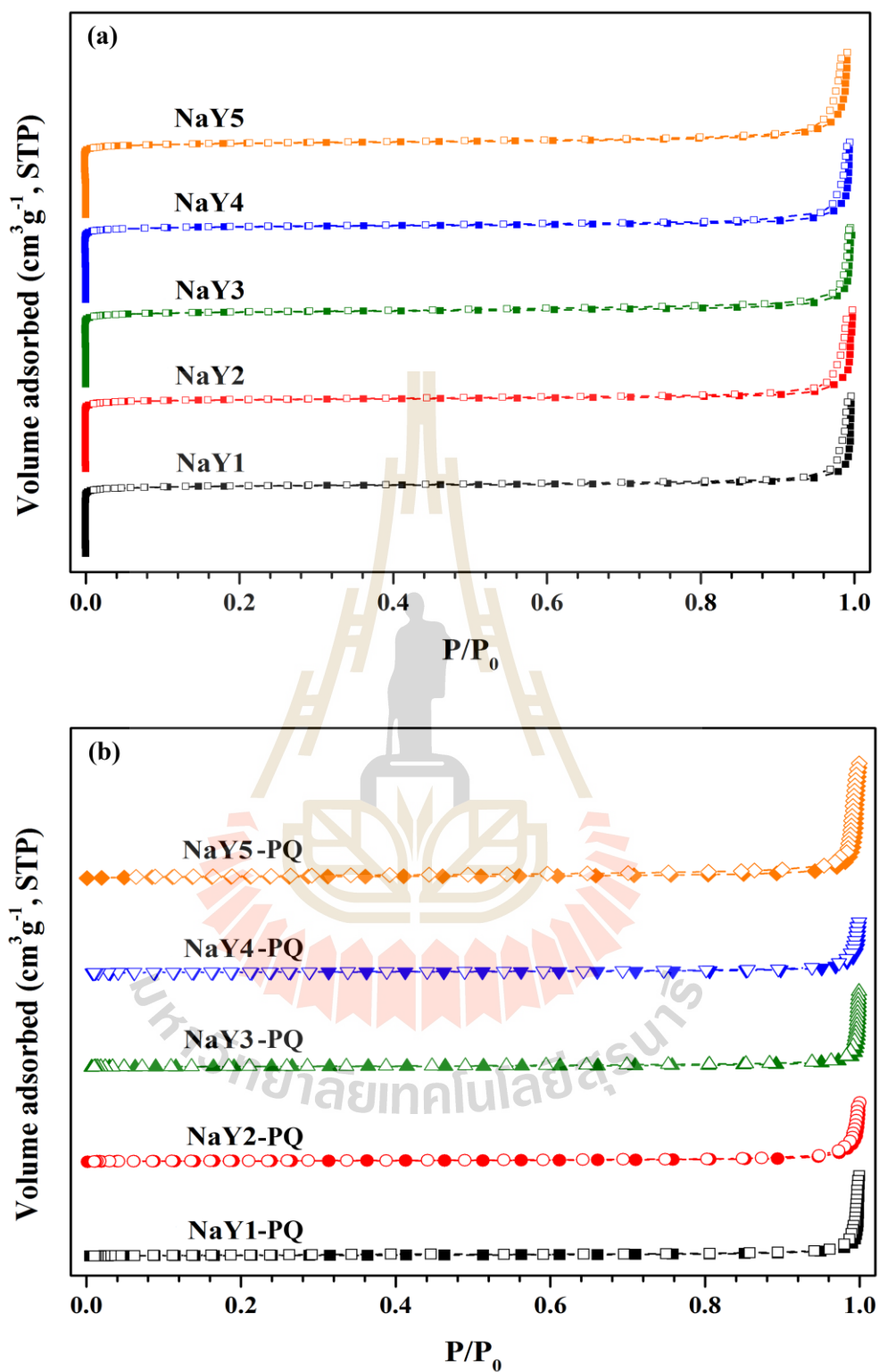


**Figure 4.2** Nitrogen adsorption-desorption isotherm of (a) NaY with various Si/Al ratio and (b) paraquat adsorbed NaY.

### 4.3.3 Morphology

The morphology of zeolite NaYs with various Si/Al ratio from SEM are shown in Figure 4.3. The particles of all zeolite NaY are uniform in size and smaller than 1  $\mu\text{m}$ . The particle size of the crystals is approximately 100-200 nm. However, the particle size of NaY is smaller with increasing Al content.

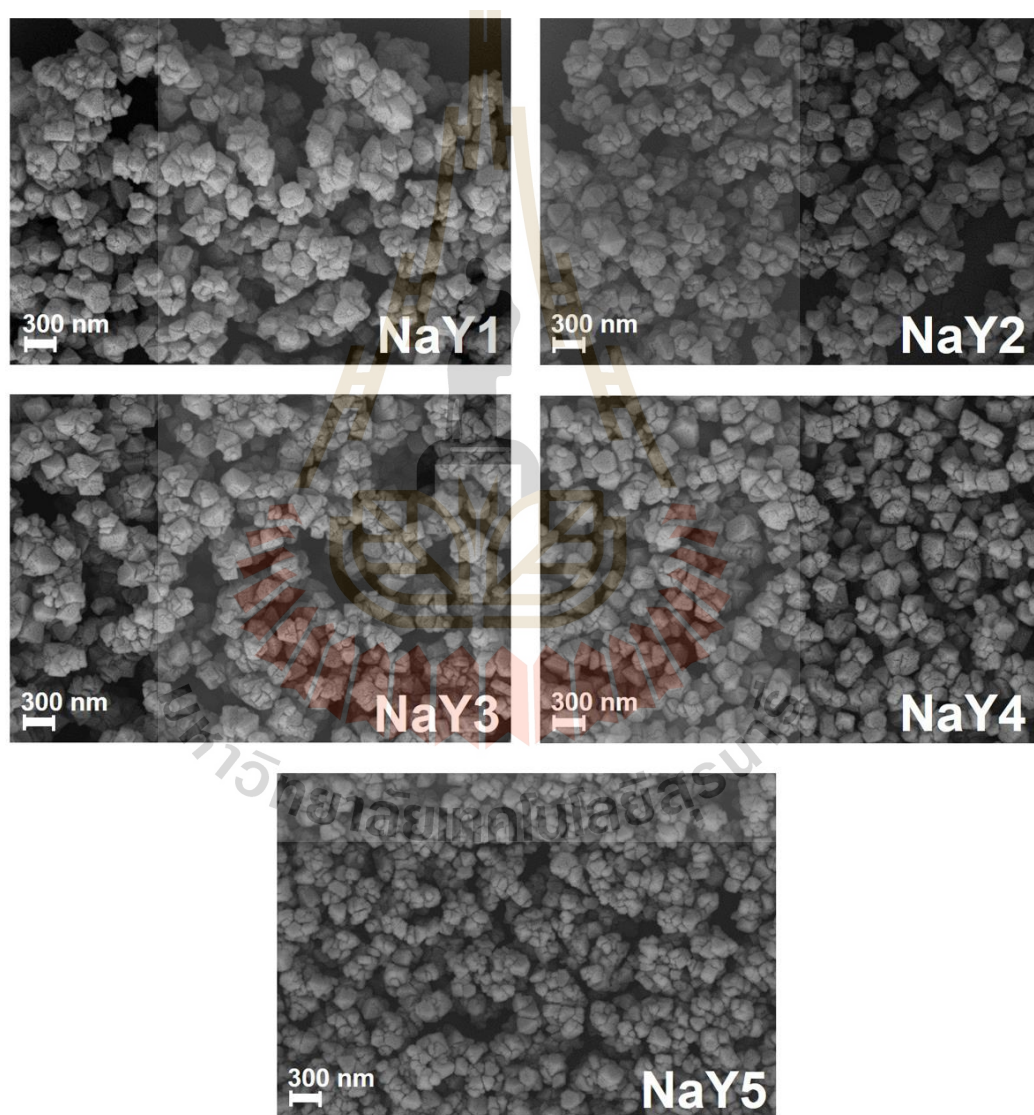


**Figure 4.3** TEM images of NaY samples with various Si/Al ratio.



#### 4.3.4 Functional groups

Figure 4.4 shows FTIR spectra of the NaY and paraquat adsorbed NaY. The bands at 900-1200  $\text{cm}^{-1}$  are attributed to asymmetrical stretching vibrations corresponding to the tetrahedral Si, Al atoms. The band between 700 and 900  $\text{cm}^{-1}$  is assigned to Si-O symmetrical stretching vibrations, while the band appearing at 550 to 555  $\text{cm}^{-1}$  arises from the presence of structural double D6R rings in the case of FAU(Y) zeolite. The band between 465 and 455  $\text{cm}^{-1}$  corresponds to the structure insensitive internal tetrahedral bending bond, i.e., T-O<sub>4</sub> (T: Si or Al) (Morales-Pacheco et al., 2011; Lutz, 2014). Paraquat shows characteristic peaks at 3055 and 3018  $\text{cm}^{-1}$  corresponding to the C-H tension mode of the methyl groups on the aromatic ring in the paraquat molecule. Bands between 1641 and 1194  $\text{cm}^{-1}$  are attributed to the C-C tension mode and the C-H deformation mode in the aromatic ring plane (Brigante and Avena, 2014). After paraquat adsorption, peaks of functional groups in paraquat are observed in the spectra of spent NaY samples. Moreover, the new peaks are appeared at 1639, 1504, 1459  $\text{cm}^{-1}$  corresponded to the binding between the herbicide and NaY zeolite. This binding generates binary surface species SiO<sub>2</sub>-PQ<sup>2+</sup>, the formation is mainly driven by electrostatic interactions, where negatively charged groups of NaY could bind the dication by forming ionic pairs or outer-sphere complexes (Brigante and Avena, 2014). Two bands at 3500  $\text{cm}^{-1}$  and 3732  $\text{cm}^{-1}$  (as shown in Figure 4.4) attribute to silanol nests in the porous matrix and both isolate external and internal silanol groups, respectively (Grand et al., 2017). The 3732  $\text{cm}^{-1}$  band is not observed in NaY1 sample with a lower amount of Al (high Si/Al ratio). This evidence confirms that NaY1 is hydrophobic.

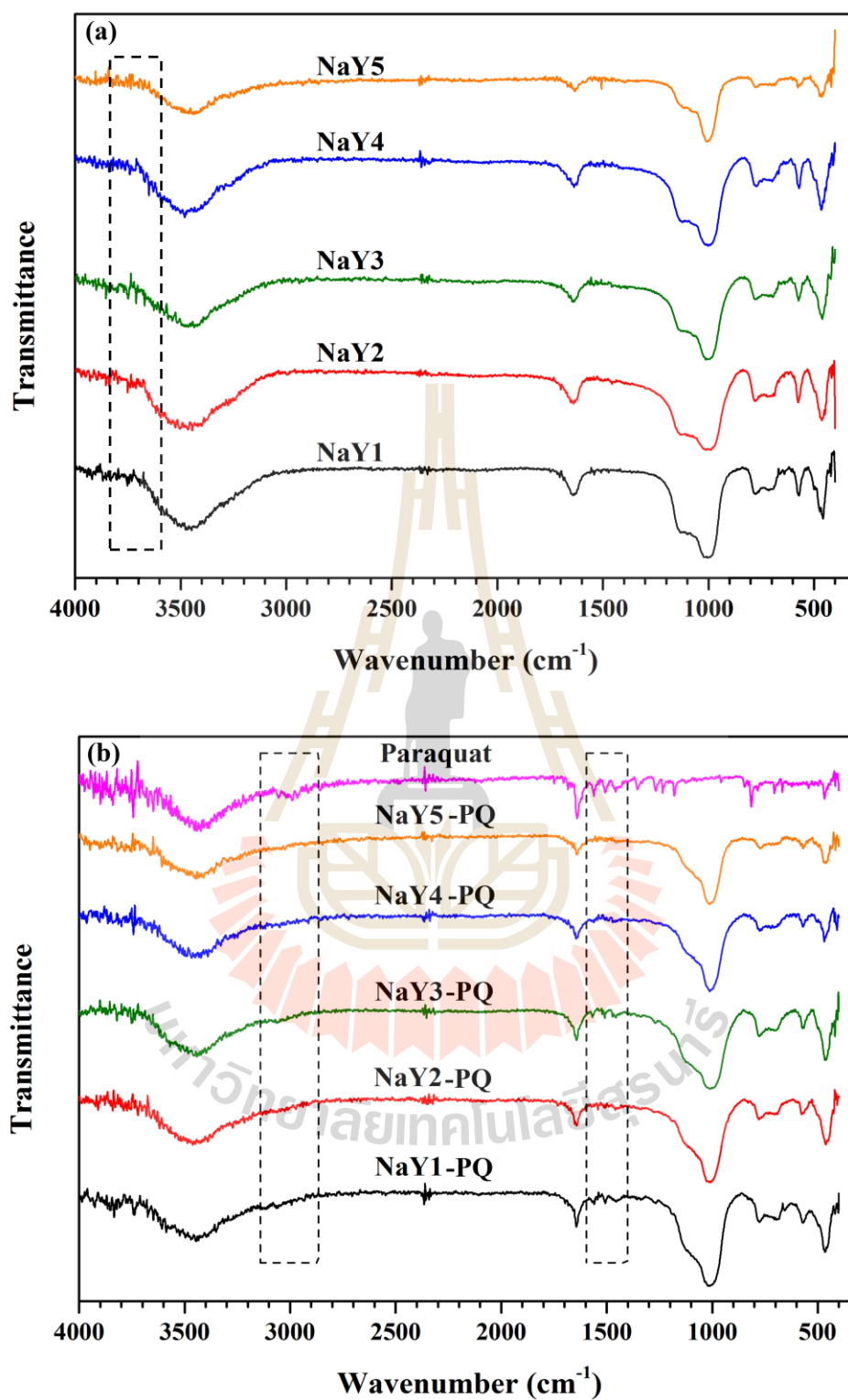


**Figure 4.4** Nitrogen adsorption-desorption isotherm of (a) NaY with various Si/Al ratio and (b) paraquat adsorbed NaY.

#### 4.3.5 Basicity of NaY

The CO<sub>2</sub>-TPD profiles of NaY samples are shown in Figure 4.5. All NaY samples show one peak between 190 and 370 °C contributing to a weak basicity (Rakmae et al., 2016). The basicity of NaY samples is summarized in Table 4.2. NaY1 with the higher Si/Al ratio (lower Al content) has the highest basicity.

**Table 4.2** Basicity amount of NaY samples.

Adsorbent	Basicity amount (mmol/g)			Total
	100-200 °C	200-400 °C	400-600 °C	
NaY1 (-20% Al)	0.030	0.210	0.034	0.274
NaY2 (-10% Al)	0.018	0.202	0.032	0.252
NaY3 Normal	0.013	0.180	0.029	0.222
NaY4 (+10% Al)	0.012	0.175	0.025	0.212
NaY5 (+20% Al)	0.010	0.158	0.024	0.192

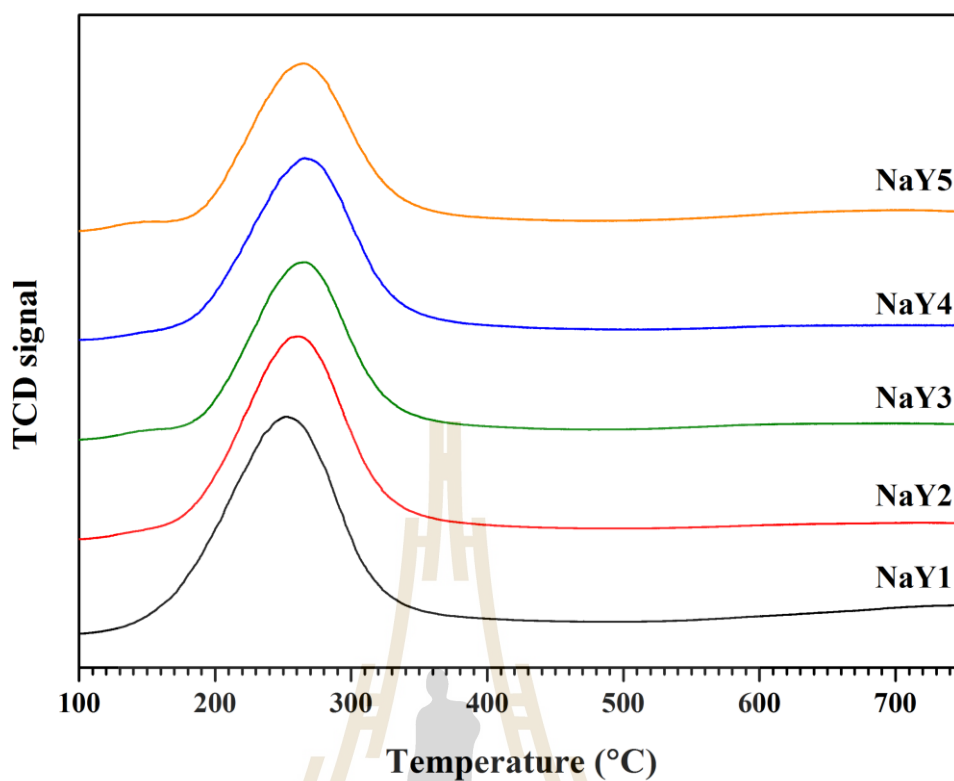


**Figure 4.5** TCD signal of NaY with various Si/Al.

#### 4.4 Paraquat adsorption

The amount of paraquat adsorbed on all zeolite NaY adsorbents at various equilibrium concentrations are shown in Figure 4.6. The amount of paraquat adsorbed on all NaY adsorbents increases sharply at very low equilibrium concentrations implying that paraquat adsorption on these adsorbents are chemisorption. The isotherms of paraquat adsorbed on NaY samples based on Giles classification are class H (high affinity) sub-group 2 which is a strong adsorption (Giles et al., 1960). The adsorption curve tends to be a plateau indicating a formation of paraquat monolayer on the adsorbent surface. The similar adsorption behavior is reported on zeolite NaY (Rongchapo et al., 2013) and zeolite NaX (Rongchapo et al., 2015).

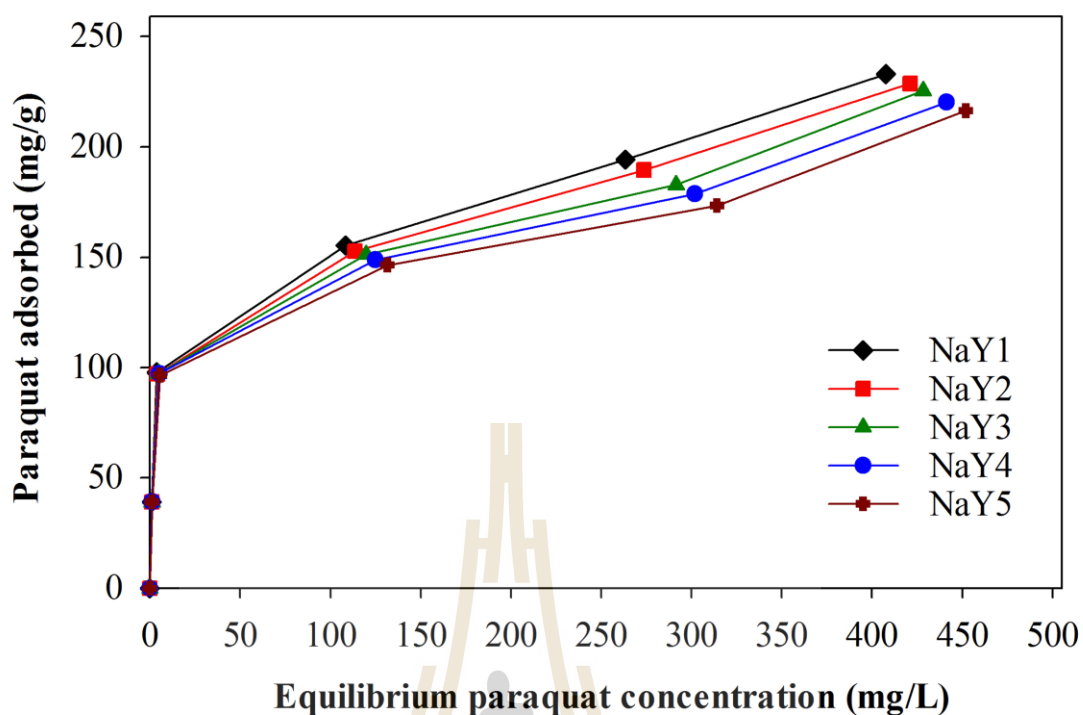


**Figure 4.6** Adsorption isotherm of paraquat on Mt and modified Mt samples.

The amount of paraquat adsorbed is different at high paraquat concentration. This may be because paraquat adsorbs on NaY by ion exchange with  $\text{Na}^+$  according to XRD results, the  $I_{(220)}/I_{(311)}$  changed after paraquat adsorption (Rongchapo et al., 2017). Moreover, paraquat probably adsorbs by hydrophobic adsorption. Osakoo et al., (2017) propose that C and N atoms in paraquat molecules interacted with oxygen atom on NaY-SBA-15 composite.

The adsorption of paraquat on NaY samples follows Langmuir isotherms indicating a monolayer adsorption. The Langmuir parameters are summarized in Table 4.3. The adsorption of paraquat on NaY1 had the highest  $K_L$  values indicate that the highest affinity of paraquat molecules to the binding sites (Giles et al., 1960). The maximum adsorption capacity ( $q_m$ ) of the adsorbents on NaY1 with the lower Al

content is the highest (233 mg/g-adsorbent) followed by NaY2, NaY3, NaY4 and NaY5. Although NaY1 has the lowest surface area, it has the highest adsorption capacity. Paraquat dication could ion exchange with cation of zeolite (Rongchapo et al., 2013). The exchange capacity depends on Si/Al ratio. When an Al atom is present in the zeolite framework, a negative charge is generated and the balancing cation is required. However, the lower aluminium content has the highest capacity. The result may be because the high basicity of NaY1. This corresponded to the effect of pH on paraquat adsorption. The lower amount adsorbed at the lower pH indicates a competition between proton and paraquat to the adsorption sites. A similar effect is reported on adsorption of paraquat on silica (Brigante and Avena, 2014). Another reason may be the high hydrophobicity of NaY1. This similar behavior is reported on NaY/SBA-15 composite (Osakoo et al., 2017).

**Table 4.3** Langmuir parameters of paraquat adsorption on NaY with various Si/Al ratio.

Adsorbent	Langmuir parameters		
	$q_m$ (mg/g)	$K_L$ (L/mg)	$R^2$
NaY1 (-20% Al)	233	0.0462	0.9771
NaY2 (-10% Al)	227	0.0445	0.9760
NaY3 Normal	222	0.0435	0.9721
NaY4 (+10% Al)	213	0.0438	0.9724
NaY5 (+20% Al)	208	0.0423	0.9696

## 4.5 Conclusions

High purity of FAU Y is successfully synthesized from rice husk silica by using hydrothermal method. Si/Al ratio of the obtained FAU zeolites is in the range of 2.1-2.4 and particle sizes of 100-300 nm. The surface areas of zeolite NaY samples are between 789 and 856 m<sup>2</sup>/g. The highest Si/Al ratio (lower Al content) of FAU sample has the highest basicity (0.274 mmol/g). All FAU samples can be used as adsorbents for paraquat. The adsorption of paraquat on NaY samples follows Langmuir isotherm. The capacity of the adsorbents is in the range of 210-240 mg/g-adsorbent. FAU sample with the Si/Al ratio 2.4 has the higher adsorption capacity. The surface areas of the FAU samples decrease from about 800 to about 30 m<sup>2</sup>/g indicating that paraquat adsorbs in the cavity of the zeolite.

## 4.6 References

- Baba, T., Sawada, H., Takahashi, T., and Abe, M. (2002). Chemisorption study of hydrogen and methane by <sup>1</sup>H MAS NMR and conversion of methane in the presence of ethylene on Ag-Y zeolite. **Applied Catalysis A. General**. 231: 55-63.
- Boparai, H. K., Joseph, M., and O'Carroll, D. M. (2011). Kinetics and thermodynamics of cadmium ion removal by adsorption onto nanozerovalent iron particles. **Journal of Hazardous Materials**. 186: 458-465.
- Brigante, M. and Avena, M. (2014). Synthesis, characterization and application of a hexagonal mesoporous silica for pesticide removal from aqueous solution. **Microporous and Mesoporous Materials**. 191: 1-9.

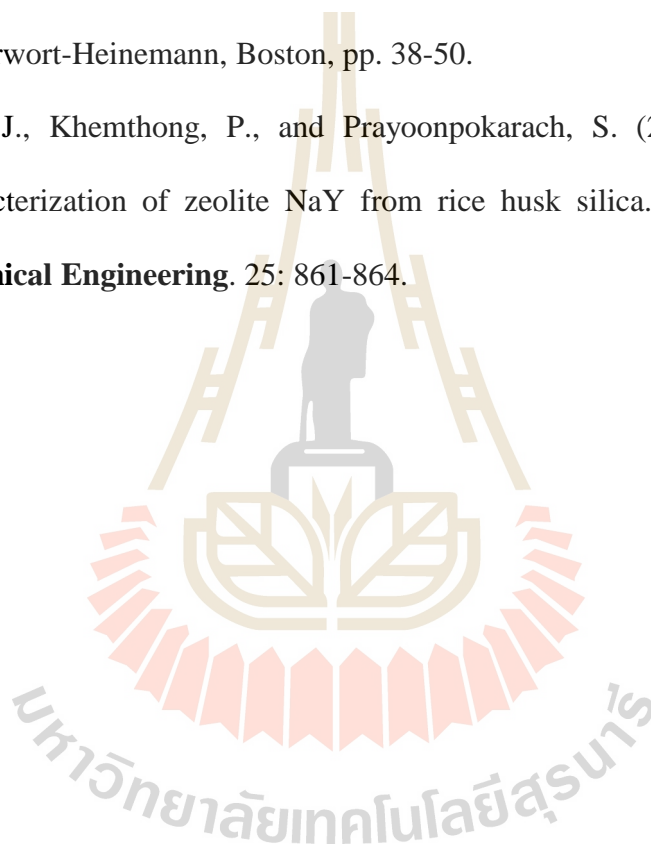
- Cundy, C. S. and Cox, P. A. (2005). The hydrothermal synthesis of zeolites: Precursors, intermediates and reaction mechanism. **Microporous and Mesoporous Materials**. 82: 71-78.
- Giles, C.H., Macewan, T.H., Nakhwa, S.N., and Smith, D. (1960). Study in adsorption Part XI. A system of classification of solution adsorption isotherm, and its use in diagnosis of adsorption mechanism and in measurement of specific surface areas of solids. **Journal of the Chemical Society**. 4: 3973-3993.
- Grand, J., Talapaneni, S. N., Vicente, A., Fernandez, C., Dib, E., Aleksandrov, H. A., Vayssilov, G. N., Retoux, R., Boullay, P., Gilson, J.-P., Valtchev, V., and Mintova, S. (2017). One-pot synthesis of silanol-free nanosized MFI zeolite. **Nature Materials**. 16: 1010-1015.
- Ibrahim, K. M. and Jbara, H. A. (2009). Removal of paraquat from synthetic wastewater using phillipsite-faujasite tuff from Jordan. **Journal of Hazardous Materials**. 163: 82-86.
- Khemthong, P., Klysubun, W., Prayoonpokarach, S., and Wittayakun, J. (2010). Reducibility of cobalt species impregnated on NaY and HY zeolites. **Materials Chemistry and Physics**. 121(1-2): 131-137.
- Kaduk, J. and Faber, J. (1995). Crystal structure of zeolite y as a function of ion exchange. **Rigaku Journal**. 12: 14-34.
- Kozlov A, Asakura K., and Iwasawa, Y. (1998). Synthesis and characterization of vanadium (IV) complexes in NaY zeolite supercages. **Microporous Mesoporous Materials**. 21: 571-579.



- Liou, T. H. (2004). Preparation and characterization of nano-structured silica from rice husk. **Materials Science and Engineering A**. 364: 313-323.
- Lutz, W. (2014). Zeolite Y: Synthesis, modification, and properties-A case revisited. **Advances in Materials Science and Engineering**. 2014: 1-20.
- Mohamed, R. M., Mkhallid, I. A., and Barakat, M. A. (2015). Rice husk ash as a renewable source for the production of zeolite NaY and its characterization. **Arabian Journal of Chemistry**. 8: 48-53.
- Morales-Pacheco, P., Domínguez, J.M, Bucio, L., Alvarez, F., Sedran, U., and Falco, M. (2011). Synthesis of FAU(Y)- and MFI(ZSM5)-nanosized crystallites for catalytic cracking of 1,3,5-triisopropylbenzene. **Catalysis Today**. 166: 25-38.
- Nakayama, M., Yano, J., Nakaoka, K., and Ogura, K. (2003). Spectroscopic studies on the incorporation of polypyrrole into zeolite channels. **Synthetic Metal**. 138(3): 419-422.
- Nur, H., Manan, A. F. N. A., Wei, L., Muhid, M. N. M., and Hamdan, H. (2005). Simultaneous adsorption of a mixture of paraquat and dye by NaY zeolite covered with alkylsilane. **Journal of Hazardous Materials**. B117: 35-40.
- Osakoo, N., Pansakdanon, C., Sosa, N., Deekamwong, K., Keawkumay, C., Rongchapo, W., Prayoonpokarach, S., and Wittayakun, J. (2017). Characterization and comprehension of zeolite NaY/mesoporous SBA-15 composite as adsorbent for paraquat. **Materials Chemistry and Physics**. 193: 470-476.
- Petkowicz, D. I., Rigo, R. T., Radtke, C., Pergher, S. B., and Santos, J. H. Z. (2008). Zeolite NaA from Brazilian chrysotile and rice husk. **Microporous and Mesoporous Materials**. 116: 548-554.

- Rakmae, S., Keawkumay, C., Osakoo, N., Montalbo, K. D., de Leon, R. L., Kidkhunthod, P., Chanlek, N., Roessner, F., Prayoonpokarach, S., and Wittayakun, J. (2016). Realization of active species in potassium catalysts on zeolite NaY prepared by ultrasound-assisted impregnation with acetate buffer and improved performance in transesterification of palm oil. **Fuel**. 184: 512-517.
- Rongchapo, W., Deekamwong, K., Loiha S., Prayoonpokarach, S., and Wittayakun, J. (2015). Paraquat adsorption on NaX and Al-MCM-41. **Water Science and Technology**. 71: 1347-1353.
- Rongchapo, W., Sophiphun, O., Rintramee, K., Prayoonpokarach, S., and Wittayakun, J. (2013). Paraquat adsorption on porous materials synthesized from rice husk silica. **Water Science and Technology**. 68: 863-869.
- Saceda, J. J. F., de Leon, R. L., Rintramee, K., Prayoonpokarach, S., and Wittayakun, J. (2011). Properties of silica from rice husk and rice husk ash and their utilization for zeolite Y synthesis. **Química Nova**. 34: 1394-1397.
- Singh, N. (2009). Adsorption of herbicides on coal fly ash from aqueous solutions. **Journal of Hazardous Materials**. 168: 233-237.
- Su, F., Lu, C., Kuo, S. C., and Zeng, W. (2010). Adsorption of CO<sub>2</sub> on amine functionalized Y-type zeolites. **Energy Fuels**. 24: 1441-1448.
- Suntres, Z. E. (2002). Role of antioxidants in paraquat toxicity. **Toxicology**. 180: 65-77.
- Tan, G. and Xiao, D. (2009). Adsorption of cadmium ion from aqueous solution by ground wheat stems. **Journal of Hazardous Materials**. 164: 1359-1363.

- Tan, W. C., Yap, S. Y., Matsumoto, A., Othman, R., and Yeoh, F. Y. (2011). Synthesis and characterization of zeolites NaA and NaY from rice husk ash. **Adsorption**. 17: 863-868.
- Treacy, M. M. J., Higgins, J. B. (2007). **Collection of Simulated XRD Powder Patterns for Zeolites**. 5<sup>th</sup> ed., IZA, Elsevier, Amsterdam, ISBN 0444530673.
- Thomas, W. J. and Crittenden, B. (1998). **Adsorption Technology and Design**. Butterworth-Heinemann, Boston, pp. 38-50.
- Wittayakun, J., Khemthong, P., and Prayoonpokarach, S. (2008). Synthesis and characterization of zeolite NaY from rice husk silica. **Korean Journal of Chemical Engineering**. 25: 861-864.



# CHAPTER V

## EFFECT OF ALUMINIUM SOURCE AND WATER CONTENT ON TEXTURAL PROPERTY AND MORPHOLOGY OF FAUJASITE NANOZEOLITE

### Abstract

The objective of this study is to synthesize FAU type zeolite by hydrothermal method with different aluminium source and amount of water. The particle size of FAU crystals synthesized from sodium aluminate is smaller than that from aluminium powder. Moreover, the smaller size is produced from the synthesis with less water content. Nano-sized FAU crystals are obtained from the synthesis with sodium aluminate but with the presence of GIS impurity. Thus, further syntheses with sodium aluminate are performed using different amount of water. The amount of water is increased in the following order: Y1-180 > Y1-140 > Y1-92. The SEM images of the FAU samples show that Y1-140 and Y1-92 have nano-sized crystals. However, the XRD patterns indicate that only Y1-140 nanocrystals have pure FAU phase with Si/Al ratio of 1.64, surface area of 701 m<sup>2</sup>/g and micropore volume of 0.30 cm<sup>3</sup>/g.

## 5.1 Introduction

FAU zeolite has a unit structure containing sodalite cages which arrange to form supercages (11.0 x 13.0 Å) with large pore (7.4 x 7.4 Å). FAU zeolites have high potential for various applications such as catalysis, sensing, ion exchange, and absorption for separation of various chemical species (Rasouli et al., 2012; Sharma, 2015; Nakrani et al., 2017). The potential FAU zeolite can be improved by decreasing the crystal to nano-size. The smaller size decreases diffusion path lengths, increases external surface area and increases surface reactivity (Nakrani et al., 2017).

Nanocrystalline FAU is nanosized crystals with a large pore volume, external surface area with high external surface acid sites. It shows a high activity and good stability (Rasouli et al., 2012; Awala et al., 2015). There are several parameters in the synthesis of nanocrystalline zeolites, for example the silica source, directing agent organic structure, gel composition, reaction temperature, aging time and crystallization time (Mintova and Valtchev, 1999; Morales-Pacheco et al., 2011; Mintova and Ng, 2013).

Mintova et al. (1999, 2003) synthesized colloidal crystals of FAU zeolites with a mean crystal size between 40 to about 80 nm using 15-crown-5 ether as a co-temple. Holmberg et al. (2003, 2004) reported the synthesis of small FAU using tetramethylammonium bromide (TMABr) as a co-temple to produce the crystals with mean diameter of 32-120 nm. Li et al. (2002) studied nucleation and crystal growth kinetics of nanosized FAU crystallites from clear solutions. The influence of the growth limiting nutrient ( $\text{Na}^+$ ) on the crystallization process is observed. Valtchev and Bozhilov (2004) also studied the formation of FAU zeolites at room temperature using electron microscope. Song et al. (2005) synthesized nanocrystalline FAU Y

with crystal sizes of 23 and 50 nm. Larsen (2007) reported the synthesis, characterization and applications of FAU Y zeolites with crystal sizes of 50 nm. Morales-Pacheco et al. (2011) reported the synthesis of FAU zeolite nanocrystals from clear solutions using tetramethylammonium hydroxide and tetramethylammonium bromide as templates. The mean crystal sizes between 20 and 40 nm are obtained. The presence of Brønsted and Lewis acid sites on the surface of nanocrystalline FAU zeolite relates to the zeolite structure, structural aluminum content and pore diameters. Awala et al. (2015) reported the synthesis of FAU Y nanocrystals by hydrothermal method with the nucleation of nanosized FAU crystallites from clear solutions at low crystallization temperature. The obtained FAU nanozeolite showed the nanocrystal sizes between 10-50 nm with a narrow particle size distribution, high crystalline yields (above 80%), micropore volumes ( $0.30 \text{ cm}^3/\text{g}$ ) comparing to micrometre-sized crystals, Si/Al ratios of 2.1 and excellent thermal stability. These properties indicated the many potential applications in areas of catalysis, separation, environmental remediation, decontamination and drug delivery (Awala et al., 2015).

In Chapter IV, zeolite FAU (NaY) is synthesized with various Si/Al (2.15-2.40). The crystalline sizes are ranged from 200 to 500 nm which are not yet considered nanosized (<100 nm). The impact of the particle size over the physicochemical properties become more pronounced when the crystallites are smaller than 50 nm and even below 30 nm (Mintova et al., 2016). Small crystals exhibit greater catalytic activity because their relatively small size allows a faster diffusion of reactants into the catalyst (Salou et al., 2001). Therefore, the purpose of this work is to explore the synthesis of nanosized FAU Y zeolite. The synthesis of

FAU Y is performed using different aluminium sources including aluminium powder and sodium aluminate. The influence of water contents is also studied.

## 5.2 Experiment

### 5.2.1 Synthesis of Y1-140 and Y1-180

FAU Y zeolites are synthesized by varying water content in gel composition to  $140\text{H}_2\text{O}$  and  $180\text{H}_2\text{O}$ . The obtained samples are named Y1-140 and Y1-180, respectively. The gel molar compositions of Y1-140 and Y1-180 are as follows :

The sample Y1-140 is prepared from a turbid precursor suspension with the following chemical composition:  $7\text{Na}_2\text{O} : 0.8\text{Al}_2\text{O}_3 : 10\text{SiO}_2 : 140\text{H}_2\text{O}$ .

The sample Y1-180 is synthesized from a clear precursor suspension with a molar composition:  $7\text{Na}_2\text{O} : 0.8\text{Al}_2\text{O}_3 : 10\text{SiO}_2 : 180\text{H}_2\text{O}$ .

FAU Y zeolite with different aluminium sources and amounts of water is synthesized by hydrothermal method according to Awala et al. (2016). The starting mixtures are synthesized from solution A (sodium aluminate solution) and solution B (sodium silicate solution). Amounts of materials for the synthesis of FAU Y using the different amounts of water with aluminium powder and sodium aluminate as aluminium sources are shown in Table 5.1 and 5.2, respectively.

**Table 5.1** Amounts of materials for the synthesis of FAU Y (Y1-180 and Y1-140) with aluminium powder.

Materials	Y1-140	Y1-180
<b>Solution A (NaAl<sub>2</sub>O<sub>3</sub>)</b>		
NaOH	2.17	2.17
H <sub>2</sub> O	4.70	7.67
Aluminium powder	0.24	0.24
<b>Solution B (Na<sub>2</sub>SiO<sub>3</sub>)</b>		
NaOH	0.95	0.95
H <sub>2</sub> O	1.57	2.53
Ludox HS-40	11.11	11.11

**Table 5.2** Amounts of materials for the synthesis of FAU Y (Y1-180 and Y1-140) with sodium aluminate (NaAlO<sub>2</sub>).

Materials	Y1-140	Y1-180
<b>Solution A (NaAl<sub>2</sub>O<sub>3</sub>)</b>		
NaOH	2.00	2.00
H <sub>2</sub> O	4.67	7.67
NaAlO <sub>2</sub>	0.81	0.81
<b>Solution B (Na<sub>2</sub>SiO<sub>3</sub>)</b>		
NaOH	0.88	0.88
H <sub>2</sub> O	1.56	2.56
Ludox HS-40	11.11	11.11



### 5.2.2 Synthesis of Y1-180 and Y1-140 using aluminium powder

FAU Y zeolites (Y1-180 and Y1-140 using aluminium powder) are synthesized as follows: initially, solution A is prepared by dissolving aluminium powder (325 mesh, 99.5%, Alfa Aesar) in sodium hydroxide (97%, Sigma-Aldrich) and double distilled (DD) H<sub>2</sub>O, slowly added of aluminium powder. The mixture is stirred until clear (3 h). Solution B is prepared by dissolving Ludox HS-40 (40 wt. % SiO<sub>2</sub>, pH=9.8, Aldrich) in sodium hydroxide and DD H<sub>2</sub>O. A turbid solution is obtained after shaking. In order to get clear suspension, the container is placed in an oven at 90 °C for 5-10 min.

### 5.2.3 Synthesis of Y1-180 and Y1-140 using sodium aluminate

FAU Y zeolites (Y1-180 and Y1-140 using sodium aluminate) are synthesized as follows: initially, solution A is prepared by dissolving sodium aluminate (Al<sub>2</sub>O<sub>3</sub> ~ 50-56 wt. %, Na<sub>2</sub>O ~ 40-45 wt. %, Aldrich) in sodium hydroxide and DD H<sub>2</sub>O. The mixture is stirred until clear (1 h). Solution B is prepared by dissolving Ludox HS-40 in sodium hydroxide and DD H<sub>2</sub>O. A turbid solution is obtained after shaking. In order to get clear suspension, the container is placed in an oven at 90 °C for 5-10 min.

### 5.2.4 Aging and crystallization

Solution A is added drop wise under vigorously stirring to the solution B, during the mixing, solution B is kept in ice. The resulting clear suspension of Y1-180 and Y1-140 is aged by shaking for 48 h at room temperature. Hydrothermal crystallization is performed at 90 °C for rapid crystallization time of 4 h. The solid products from all syntheses are recovered by centrifugation (20,000 rpm for 20 min) followed by dispersion in double distilled water, this procedure is repeated several

times until the final colloidal suspensions reached pH of 7 and then freeze-dried prior further characterization.

## **5.3 Characterization**

### **5.3.1 X-ray diffraction (XRD) analysis**

Powder samples are analyzed using a PANalytical X'Pert Pro diffractometer with CuK $\alpha$  monochromatized radiation ( $\lambda = 1.5418 \text{ \AA}$ ). The samples are scanned in the range  $3\text{-}50^\circ 2\theta$  with a step size of  $0.02^\circ$ .

### **5.3.2 N<sub>2</sub> adsorption-desorption analysis**

Nitrogen adsorption-desorption isotherms are obtained from a Micromeritics ASAP 2020 volumetric adsorption analyzer. Samples are degassed at  $250^\circ\text{C}$  under vacuum overnight prior to the measurement. The external surface area and micropore volume are estimated by alpha-plot method using Silica-1000 ( $22.1 \text{ m}^2\text{g}^{-1}$  assumed) as a reference. The micropore and mesopore size distributions of solids are extracted from adsorption branch by the Nonlocal Density Functional Theory (NLDFT) and from the desorption branch using the Barret-Joyner-Halenda (BJH) algorithm, respectively.

### **5.3.3 Scanning electron microscopy (SEM)**

Solid samples are dispersed on carbon tape and then all samples are coated with Pt. The morphology of solids is determined by a Scanning electron microscopy (SEM) using a MIRA LMH operated at 30 kV.

### **5.3.4 Dynamic light scattering (DLS) analysis**

The hydrodynamic diameters of the FAU Y nanoparticles in the suspensions are determined with a Malvern Zetasizer Nano. The analyses are

performed on samples after purification with a solid concentration of 10 wt.% at pH=8. The back scattering geometry (scattering angle  $173^\circ$ , HeNe laser with 3 mW output power at 632.8 nm wavelength) allows measurements at high sample concentration, since a complete penetration of the incident light through the sample is not required.

### 5.3.5 Chemical analysis

The chemical composition of the FAU samples is determined by inductively coupled plasma (ICP) optical emission spectroscopy using a Varian ICP-OES 720-ES. The samples are prepared by acid digestion method and then diluted to a final volume of 100 mL.

## 5.4 Results and discussion

### 5.4.1 Phase and crystallinity of FAU Y with different aluminium sources

The X-ray diffraction (XRD) patterns of FAU Y zeolites (Y1-180-Alpowder, Y1-180-NaAlO<sub>2</sub>, Y1-140-Alpowder and Y1-140-NaAlO<sub>2</sub>) are shown in Figure 5.1-5.2. All samples show the peaks corresponding to the pure FAU. Sharper peaks of Y1-180-Alpowder and Y1-180-NaAlO<sub>2</sub> illustrated the increase size of its individual particles. Y1-140-Alpowder and Y1-140-NaAlO<sub>2</sub> exhibit broad peaks with intensities similar to micrometre-sized crystals (Awala et al., 2015). The highest intensity of Y1-180-Alpowder corresponded to high crystallinity (as shown in Figure 5.1). Crystallinity of FAU Y samples depends on the type of aluminium source. This may be attributed to the different reactivities of the Al species in the gels formed toward bonding with Si species during the gelation process (Reddy and Song, 1996). In comparison between Y1-180 and Y1-140 with different amounts of water, the

intensity of Y1-180 with high amount of water is higher than that of Y1-140 indicating that crystallinity of FAU Y samples is also depended on water content. This is because the addition of water to the synthetic system affects the solubility of aluminium source and the hydrolysis of inorganic species (Xu et al., 2007).

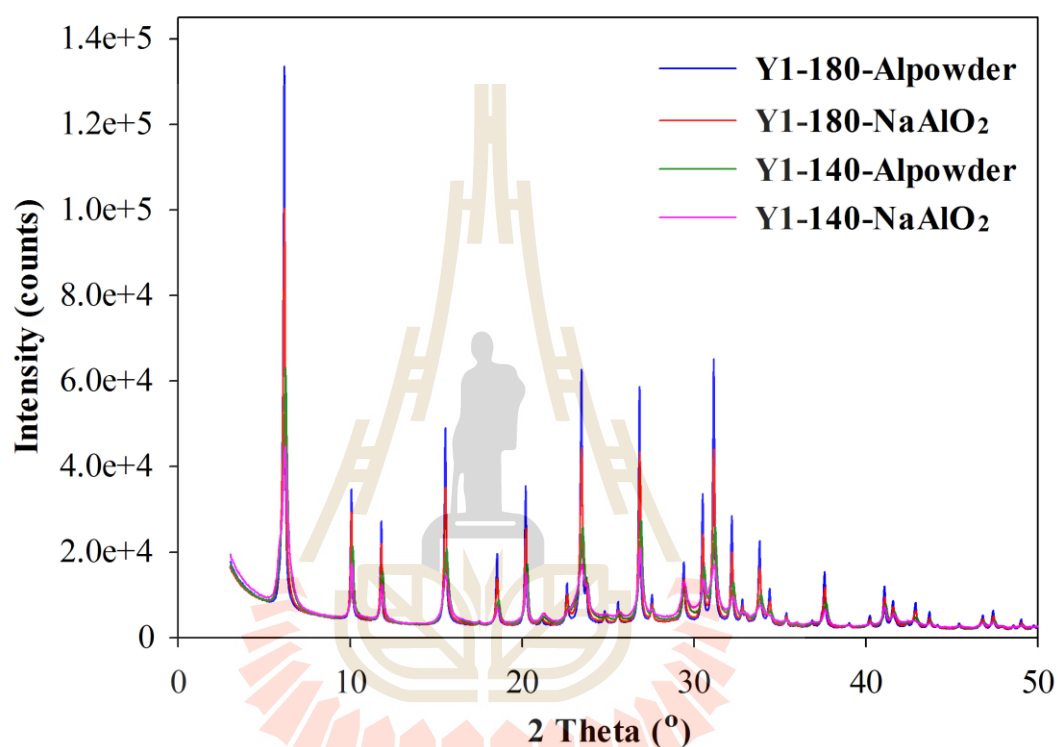


**Figure 5.1** XRD patterns of FAU Y samples with the same scale to compare crystallinity.

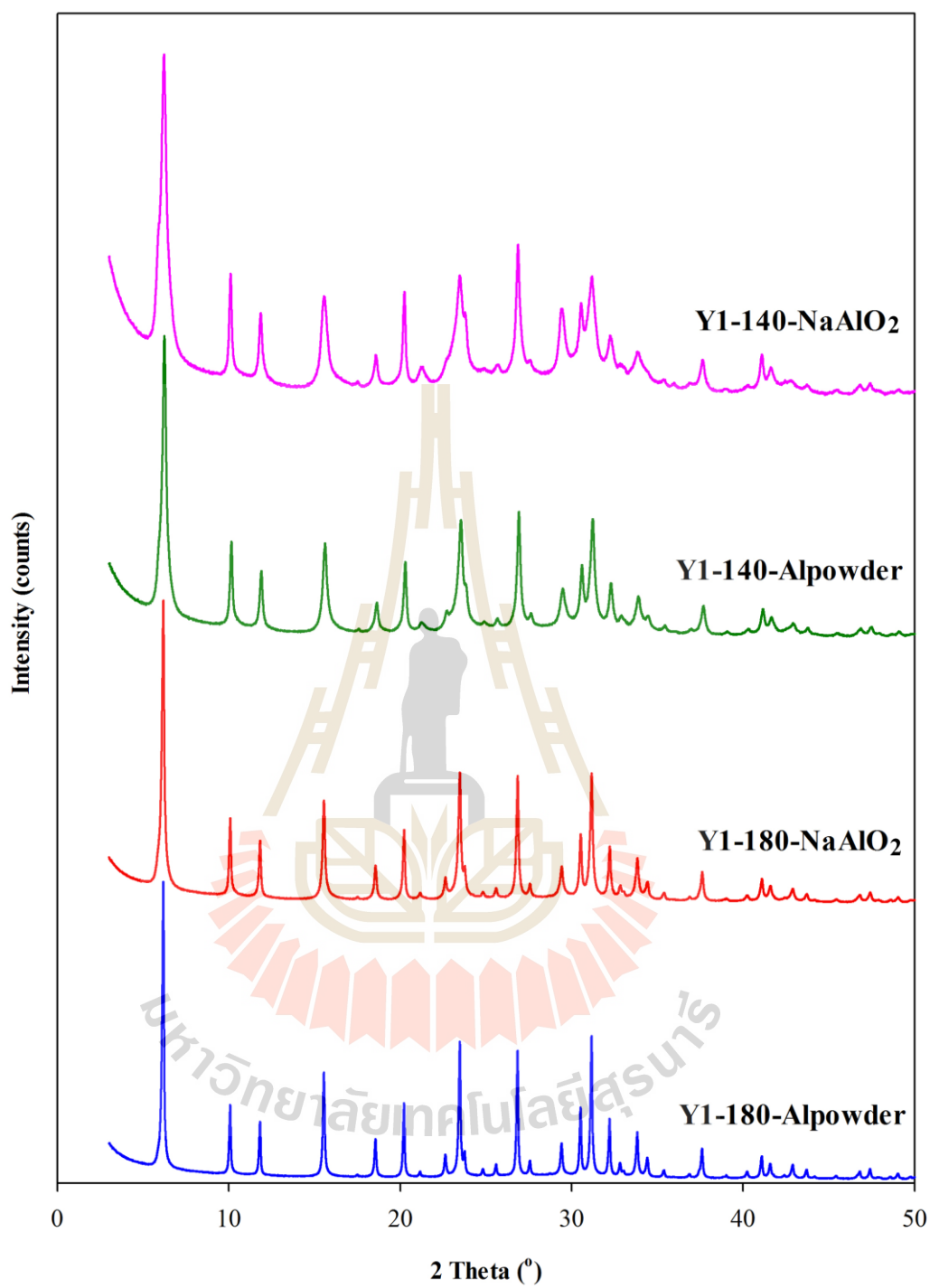


**Figure 5.2** XRD pattern of Y1-180 and Y1-140 with different aluminium sources.

#### 5.4.2 Morphology of FAU Y nanozeolites

The morphology of the FAU Y crystals from SEM is shown in Figure 5.3A-5.3D. The synthesized FAU Y samples have different crystal morphologies. The smallest crystalline sizes are observed for Y1-140-NaAlO<sub>2</sub> sample. The sizes are ranged of 50-100 nm with rectangular and sphere crystalline crystals of FAU Y particles. While Y1-140-Al powder with different aluminium source, crystalline sizes are bigger than those of Y1-140-NaAlO<sub>2</sub>. The sizes are between 100 and 300 nm with the same shapes of crystalline crystals. FAU zeolite synthesized using sodium aluminate has a smaller crystalline size than that of aluminium powder. This is because the acidic radical of aluminum source affects the crystallization (Aly et al., 2011). Similar behavior is also reported on the synthesis of ZSM-5 zeolite by using sodium aluminate, aluminum chloride and aluminum nitrate as aluminium sources. The average crystalline size is in the order: sodium aluminate (78.56 nm) < aluminum nitrate (104.87 nm) < aluminum chloride (112.3 nm) (Aly et al., 2011).

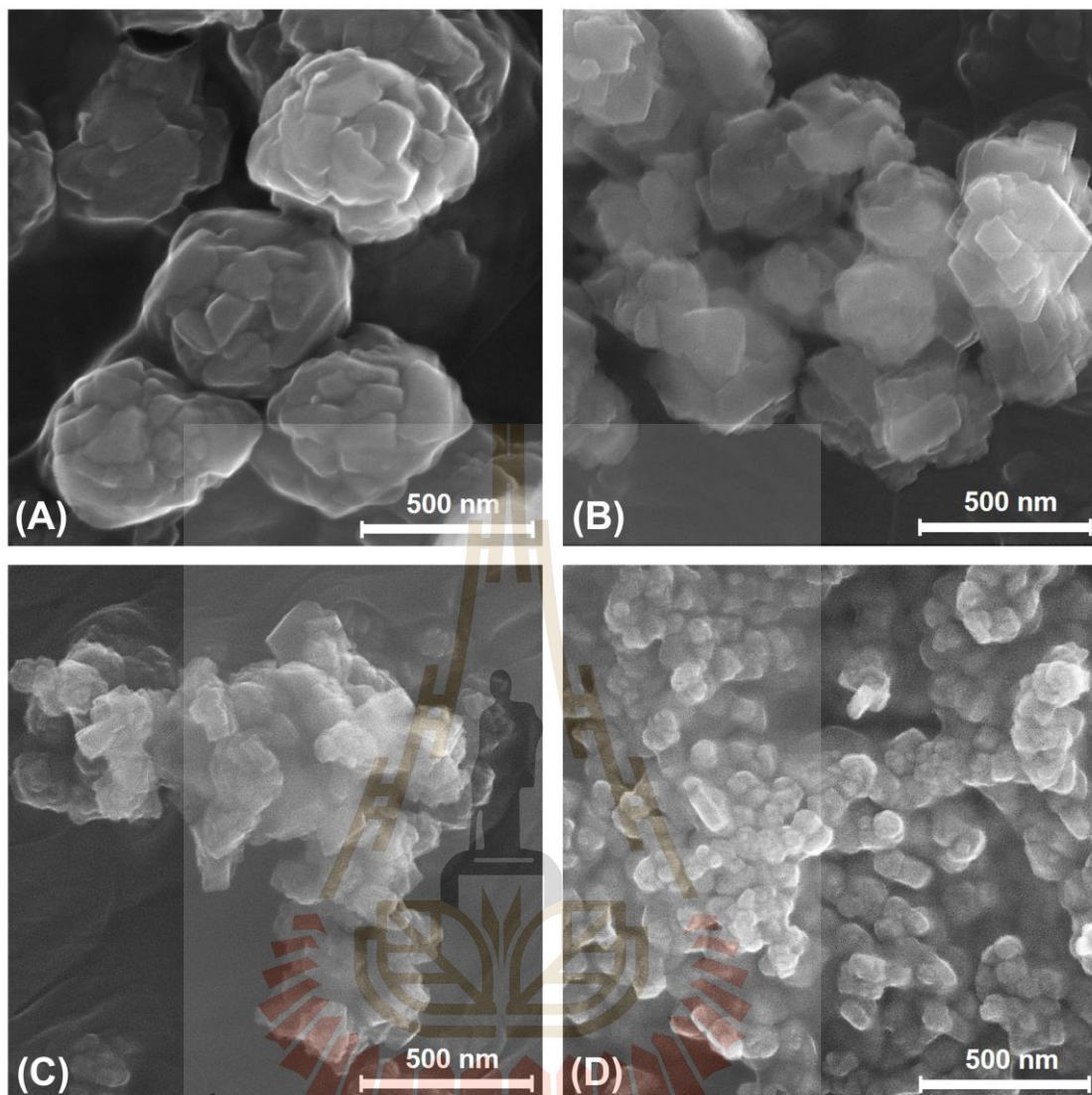


**Figure 5.3** SEM images of Y1-180 and Y1-140 with different aluminium sources

(A) Y1-180-Alpowder, (B) Y1-180-NaAlO<sub>2</sub>, (C) Y1-140-Alpowder  
and (D) Y1-140-NaAlO<sub>2</sub>.

With increasing amount of water in the synthesis of FAU Y zeolite, crystalline sizes of Y1-180-Alpowder and Y1-180-NaAlO<sub>2</sub> are bigger than those of Y1-140-Alpowder and Y1-140-NaAlO<sub>2</sub>. The highly aggregation from rectangular shape to spherical shape of Y1-180-Alpowder and Y1-180-NaAlO<sub>2</sub> crystals is observed. This is because the degree of dilution is increased, crystal size rises and aggregates become increasingly numerous. The product obtained from the most diluted mixture contained primarily crystal aggregates (Mostowicz and Berak, 1985). This behavior is similar to the formation of larger zeolite crystals (400 nm) with high water content of the synthesis FAU nanozeolite (Awala et al., 2015). The crystal sizes are in the range from 300 to 500 nm. The size of the crystals corresponded with the dynamic light scattering (DLS) results are shown in Figure 5.4.

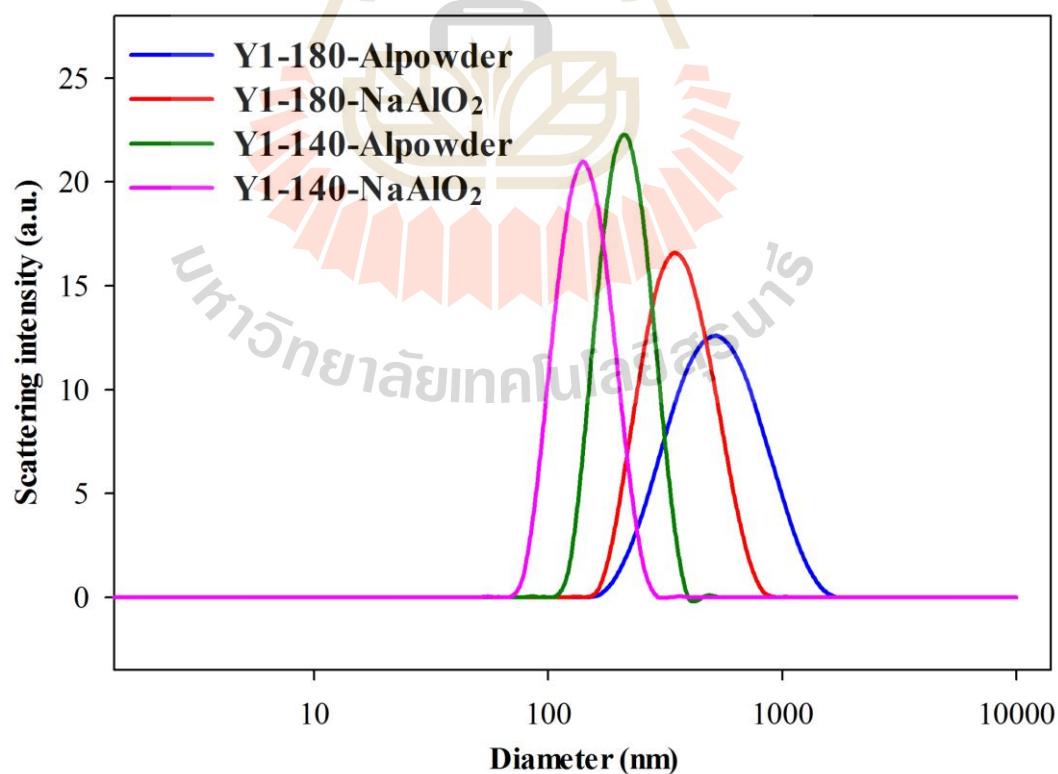


**Figure 5.4** DLS curves of Y1-180 and Y1-140 with different aluminium sources.



### 5.4.3 N<sub>2</sub> adsorption-desorption isotherms of FAU Y zeolite

Nitrogen adsorption-desorption isotherms of FAU Y samples are shown in Figure 5.5. Y1-180-Alpowder and Y1-180-NaAlO<sub>2</sub> exhibit a Type I isotherms with a sharp uptake at low relative pressures followed by horizontal adsorption and desorption branches. In contrast, samples Y1-140-Alpowder and Y1-140-NaAlO<sub>2</sub> showed a mix of Type I and IV isotherms with a H1-type hysteresis. This characteristic corresponded with textural pores formed by the close packing of monodispersed and well-shaped nanosized crystallites (Awala et al., 2015). The total pore volumes for samples Y1-140-Alpowder and Y1-140-NaAlO<sub>2</sub> is 0.47 and 0.53 cm<sup>3</sup>/g (as shown in Table 5.3), respectively, while sample Y1-180-Alpowder and Y1-180-NaAlO<sub>2</sub> have total pore volume of 0.37 and 0.43 cm<sup>3</sup>/g, respectively.

The difference in total pore volume is due to the decrease in particle size from 500 nm to 50 nm. The high micropore volume (0.30 cm<sup>3</sup>/g) of Y1-140-NaAlO<sub>2</sub> with the smallest nanocrystals is similar to template-free nanosized faujasite-type (Awala et al., 2015). Moreover, Y1-140-NaAlO<sub>2</sub> with the smallest nanocrystals has a high external surface area of 138 m<sup>2</sup>/g. The external surface areas of Y1-180-NaAlO<sub>2</sub>, Y1-180-Alpowder and Y1-140-Alpowder are 106, 84 and 43 m<sup>2</sup>/g, respectively. High external surface area of synthesized FAU Y using sodium aluminate with low water content is observed.

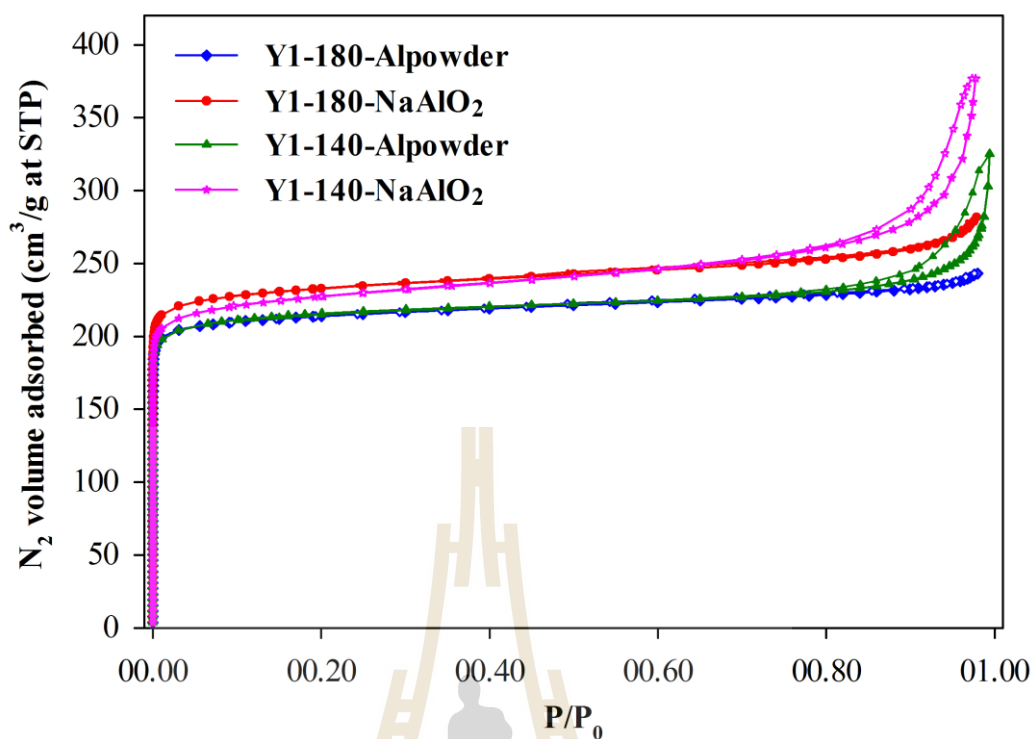


**Figure 5.5**  $N_2$  adsorption-desorption isotherm of Y1-180 and Y1-140 with different aluminium sources.

**Table 5.3** Textural properties of Y1-180 and Y1-140 with different aluminium sources.

FAU Y	Surface area (m <sup>2</sup> /g)	Micropore area (m <sup>2</sup> /g)	External surface area (m <sup>2</sup> /g)	Micropore volume (cm <sup>3</sup> /g)	Total pore volume (cm <sup>3</sup> /g)
Y1-180-Alpowder	654	570	84	0.30	0.37
Y1-180-NaAlO <sub>2</sub>	713	607	106	0.31	0.43
Y1-140-Alpowder	690	647	43	0.32	0.47
Y1-140-NaAlO <sub>2</sub>	701	563	138	0.30	0.53

#### 5.4.4 Chemical composition of FAU Y zeolite

The chemical composition by ICP analysis of Y1-180 and Y1-140 synthesized using aluminium powder and sodium aluminate summarized in Table 5.4. The ICP analysis of samples Y1-180-Alpowder, Y1-180-NaAlO<sub>2</sub> Y1-140-Alpowder and Y1-140-NaAlO<sub>2</sub> revealed that the elemental composition of FAU Y zeolites is not significant difference from those of FAU Y zeolites. The Si/Al ratio of Y1-180 and Y1-140 with different aluminium sources is in the range from 1.69 to 1.74.

**Table 5.4** Chemical composition of Y1-180 and Y1-140 with different aluminium sources.

FAU Y	Atomic (%)			Si/Al
	Na	Si	Al	
Y1-180-Alpowder	9.93	21.59	12.43	1.74
Y1-180-NaAlO <sub>2</sub>	11.10	23.88	13.99	1.71
Y1-140-Alpowder	12.44	26.84	15.53	1.73
Y1-140-NaAlO <sub>2</sub>	11.75	23.76	14.53	1.69

#### 5.4.5 Optimization of water content for FAU Y synthesis

As the synthesis FAU Y zeolite using of aluminium powder and sodium aluminate as aluminium sources with different amounts of water (180H<sub>2</sub>O and 140H<sub>2</sub>O in gel composition), the synthesized FAU Y using sodium aluminate with low water content (140H<sub>2</sub>O) had the smallest nanosized crystals (50-100 nm) with high total pore volume and external surface area. In order to obtain the nanosized crystals smaller than 50-100 nm, the synthesis of FAU Y using sodium aluminate and

lower amount of water ( $92\text{H}_2\text{O}$  in gel composition) is studied. Y1-180 and Y1-140 samples show the diffraction peaks corresponding to pure FAU Y (Figure 5.6). While Y1-92 show additional peaks corresponding to GIS type zeolite. The phase transformation is due to the lower amount of water for FAU Y synthesis. This result suggests that crystallization rate is very fast thus GIS type zeolite is formed. This could be attributed to the low water content in the synthesis accelerated the growth of zeolite crystals (Shirazian et al., 2014).

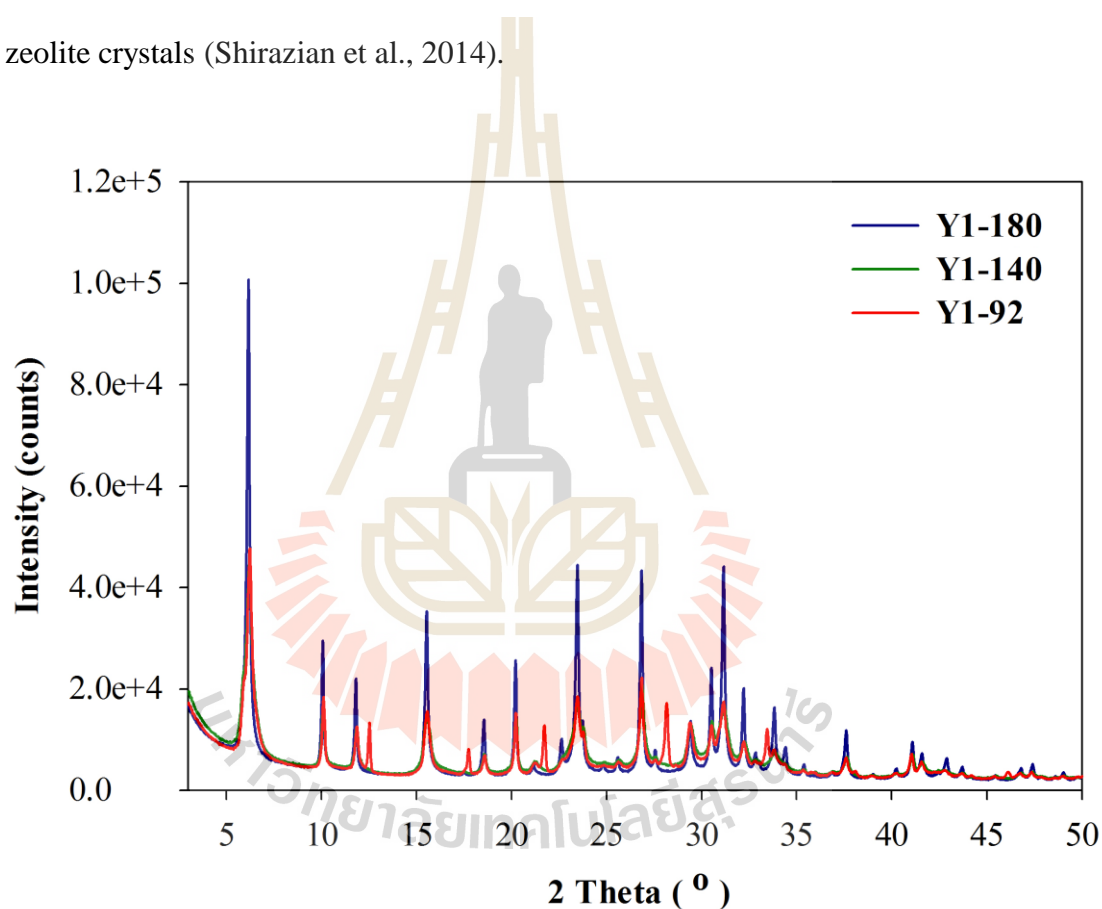


**Figure 5.6** XRD patterns of Y1-180, Y1-140 and Y1-92 using sodium aluminate.

As seen from the SEM images (Figure 5.7), Y1-92 show the smallest crystal sizes in the range from 50 to 100 nm with rectangular shape. However, the crystal sizes and the shape of Y1-92 are similar to those of Y1-140. Therefore, these observations could be summarized that the optimum water content for FAU Y synthesis using sodium aluminate is  $140\text{H}_2\text{O}$ .

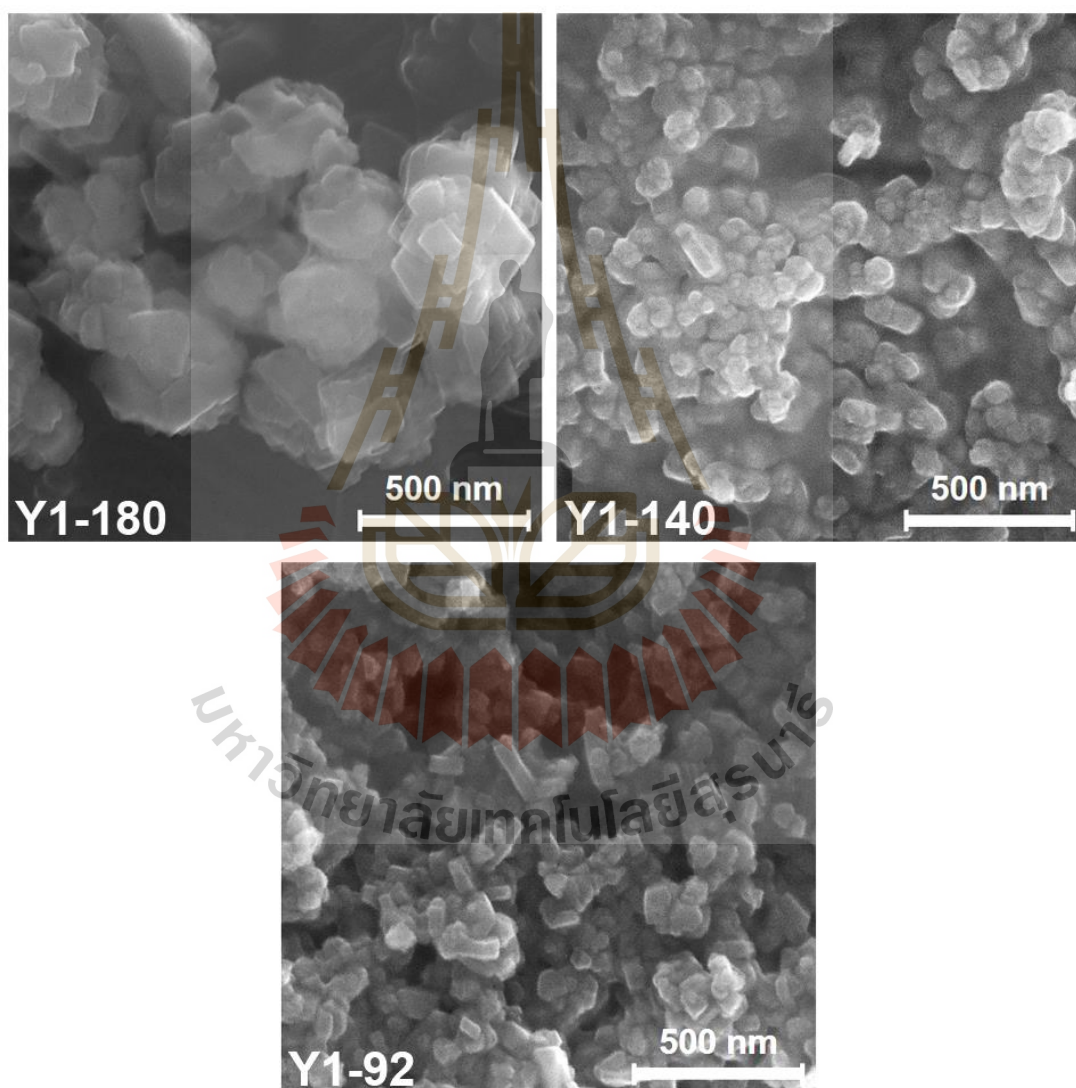


**Figure 5.7** SEM images of Y1-180, Y1-140 and Y1-92 using sodium aluminate.

## 5.5 Conclusions

The effect of aluminium sources (aluminium powder and sodium aluminate) and water contents on the textural properties and morphologies of FAU Y nanozeolite is investigated. FAU Y nanozeolite is successfully synthesized using hydrothermal method with the rapid crystallization time of 4 h. The smallest crystalline sizes are observed for Y1-140-NaAlO<sub>2</sub> sample (synthesis using sodium aluminate with lower content of water). The sizes are ranged of 50-100 nm with rectangular and sphere crystalline crystals of FAU Y particles. The nanocrystals showed the porosity with highly crystalline FAU type zeolites. The Si/Al ratio of Y1-180 and Y1-140 with different aluminium sources is in the range from 1.69 to 1.74. With decreasing water content to 92H<sub>2</sub>O, FAU Y zeolite is transformed to GIS-type zeolite. The optimum water content for the synthesis of FAU Y using sodium aluminate is 140H<sub>2</sub>O.

## 5.6 References

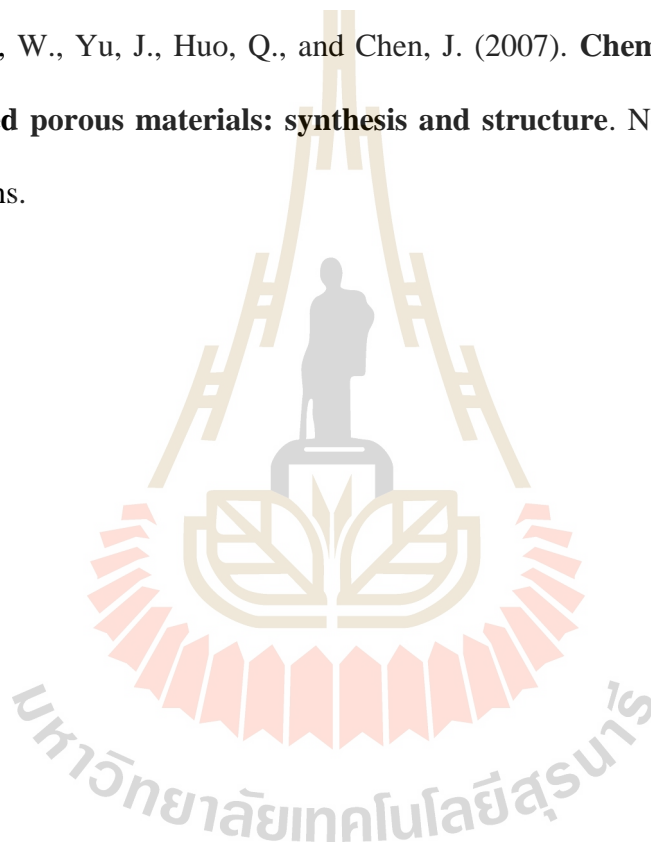
- Aly, H. M., Moustafa, M. E., and Abdelrahman, E. A. (2013). Influence of aluminum source on the synthesis of nanosized ZSM-5 zeolite. **Der Chemica Sinica**. 4: 68-72.
- Awala, H., Gilson, J.-P., Retoux, R., Boullay, P., Goupil, J.-M., Valtchev, V., and Mintova, S. (2015). Template-free nanosized faujasite-type zeolites. **Nature Materials**. 14: 447-451.
- Holmberg, B. A., Wang, H., Norbeck, J. M., and Yan, Y. (2003). Controlling size and yield of zeolite Y nanocrystals using tetramethylammonium bromide. **Microporous and Mesoporous Materials**. 59: 13-28.

- Holmberg, B. A., Wang, H., and Yan, Y. (2004). High silica zeolite Y nanocrystals by dealumination and direct synthesis. **Microporous and Mesoporous Materials**. 74: 189-198.
- Larsen, S. C. (2007). Nanocrystalline zeolites and zeolite structures: Synthesis, characterization, and applications. **Journal of Physical Chemistry C**. 111: 18464-18474.
- Li, Q., Creaser, D., and Sterte, J. (2002). An investigation of the nucleation/crystallization kinetics of nanosized colloidal faujasite zeolites. **Chemistry of Materials**. 14: 1319-1324.
- Mintova, S., Grand, J., and Valtchev, V. (2016). Nanosized zeolites: Quo Vadis? **Comptes Rendus Chimie**. 19: 183-191.
- Mintova, S. and Ng, E. P. (2013). Zeolite Nanoparticles. **Comprehensive Inorganic Chemistry II (Second Edition): From Elements to Applications**. 5: 285-302.
- Mintova, S. and Valtchev, V. (1999). Synthesis of nanosized FAU-type zeolite. **Studies in Surface Science and Catalysis**. 125: 141-148.
- Mintova, S., Valtchev, V., and Bein, T. (2003). Formation of colloidal molecular sieves: Influence of silica precursor. **Colloids and Surfaces A: Physicochemical and Engineering Aspects**. 217: 153-157.
- Morales-Pacheco, P., Alvarez, F., Bucio, L., and Domínguez, J. M. (2009). Synthesis and structural properties of zeolitic nanocrystals II: FAU-type zeolites. **Journal of Physical Chemistry C**. 113: 2247-2255.

- Morales-Pacheco, P., Domínguez, J. M., Bucio, L., Alvarez, F., Sedran, U., and Falco, M. (2011). Synthesis of FAU(Y)- and MFI(ZSM5)-nanosized crystallites for catalytic cracking of 1,3,5-triisopropylbenzene. **Catalysis Today**. 166: 25-38.
- Mostowicz, R. and Berak, J. M. (1985). Factors Influencing the Crystal Morphology of ZSM-5 Type Zeolites. **Studies in Surface Science and Catalysis**. 24: 65-72.
- Nakrani, D., Belani, M., Bajaj, H. C., Somani, R. S., and Singh, P. S. (2017). Concentrated colloidal solution system for preparation of uniform Zeolite-Y nanocrystals and their gas adsorption properties. **Microporous and Mesoporous Materials**. 241: 274-284.
- Rasouli, M., Yaghobi, N., Chitsazan, S., and Sayyar, M. H. (2012). Adsorptive separation of meta-xylene from C<sub>8</sub> aromatics. **Chemical Engineering Research and Design**. 90: 1407-1415.
- Reddy, K. M. and Song, C. (1996). Synthesis of mesoporous molecular sieves: influence of aluminum source on Al incorporation in MCM-41. **Catalysis Letters**. 36: 103-109.
- Sharma, P., Han, M. H., and Cho, C. H. (2015). Synthesis of zeolite nanomolecular sieves of different Si/Al ratios. **Journal of Nanomaterials**. 2015: 1-9.
- Shirazian, S., Parto, S. G., and Ashrafizadeh, S. N. (2014). Effect of water content of synthetic hydrogel on dehydration performance of nanoporous LTA zeolite membranes. **International Journal of Applied Ceramic Technology**. 11: 793-803.



- Song, W., Li, G., Grassian, V. H., and Larsen, S. C. (2005). Development of improved materials for environmental applications: Nanocrystalline NaY zeolites. **Environmental Science and Technology**. 39: 1214-1220.
- Valtchev, V. P. and Bozhilov, K. N. (2004). Transmission Electron Microscopy Study of the Formation of FAU-Type Zeolite at Room Temperature. The **Journal of Physical Chemistry B**. 108: 15587-15598.
- Xu, R., Pang, W., Yu, J., Huo, Q., and Chen, J. (2007). **Chemistry of zeolites and related porous materials: synthesis and structure**. New York: John Wiley & Sons.



# CHAPTER VI

## INCORPORATION OF VANADIUM IN FAUJASITE NANOZEOLITE

### Abstract

The objective of this study is to synthesize nanosized FAU zeolites incorporated with vanadium (V-FAU) using the one-pot hydrothermal method with various water contents. The effect of water contents on the size, morphology and crystallinity of V-FAU nanocrystallines is investigated. The crystallization time is also optimized. The synthesized zeolite nanoparticles are characterized by X-ray powder diffraction (XRD), scanning electron microscope (SEM), transmission electron microscope (TEM), dynamic light scattering (DLS) analysis, Inductively-coupled plasma spectroscopy (ICP). Acidity of V-FAU samples is investigated by Fourier transform infrared spectroscopy (FTIR) using pyridine as a probe molecule. V-FAU with a high crystallinity and pure phase is obtained from the crystallization time of 6 h. Crystalline shapes and sizes of V-FAU zeolite particles with various water contents are different. V-FAU from the synthesis gel with high water content exhibits characteristic rectangular shape of crystals around 100-300 nm. In contrast, V-FAU from the synthesis gel with lower water content shows spherical shape of zeolite crystals with the crystalline sizes of 500 nm. The V-FAU samples have specific surface area ranging from 550 to 686 m<sup>2</sup>/g and micropore volume of 0.30

cm<sup>3</sup>/g. The Si/Al ratio of V-FAU samples is ranged from 1.56 to 1.79. Vanadium is detected in all V-FAU samples and the incorporation in FAU structure is confirmed by DR UV-Vis spectroscopy. The number of acid sites, Brønsted site and Lewis sites of V-HY are higher than that of HY. The higher of acidity of V-HY zeolite is beneficial as a catalyst for reactions.

## 6.1 Introduction

Vanadium-incorporated zeolites are used as selective oxidation catalysts. The activity and selectivity of vanadium containing zeolite are sensitive to the nature of vanadium species in the zeolites including oxidation state, coordination, dispersion (Roozeboom et al., 1980; Went et al., 1990; Das et al., 1993; Whittington and Anderson, 1993; Chao et al., 1997; Teixeira-Neto et al., 2009). Zeolite containing vanadium provides desired redox properties, structural and shape selective properties. Microporous crystalline zeolites have high thermal stabilities, high surface areas and pore volumes. In addition, the acidity could be controlled (Chao et al., 1997; Teixeira-Neto et al., 2009).

Teixeira-Neto et al. (2009) reviewed the preparation methods for the incorporation of vanadium into zeolite such as ion-exchange, impregnation, chemical vapor deposition and one-pot hydrothermal synthesis. For ion-exchange method, protons or sodium ions are exchanged with vanadyl cations, VO<sup>2+</sup>. However, low pH values lead to a competition between H<sup>+</sup> and VO<sup>2+</sup> ions, which may cause the incorporation of limited vanadium amounts. Thus, impregnation method is another choice to introduce vanadium. However, this method may lead to an aggregation of V<sub>2</sub>O<sub>5</sub>. For chemical vapor deposition method, the vanadium species are vaporized at

high temperature and deposited on zeolite surfaces but this method lead to a poor dispersion at the external surface. The most employed preparation method is one-pot synthesis in which a vanadium source such as  $V_2O_5$ ,  $VOSO_4$  is introduced to the synthesis gel to form vanadosilicate. Vanadium incorporated zeolites prepared by one-pot synthesis are still the best method which can compromise between vanadium concentration and metal dispersion (Teixeira-Neto et al., 2009).

The most studied zeolite prepared by one-pot synthesis is ZSM-5 (Centi et al., 1992). Many techniques, including  $^{51}V$  nuclear magnetic resonance (NMR), X ray photoelectron spectroscopy (XPS), electron paramagnetic resonance (EPR) and diffuse reflectance UV-visible spectroscopy (DR-UV-Vis) are used to propose a model of the coordination vanadium sites in the zeolite structure. Kim et al. (1997) reported the incorporation of vanadium into ZSM-5, MOR and FAU Y zeolites by using one-pot hydrothermal method. The substitution of vanadium into the zeolite framework structure could be applied to the large pore zeolites and the vanadium containing zeolites had selective catalytic properties in various oxidation reactions. However, the crystalline sizes of vanadium containing zeolites are ranged from 5 to 10  $\mu m$ .

Faujasite (FAU) zeolite is one of the most promising materials because of its well-defined channels making a large supercage ( $11.0 \times 13.0 \text{ \AA}$ ) with a large pore size ( $7.4 \times 7.4 \text{ \AA}$ ), large surface area, and excellent thermal stability. From these properties, FAU zeolite can be used in many applications such as ion exchange, adsorption, catalysis and membrane separation (Mintova and Valtchev, 1999; Nakrani et al., 2016; Dang et al., 2017).

FAU zeolites with nanocrystalline are have potential properties including small crystallites between 10-50 nm with a narrow particle size distribution, high micropore volumes ( $0.30 \text{ cm}^3/\text{g}$ ) and excellent thermal stability leading to increase the catalytic performance (Awala et al., 2015). Moreover, nanocrystalline FAU zeolites are synthesized using hydrothermal method without template. Nanocrystalline FAU zeolite has larger pore volume, more external surface area with containing high external surface acid sites and it exhibits high activity and stability (Rasouli et al., 2012; Awala et al., 2015).

The purpose of this study is to adapt the hydrothermal synthesis from Awala et al. (2015) by incorporating of vanadium into FAU zeolite to get nanosizes. However, Chapter V, the synthesis of FAU nanozeolite is optimized. Water content in the synthesis gel has an influence on crystalline size. The low water content decreases a crystallization rate leading to small zeolite crystals. The nanosized crystals of FAU Y zeolite are obtained from the synthesis using low water content. However, phase transformation of FAU Y zeolite to GIS-type zeolite is observed from the synthesis using low water content ( $92\text{H}_2\text{O}$ ). Therefore, the synthesis of V incorporation on FAU Y zeolite is conducted by varying water contents to obtain nanosized crystals. In order to get the small crystals of FAU nanozeolite with the incorporation of V, sodium aluminate is selected as an alumina source. An influence from the amount of water is also studied. Moreover, the existence of vanadium in FAU nanozeolite is analyzed by using ICP. The coordination of vanadium is determined using DR UV-Vis spectroscopy.

## 6.2 Experimental

### 6.2.1 Synthesis of V-Y83, V-Y90 and V-Y100

FAU Y zeolites with incorporation of vanadium are synthesized by varying water content in gel composition, namely, 83H<sub>2</sub>O, 92H<sub>2</sub>O and 100H<sub>2</sub>O. The samples from those syntheses are named V-Y83, V-Y90 and V-Y100, respectively. Firstly, solution A, different water contents as shown in Table 6.1, is prepared by dissolving sodium aluminate (Al<sub>2</sub>O<sub>3</sub> ~ 50-56 wt. %, Na<sub>2</sub>O ~ 40-45 wt. %, Aldrich) and sodium vanadate (99.9 wt. %, Aldrich) in double-distilled H<sub>2</sub>O. The mixture is stirred until a clear solution is obtained. Solution B is prepared by dissolving Ludox HS-40 (40 wt. % SiO<sub>2</sub>, pH=9.8, Aldrich) in sodium hydroxide (97 %, Sigma-Aldrich). A liquid solution is obtained after shaking and stirring for 5 min.

Solution A is added drop wise under a vigorously stirring to the solution B. The resulting clear suspension of V-Y83, V-Y90 and V-Y100 is aged by shaking for 48 h at room temperature. Hydrothermal crystallization is performed at 90 °C for 6 h. The solid products from all syntheses are recovered by centrifugation (20,000 rpm for 20 min) followed by dispersion in double distilled water. This procedure is repeated several times until pH of the final colloidal suspensions is 7 and then freeze-dried prior further characterization.

The gel molar composition of V incorporated FAU zeolite shown below :

V-Y83: 7Na<sub>2</sub>O : 0.8Al<sub>2</sub>O<sub>3</sub> : 10SiO<sub>2</sub> : 0.2NaVO<sub>3</sub> : 83H<sub>2</sub>O

V-Y92: 7Na<sub>2</sub>O : 0.8Al<sub>2</sub>O<sub>3</sub> : 10SiO<sub>2</sub> : 0.2NaVO<sub>3</sub> : 92H<sub>2</sub>O

V-Y100: 7Na<sub>2</sub>O : 0.8Al<sub>2</sub>O<sub>3</sub> : 10SiO<sub>2</sub> : 0.2NaVO<sub>3</sub> : 100H<sub>2</sub>O

The starting mixtures are prepared from solution A (sodium aluminate and sodium vanadate solution) and solution B (sodium silicate solution). Amount of each component for the synthesis of FAU Y is shown in Table 6.1.

**Table 6.1** Amount of materials in gram for the synthesis of V incorporated FAU Y zeolite with various water contents

Materials	V83	Y92	V100
<b>Solution A</b>			
NaVO <sub>3</sub>	0.16	0.16	0.16
NaAlO <sub>2</sub>	1.03	1.03	1.03
H <sub>2</sub> O	4.00	5.00	6.00
<b>Solution B</b>			
NaOH	3.37	3.37	3.37
Ludox HS-40	10.00	10.00	10.00

## 6.3 Characterization

### 6.3.1 X-ray diffraction (XRD) analysis

Powder samples are analyzed using a PANalytical X'Pert Pro diffractometer with CuK $\alpha$  monochromatized radiation ( $\lambda = 1.5418 \text{ \AA}$ ). The samples are scanned in the  $2\theta$  range of  $3\text{-}50^\circ$  with a step size of  $0.02^\circ$ .

### 6.3.2 N<sub>2</sub> adsorption-desorption analysis

Nitrogen adsorption-desorption isotherms are obtained using Micromeritics ASAP 2020 volumetric adsorption analyzer. Samples are degassed at  $250 \text{ }^\circ\text{C}$  under vacuum overnight prior to the measurement. The external surface area and micropore volume are estimated by alpha-plot method using Silica-1000 (22.1

m<sup>2</sup>/g assumed) as a reference. The micropore and mesopore size distributions of solids are extracted from adsorption branch by the Nonlocal Density Functional Theory (NLDFT) and from the desorption branch using the Barret-Joyner-Halenda (BJH) algorithm, respectively.

### **6.3.3 Scanning electron microscopy (SEM)**

Morphology of solids is studied by SEM using a MIRA LMH operated at 30 kV. Solid samples are dispersed on carbon tape coated with Pt.

### **6.3.4 Transmission electron microscopy (TEM)**

The crystal sizes of V-FAU zeolite are determined by TEM using a JEOL 2010 FEG and a FEI LaB6 TECNAI G230UT operated at 200 kV and 300 kV, respectively. Diluted colloidal suspensions of FAU nanomaterials are sonicated for 15 min and then 2-3 drops of fine particle suspensions are dried on carbon-film-covered 300-mesh copper electron microscope grids.

### **6.3.5 Chemical analysis**

The chemical composition of the FAU samples is determined by inductively coupled plasma (ICP) optical emission spectroscopy using a Varian ICP-OES 720-ES. The samples are prepared by acid digestion method and then diluted to a final volume of 100 mL.

### **6.3.6 Pyridine adsorption**

The Brønsted and Lewis acidities of the samples are measured by pyridine adsorption using in-situ IR spectroscopy. Prior to pyridine adsorption/desorption measurements V-FAU and FAU nanosized samples are transformed to proton form by ion-exchange with a solution of 0.2 M of NH<sub>4</sub>Cl (1 h at



25 °C). This procedure is repeated twice and then the solutions are purified by two-step centrifugation, washed with H<sub>2</sub>O and calcined at 370 °C.

FTIR spectrum of the V-FAU and FAU samples is obtained using KBr dilution and fine KBr powder as a reference. To analyze acidity, sample is heat treated at 350 °C for 4 h and cooled to room temperature. Pyridine adsorption is performed at room temperature and then evacuated for 15 min at the 150 °C and before recording the spectrum. The desorption of the probe molecule is successively monitored stepwise, by evacuating the sample for 10 min at room temperature, 50, 100, 150, 200, 250, 300 and 350 °C and cooling to room temperature between each step, to record the spectrum. According to Emeis (1993), Zhang et al. (2012) and Jia et al., (2017) the density and concentration of acid sites on three catalysts are calculated by the following equations,

$$CL = (\pi/IMECL) \times (r^2/w) \times A_{1450} \quad (6.1)$$

$$CB = (\pi/IMECB) \times (r^2/w) \times A_{1540} \quad (6.2)$$

where CL and CB (μmol/g) are the concentration of L and B acid sites; A<sub>1450</sub> and A<sub>1540</sub> is integrated areas of bands at 1450 and 1545 cm<sup>-1</sup>; π/IMECL and π/IMECB are integration molar extinction coefficients, 2.22 and 1.67 cm/μmol, respectively, r (cm) is the sample radius, and w (g) is the sample weight.

### 6.3.7 Diffuse reflectance (DR) UV-Vis spectroscopy

The coordination of vanadium in FAU zeolite is analyzed using DR UV-Vis spectroscopy. The spectra are recorded by a Cary 300 instrument. The powders are filled in a hole of a sample holder (3 mm in diameter and 2 mm deep), and pressed to get the smoothed surface.

## 6.4 Results and discussion

### 6.4.1 Phase and crystallinity of V-FAU

XRD patterns of V-FAU zeolites synthesized with different water content (V-Y83, V-Y92 and V-Y100) are shown in Figure 6.1-6.2. All samples showed similar patterns, characteristic of FAU phase with sharp peaks indicating high crystallinity. In comparison to FAU sample (Figure 6.1), the diffraction patterns of samples do not show any peaks of impurity phase. In addition, there are no peak shifts. The results indicate that the pure FAU is obtained. The cubic unit cell parameter is estimated to be 24.832 Å (as shown in Figure 6.3).

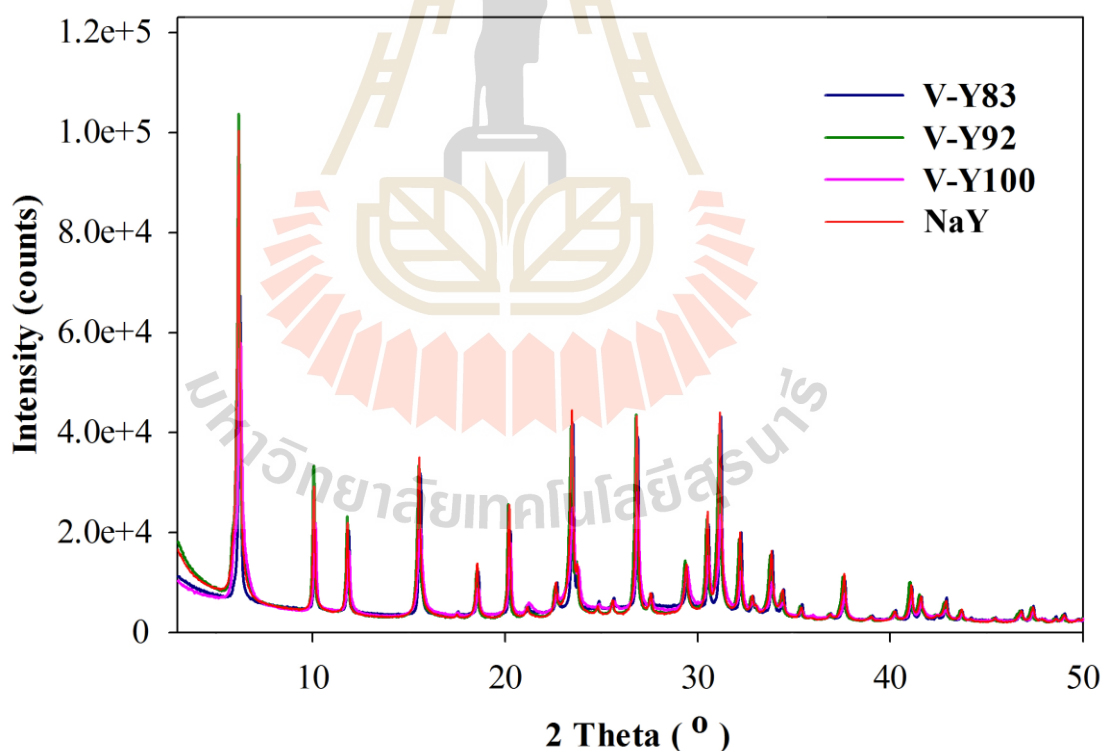


**Figure 6.1** XRD patterns of V-Y83, V-Y92, V-Y100 comparing to NaY.

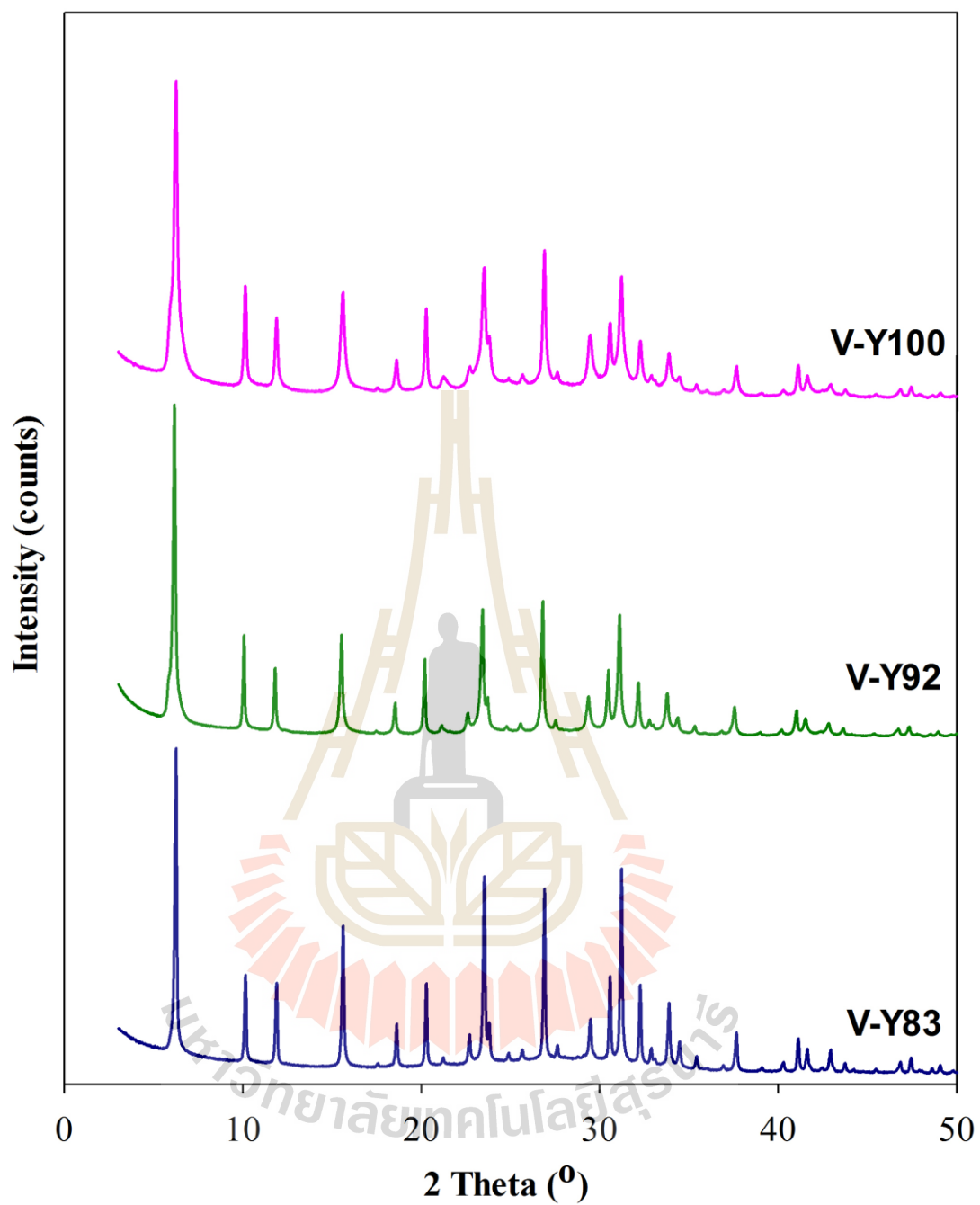


**Figure 6.2** XRD patterns of V-FAU synthesized from the gels with different water content.

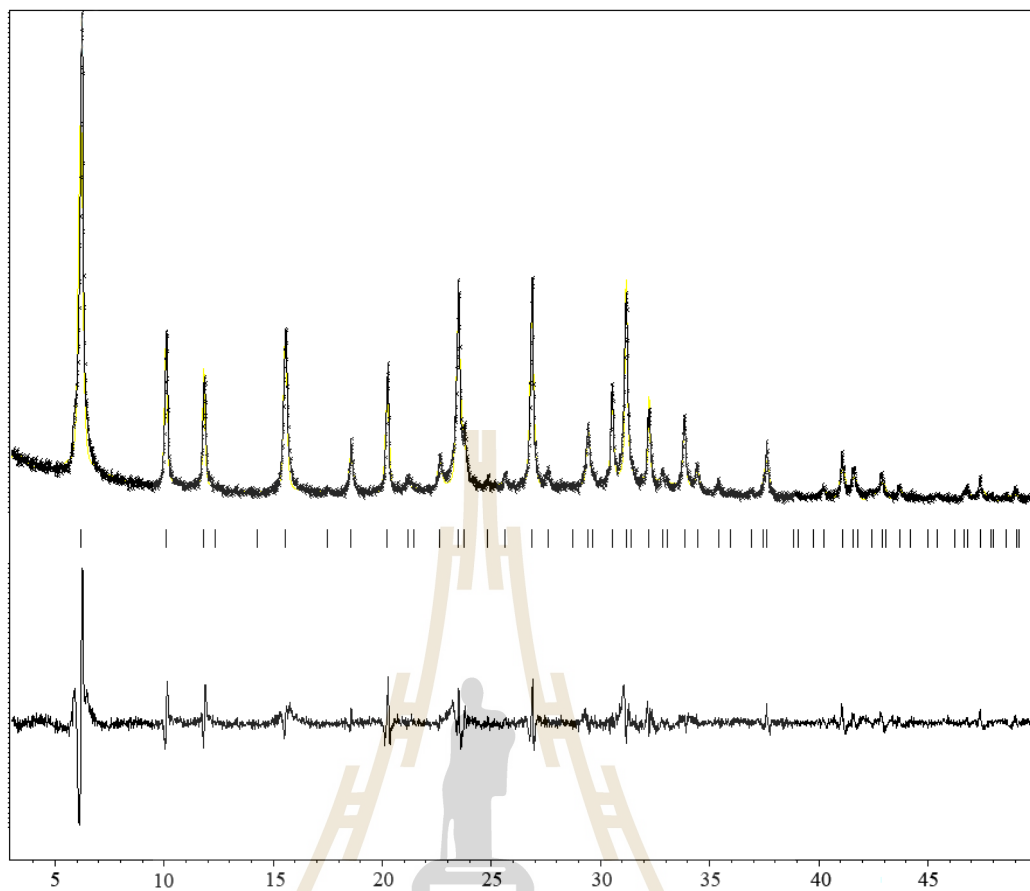


**Figure 6.3** Pattern fitting (Le Bail method) of V-Y92. Vertical ticks correspond to line indexing of the FAU phase. Difference plots between calculated and experimental points are shown at the bottom of the pattern.

#### 6.4.2 Morphology of V-FAU Y with different water contents

The SEM micrographs of V-Y83, V-Y92, V-Y100 in Figure 6.4 reveal crystalline shape and sizes. V-Y92 and V-Y100 are polycrystals with the size about 200-400 nm and 100-300 nm, respectively. V-Y83 has a less uniform shape with particle size around 500 nm. Moreover, the large particles of V-Y83 partially contain amorphous phase. The morphologies (shape and size) of V-FAU zeolite have some varieties caused by the different water contents. The smallest crystal sizes are obtained from the synthesis gel with high water content. This SEM images are different from the previous study of the synthesis FAU nanozeolites with various water content. The smallest crystal sizes obtained from the synthesis FAU Y with low water content. The incorporation of vanadium in FAU using hydrothermal method could lead to small particle sizes of FAU zeolite. The addition of vanadium may condense aluminosilicate leading to low crystallization rate of the synthesis to get small crystal sizes.

Crystalline particles of sample V-Y92 are shown in the TEM images (Figure 6.5). The V-Y92 crystals exhibit the typical zeolite Y octahedral morphology with well-defined shape (Awala et al., 2015). The mean diameter of the nanocrystallite V-Y92 zeolite is about 200 nm.

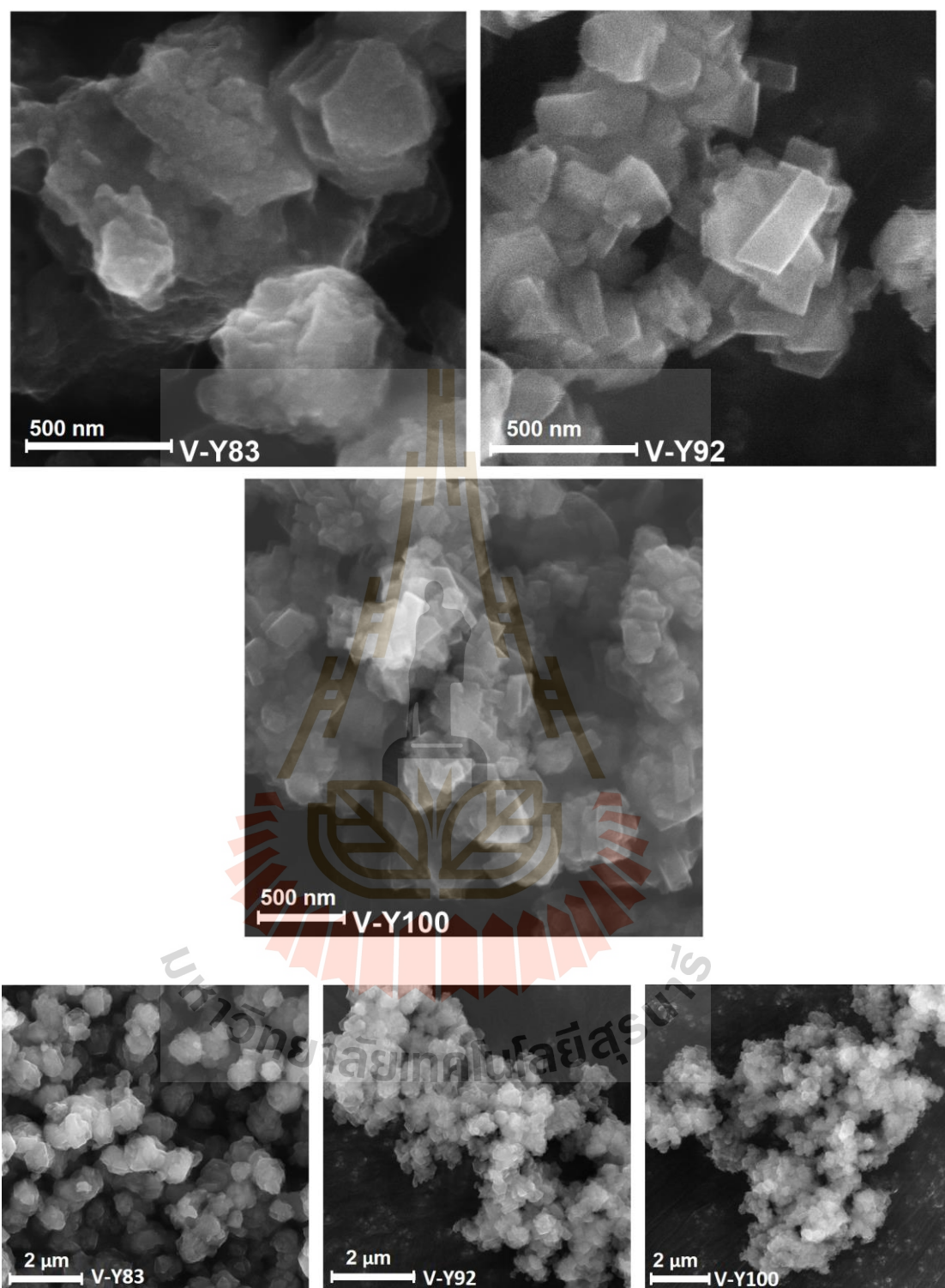


**Figure 6.4** SEM images of V-FAU with different water content.

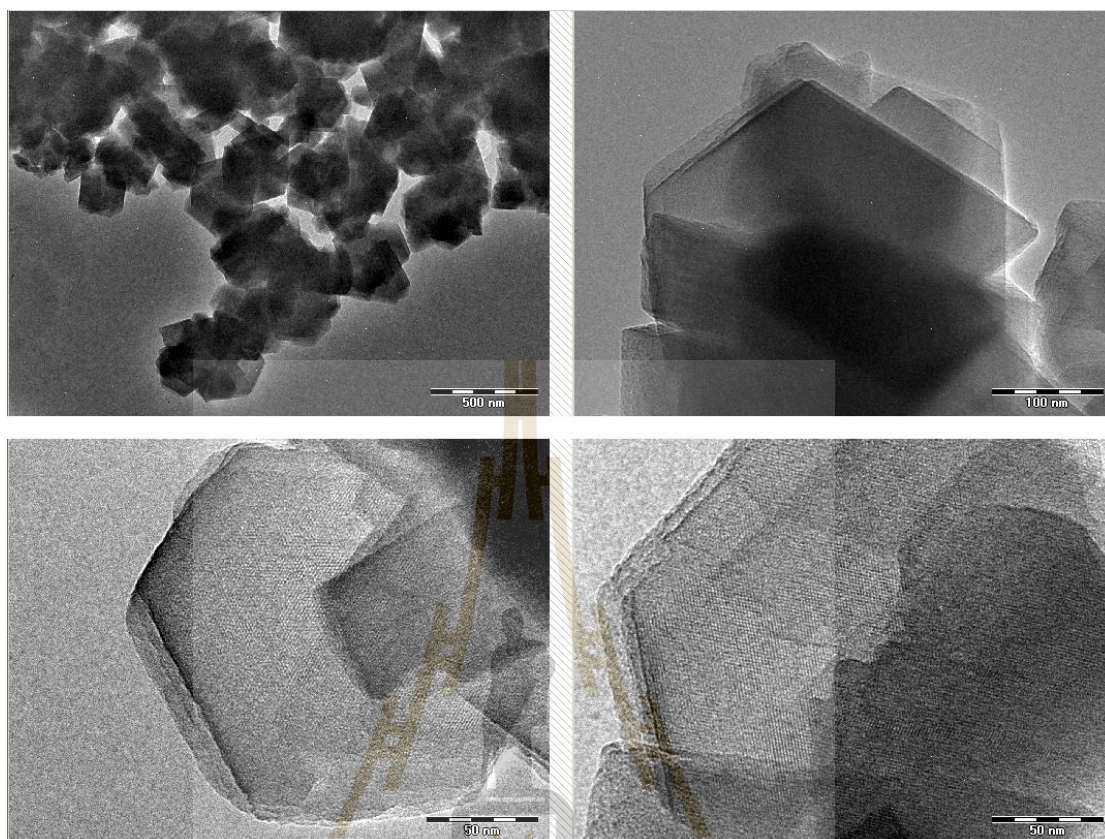


**Figure 6.5** TEM images of V-Y92 with nanosized particles with high magnification.

#### 6.4.3 N<sub>2</sub> adsorption-desorption isotherms of V-FAU

The N<sub>2</sub> adsorption-desorption isotherms of V-Y83, V-Y92, V-Y100 are displayed in Figure 6.6. The textural properties (surface area, external surface area, micropore volume and total pore volume) are summarized in Table 6.2. Zeolites V-V92 and V-Y100 exhibit a type I(a) isotherm corresponding microporous solids having relatively small external surfaces (Thommes et al., 2015). A sharp uptake at low relative pressures corresponds to the adsorption in narrow micropores, resulting in micropore filling at very low  $P/P_0$ . Zeolite V-Y83 also exhibits the isotherm type I(a) with type H4 hysteresis loop corresponding to aggregated crystals of zeolites

(Thommes et al., 2015). The small hysteresis loop indicates the presence of mesopores in the V-Y83 nanozeolite (Kabalan et al., 2016). This result is consistent with the SEM image of V-Y83 which contained amorphous phase leading to lower surface area and micropore volume. All V-FAU samples exhibit BET specific surface area ranging from 550 to 686  $\text{m}^2/\text{g}$ . V-V92 and V-Y100 show micropore volume of 0.31 and 0.30  $\text{cm}^3/\text{g}$ , respectively. Their external surface areas are 72 and 75  $\text{m}^2/\text{g}$ , respectively. While pore volumes of sample V-Y83 is lower (0.14  $\text{cm}^3/\text{g}$ ). However, total pore volume of three V-FAU samples are similar. Moreover, V-Y83 has high external surface area, 114  $\text{m}^2/\text{g}$ . This property could lead to a better diffusion of substrates when it is used as a catalyst.

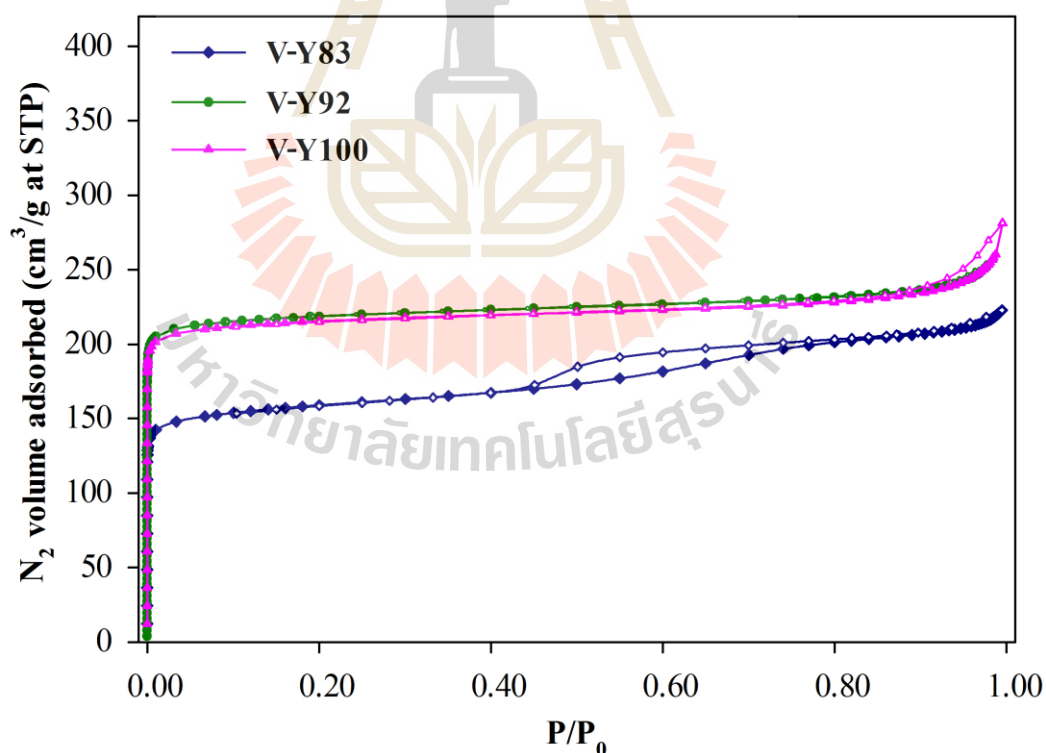


**Figure 6.6**  $\text{N}_2$  adsorption-desorption isotherm of V-FAU nanozeolites.



**Table 6.2** Textural properties of V-Y83, V-Y92 and V-Y100.

Sample	Surface area (m <sup>2</sup> /g)	Micropore area (m <sup>2</sup> /g)	External surface area (m <sup>2</sup> /g)	Micropore volume (cm <sup>3</sup> /g)	Total pore volume (cm <sup>3</sup> /g)
V-Y83	513	399	114	0.14	0.33
V-Y92	666	594	72	0.31	0.39
V-Y100	686	611	75	0.30	0.59

#### 6.4.4 Chemical composition of V-FAU zeolites

Results from elemental analysis of V-FAU zeolites from ICP are summarized in Table 6.3 Na, Si, Al and V are detected in all samples. V-Y83 has a higher Si/Al ratio than other samples probably due to a higher vanadium content. It is possible that the frame work Al atoms are replaced by V atoms. The high Si/Al of V-Y83, compared with V-Y92 and V-Y100, could be from the presence of amorphous silica.

**Table 6.3** Chemical composition of V-Y83, V-Y92 and V-Y100.

FAU Y	Atomic (%)				Si/Al
	Na	Si	Al	V	
V-Y83	11.45	21.44	12.00	0.036	1.79
V-Y92	11.54	22.20	14.25	0.006	1.56
V-Y100	11.95	22.41	14.10	0.011	1.59

### 6.4.5 Pyridine adsorption

Figure 6.7 shows the FTIR spectra of pyridine (Py) adsorption on V-FAU samples and FAU. The spectrum is collected from desorption at the temperature of 200°C due to complete separation of the bands. The band around 1450  $\text{cm}^{-1}$  is attributed to the interaction of Py molecules with Lewis (L) acid sites, while that observed at 1545  $\text{cm}^{-1}$  corresponds to the interaction of Py with Brønsted (B) sites (El-Roz et al., 2012; Zhang et al., 2012; Jia et al., 2017). The calculated number of acid sites are shown in Table 6.4. The number of acid sites, Brønsted site and Lewis sites of V-HY are higher than that of HY. This is due to the existence of vanadium in FAU Y. The higher acidity of V-HY zeolite makes it useful as acid catalyst.

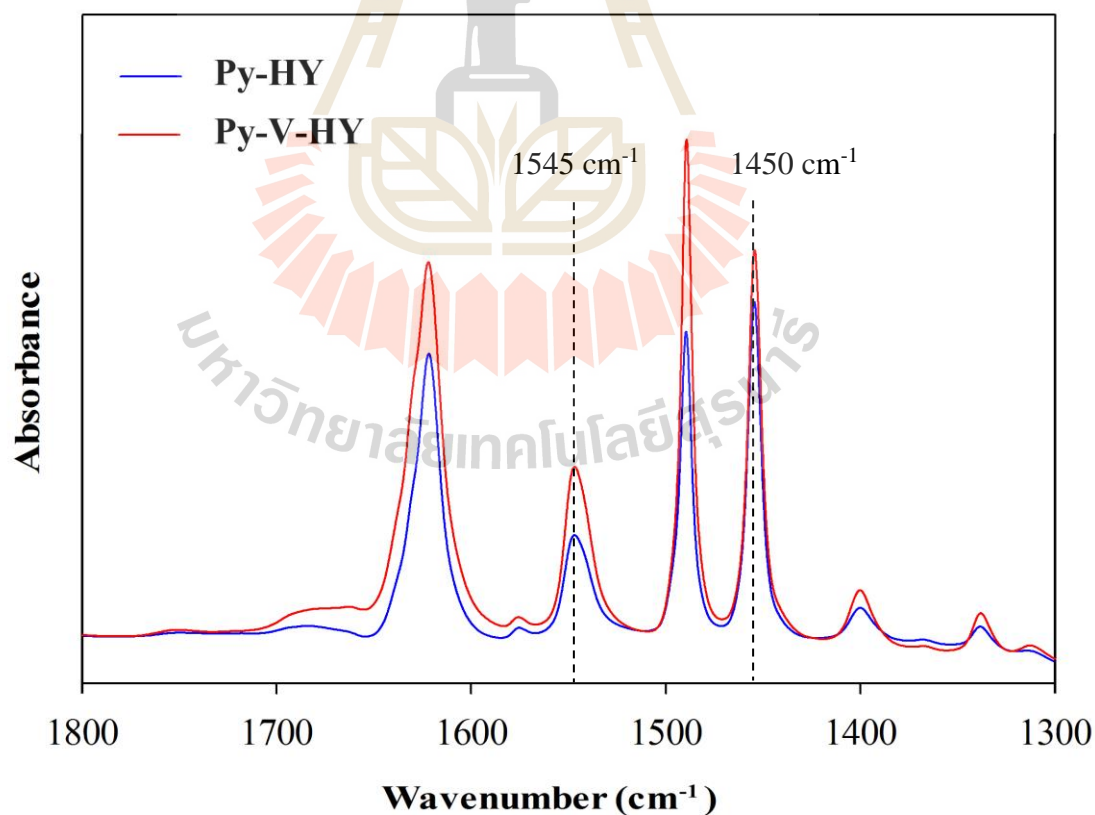


**Figure 6.7** FTIR spectra of HY and V-HY samples after pyridine adsorption.

**Table 6.4** Peak area and number of acid site.

FAU Y	Peak area (at 200°C)		Number of acid site (μmol/g)	
	Brønsted site	Lewis site	Brønsted site	Lewis site
HY	2.178	3.773	138	317
V-HY	2.600	3.844	166	325

#### 6.4.6 Characterization of V-FAU by DRUV-Vis

The diffuse reflectance UV-Vis spectra of V-Y83, V-Y92 and V-Y100 are shown in Figure 6.8. The interpretation is summarized in Table 6.4. All V-FAU samples exhibit two intense absorption bands at around 280 and 340 nm in UV region corresponding to the low-energy charge-transfer (CT) bands associated with V-O electron transfer ( $\pi \rightarrow d$ ) and ( $\pi \rightarrow d$ ), respectively. Those bands attribute to tetrahedral coordination and colorless  $V^{5+}$  ions in  $T_d$  environments. A weak band at 610 nm is assigned to the d-d transition of the  $VO^{2+}$  ion,  $b_2(d_{xy}) \rightarrow a_1(d_{x^2-y^2})$  (Chao et al., 1997; El-Roz et al., 2017). These results are summarized in Table 6.4.

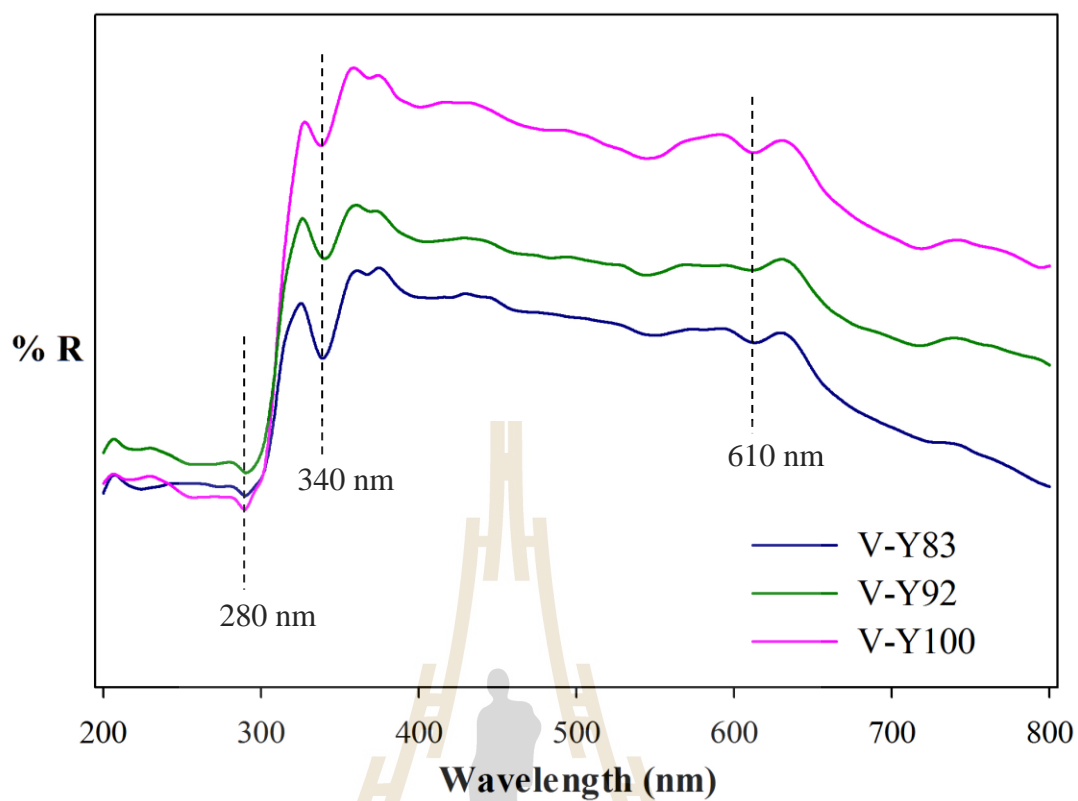


**Figure 6.8** DR UV-Vis spectra of V-Y83, V-Y92 and V-Y100.

**Table 6.5** Vanadium species in V-Y83, V-Y92 and V-Y100 zeolite based on DR UV-Vis analysis (Chao et al., 1997).

UV-Vis (nm)	V species	Symmetry
610	$\begin{array}{c} \text{O} \\    \\ \text{O}-\text{V}-\text{O} \\   \\ \text{OH}_2 \end{array}$	$\text{V}^{4+}$ in $\text{T}_d$
280, 340	$\begin{array}{c} \text{O} \\    \\ \text{O}-\text{V}-\text{O} \\   \\ \text{OH} \end{array}$	$\text{V}^{5+}$ in $\text{T}_d$

## 6.5 Conclusions

The effect of water contents on the textural properties and morphologies of vanadium incorporated FAU nanozeolite is investigated. V-FAU nanozeolite is successfully synthesized using hydrothermal method with the rapid crystallization time of 6 h. The smallest crystalline sizes are observed for V-Y100, with higher water content. The sizes are ranged of 100-300 nm with rectangular crystalline crystals of the particles. All V-FAU samples are sharp, narrow and intense peaks, corresponding to high crystallinity of the V-FAU samples. XRD patterns exhibit the pure FAU zeolite. High specific surface area (BET), ranging from 550 to 686 m<sup>2</sup>/g are observed. Vanadium is found in all FAU samples. The number of acid sites, Brønsted site and Lewis sites of V-HY are higher than that of HY. DR UV-Vis revealed that V<sup>5+</sup> ions and V<sup>4+</sup> ions incorporated in tetrahedral coordination for all V-FAU samples.

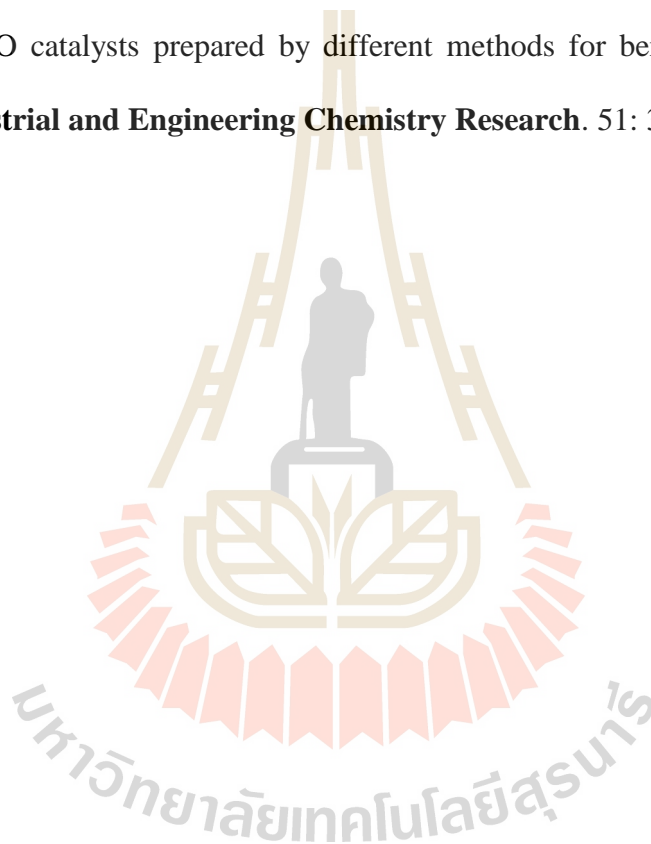
## 6.6 References

- Awala, H., Gilson, J.-P., Retoux, R., Boullay, P., Goupil, J.-M., Valtchev, V., and Mintova, S. (2015). Template-free nanosized faujasite-type zeolites. **Nature Materials**. 14: 447-451.
- Chao, K. J., Wu, C. N., Chang, H., Lee, L. J., and Hu, S. (1997). Incorporation of vanadium in mesoporous MCM-41 and microporous AFI zeolites. **Journal of Physical Chemistry B**. 101: 6341-6349.
- Dang, S., Zhao, L., Yang, Q., Zheng, M., Zhang, J., Gao, J., and Xu, C. (2017). Competitive adsorption mechanism of thiophene with benzene in FAU zeolite: The role of displacement. **Chemical Engineering Journal**. 328: 172-185.

- Das, N., Eckert, H., Hu, H., Wachs, I. E., Walzer, J. F., and Feher, F. J. (1993). Bonding states of surface vanadium(V) oxide phases on silica: structural characterization by vanadium-51 NMR and Raman spectroscopy. **Journal of Physical Chemistry**. 97: 8240-8243.
- El Roz, M., Lakiss, L., Valtchev, V., Mintova, S., and Thibault-Starzyk, F. (2012). Cold plasma as environmentally benign approach for activation of zeolite nanocrystals. **Microporous and Mesoporous Materials**. 158: 148-154.
- El-Roz, M., Lakiss, L., Telegeiev, I., Lebedev, O. I., Bazin, P., Vicente, A., and Valtchev, V. (2017). High-visible-light photoactivity of plasma-promoted vanadium clusters on nanozeolites for partial photooxidation of methanol. **ACS Applied Materials and Interfaces**. 9: 17846-17855.
- Emeis, C. A. (1993). Determination of integrated molar extinction coefficients for infrared bands of pyridine adsorbed on solid acid catalysts. **Journal of Catalysis**. 141: 347-354.
- Jia, Y., Wang, J., Zhang, K., Feng, W., Liu, S., Ding, C., and Liu, P. (2017). Nanocrystallite self-assembled hierarchical ZSM-5 zeolite microsphere for methanol to aromatics. **Microporous and Mesoporous Materials**. 247: 103-115.
- Kabalan, I., Lebeau, B., Fadlallah, M.-B., Toufaily, J., Hamieh, T., Bellat, J. P., and Daou, T. J. (2016). Hierarchical faujasite-type zeolite for molecular decontamination. **Journal of Nanoscience and Nanotechnology**. 16: 34-37.

- Kim, G.-J., Kim, J.-H., and Shoji, H. (1997). Incorporation of vanadium into ZSM-5, mordenite and Y type zeolite and their catalytic properties. **Progress in Zeolite and Microporous Materials Studies in Surface Science and Catalysis**. 105: 1101-1108.
- Mintova, S. and Valtchev, V. (1999). Synthesis of nanosized FAU-type zeolite. **Studies in Surface Science and Catalysis**. 125: 141-148.
- Nakrani, D., Belani, M., Bajaj, H. C., Somani, R. S., and Singh, P. S. (2017). Concentrated colloidal solution system for preparation of uniform zeolite-Y nanocrystals and their gas adsorption properties. **Microporous and Mesoporous Materials**. 241: 274-284.
- Rasouli, M., Yaghobi, N., Chitsazan, S., and Sayyar, M. H. (2012). Adsorptive separation of meta-xylene from C<sub>8</sub> aromatics. **Chemical Engineering Research and Design**. 90: 1407-1415.
- Roozeboom, F., Mittelmeijer-Hazeleger, M. C., Moulijn, J. A., Medema, J., De Beer, V. H. J., and Gellings, P. J. (1980). Vanadium oxide monolayer catalysts: A Raman spectroscopic and temperature-programmed reduction study of monolayer and crystal-type vanadia on various supports. **Journal of Physical Chemistry**. 84: 2783-2791.
- Thommes, M., Kaneko, K., Neimark, A. V., Olivier, J. P., Rodriguez-Reinoso, F., Rouquerol, J., and Sing, K. S. W. (2015). Physisorption of gases, with special reference to the evaluation of surface area and pore size distribution (IUPAC Technical Report). **Pure and Applied Chemistry**. 87: 1051-1069.

- Went, G. T., Oyama, S. T., and Bell, A. T. (1990). Laser Raman spectroscopy of supported vanadium oxide catalysts. **Journal of Physical Chemistry**. 94: 4240-4246.
- Whittington, B. I. and Anderson, J. R. (1993). Nature and activity of some vanadium catalysts. **Journal of Physical Chemistry**. 97: 1032-1041.
- Zhang, X., Lin, T., Li, R., Bai, T., and Zhang, G. (2012). Properties and reactivity of Fe-P-O catalysts prepared by different methods for benzylation of benzene. **Industrial and Engineering Chemistry Research**. 51: 3541-3549.





# CURRICULUM VITAE

## Mr. CHALERMPAN KEAWKUMAY

### Education

- 2005 B.Sc. (2<sup>nd</sup> Class Honors) (Chemistry), Utrraradit Rajabhat University, Thailand.
- 2010 M.Eng. (Polymer Engineering), Suranaree University of Technology, Thailand.
- 2012-2017 Ph.D. Candidate (Chemistry), Suranaree University of Technology, Thailand.

### Research exchange experience

- 2016-2017 Laboratoire Catalyse et Spectrochimie (LCS), ENSICAEN, Université Caen-Normandie, France (6 months).

### International Publications

Rakmae, S., Keawkumay, C., Osakoo, N., Montalbo, K. D., de Leon, R. L., Kidkhunthod, P., Chanlek, N., Roessner, F., Prayoonpokarach, S., and Wittayakun, J. (2016). Realization of active species in potassium catalysts on zeolite NaY prepared by ultrasound-assisted impregnation with acetate buffer and improved performance in transesterification of palm oil. *Fuel*. 184: 512-517.

Keawkumay, C., Rakmae, S., Rongchapo, W., Suppakarn, N., Prayoonpokarach, S., and Wittayakun, J. (2017). Adsorption of paraquat and pirimiphos-methyl by montmorillonite modified with tetradecylammonium chloride and intragallery templating method. *Adsorption Science and Technology*. 35(3-4): 357-371.